THE
CHEMICAL
RECORD

Performance Studies of Proton Exchange Membrane Fuel Cells with Different Flow Field Designs – Review

Muthukumar Marappan,*[a] Karthikeyan Palaniswamy,[b] Thiagarajan Velumani,[b] Kim Byung Chul,[c] Rajavel Velayutham,[c] Praveenkumar Shivakumar,[d] and Senthilarasu Sundaram*[e]

Abstract: Proton Exchange Membrane Fuel Cell (PEMFC) is majorly used for power generation without producing any emission. In PEMFC, the water generated in the cathode heavily affects the performance of fuel cell which needs better water management. The flow channel designs, dimensions, shape and size of the rib/channel, effective area of the flow channel and material properties are considered for better water management and performance enhancement of the PEMFC in addition to the inlet reactant's mass flow rate, flow directions, relative humidity, pressure and temperature. With the purpose of increasing the output energy of the fuel cell, many flow field designs are being developed continuously. In this paper, the performance of various conventional, modified, hybrid and new flow field designs of the PEMFC is studied in detail. Further the effects of channel tapering, channel bending, landing to channels width ratios, channel cross-sections and insertion of baffles/blockages/pin-fins/inserts are reviewed. The power density of the flow field designs, the physical parameters like active area, dimensions of channel/rib, number of channels; and the operating parameters like temperature and pressure are also tabulated.

Keywords: channel design, flow field, fuel cells, PEMFC, water management

[a] *M. Marappan*
Fuel Cell Research Lab
Department of Mechanical Engineering
Nandha Engineering College
(Autonomous Institution, Affiliated to Anna University)
Erode-638052, India
Tel: +91 9865923333
E-mail: muthupsgtech@gmail.com
[b] *K. Palaniswamy, T. Velumani*
Fuel Cell Energy System Lab
Department of Automobile Engineering
PSG College of Technology
Coimbatore-641004, India
E-mail: apk.auto@psgtech.ac.in
        vthiagu90@gmail.com
[c] *K. B. Chul, R. Velayutham*
Electromaterials Science Lab
Department of Printed Electronics Engineering
Sunchon National University
Jungang-Ro 255, SunCheon-Shi, JeollaNam-Do, South Korea
E-mail: bckim@scnu.ac.kr
        mek.rajavel68@gmail.com

[d] *P. Shivakumar*
Department of Mechanical Engineering
S.A. Engineering College
Chennai-600077, India
E-mail: sivapraveen09@gmail.com
[e] *S. Sundaram*
Environment and Sustainability Institute (ESI)
University of Exeter
Penryn Campus, Penryn
Cornwall TR10 9FE, UK
Tel: +44 (0)1326 259486
E-mail: S.Sundaram@exeter.ac.uk

Muthukumar Marappan is the Head of Fuel Cell Research Lab and Faculty of Mechanical Engineering in Nandha Engineering College, Erode, India. He received his Bachelor's and Master's degrees in the Stream of Mechanical Engineering from the Bharathiar University and Anna University in 1999 and 2004 respectively. He completed his Ph.D. degree in PSG College of Technology, Coimbatore, under Anna University, Chennai, India in 2016. He worked as an Assistant Production Engineer in Agni Steels Limited, Erode, India. He is having more than 18 years of teaching experience in various Engineering colleges. He has been working as the Faculty of Mechanical Engineering in Nandha Engineering College, Erode, India since 2006. He has established the Fuel Cell Research Lab in Nandha Engineering College from the funding of AICTE, New Delhi, India. His current research interests focus on the Design and development of Fuel Cell Electric Vehicles and Novel flow field designs of PEM fuel cells with high performance and Alternate fuels of I.C. Engines for an eco-friendly environment.

Karthikeyan Palaniswamy is the Head of Fuel Cell Energy System Laboratory and Professor in the Dept. of Automobile Engineering at PSG College of Technology, Coimbatore. INDIA. He has significantly contributed to fuel cell research in India and he mainly focuses on fuel cell material development, flow field optimization and design, stack development and testing, now he has moved further to develop H_2 storage, Vehicle control system and FCEV development and demonstration. He received his PhD Degree at Indian Institute of Technology Madras (IIT-M), Chennai on 2008. After successful completion of his PhD Degree at Indian Institute of Technology Madras (IIT-M), he was received BOYSCAST fellowship (2009–10) from DST, Government of India for conducting Advanced Research Training in the area of "Fuel Cells – Water Management in PEM Fuel Cells" in USA. He has received research project grants from DST-SERB, DST-UKIERI, AICTE-RPS, DST-CONACYT, DST-NPDF, CRS-NPIU, CSIR, Royal Academia, AICTE-NDF and DST-EPSRC etc. He has worked in couple of bilateral projects demonstrating his capability in the field of fuel cell and had research coordination with various universities such as the Loughborough University & University of Exeter, UK and Hanyang University and Suncheon National University, South Korea, CINVESTAV-IPN, Unidad Saltillo-Mexico, University of Toledo, OHIO, USA, Clemson University-ICAR, USA.

Thiagarajan Velumani was born in 1990 in Tamilnadu, India. He received his Bachelor's and Master's degree from Anna University, Chennai in 2012 and 2014 respectively and he completed his Doctoral degree from the same university in 2020. He worked in various government-funded projects like DST-INDO Mexican Bilateral Program, ISRO-Respond Project, and DST-UKIERI, particularly in the broad area of research in the development of energy systems like battery and fuel cell. He has more than six years of research experience in energy materials development. His current research focuses on low-cost, high energy density electrocatalyst for fuel cells and its allied applications.

Byung Chul Kim received his Ph.D. in the electrical and electrochemical characterizations of conducting polymer and hydrogel blends under the supervision of Prof. Gordon at the University of Wollongong from 1995 to 1999. He received the Japan Society of Promotion Science (JSPS) fellowship and studied by the support of Prof. Naoya Ogata at the Chitose Institute of Scicence and Technology in Japan as host institute (2000–2002). He was appointed as the invited professor at Dongguk University-Seoul in Korea and supervised 10 Ph.D. students for 7 years. He is appointed as Editorial Board of the Journal of Functional Materials and Biomolecules. He has 70 peer-reviewed publications and has supervised 15 Master and Ph.D. students to completion within the University of Wollongong and University of Dongguk University-Seoul. Currently, he is a full time Professor at the Department of Printed Electronics in the Sunchon National University, Korea. His major research interests are energy material, electrochemistry, nanotechnology and electromaterials for supercapacitors and sensors.

Rajavel Velayutham received his M.E. degree in Energy Engineering from College of Engineering, Guindy campus, Anna University, Chennai, India in 2016. Currently he is pursuing Ph.D. degree in Sunchon National University under the supervision of Prof. Byung Chul Kim. His research interests mainly focus on Super capacitor and fuel cells.

Praveenkumar Shivakumar is presently working as a Faculty of Mechanical Engineering at S.A. Engineering College, Chennai, India. He completed his B.E. (Mechanical Engineering) in 2013 followed by M.E. (Engineering Design) in 2015 under Anna University, Chennai. Currently he is pursuing Ph.D. degree on Performance enhancement and Thermal management of Proton Exchange Membrane fuel cells under Anna University, Chennai, India.
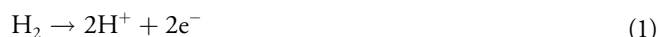

Senthilarasu Sundaram is a Senior Lecturer in Renewable Energy at the College of Engineering, Mathematics and Physical Sciences (CEMPS) at the University of Exeter. His research focus on energy materials and device architecture for the past 20 years since he started his PhD career at Bharathiar University, Coimbatore, India. Dr. Sundaram is an expert in materials design for energy conversion, water treatment, engineering for solar cell devices and fuel cells. He has published more than 130 articles in the international journals and 70 articles in the reputed conferences.
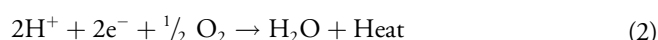
1. Introduction

1.1. Fuel Cell

Air pollution is a major problem throughout the world, which is caused by solid/liquid particles and certain gases like Nitrogen oxide (NOx), Carbon dioxide (CO$_2$), Sulphur oxide (SOx) etc. The transport sector is one of the largest contributors for carbon emissions. The pollution control has been initiated from the different sectors and adopts them through suitable sustainable alternatives. The fuel cell is one of the green power systems to overcome the air pollution by replacing IC engines.[1,2] Fuel cell technology is majorly upgraded than coal/oil-burning power plants, diesel power plants, internal combustion engines, and nuclear power plants. Fuel cell is working like battery, but it does not need recharging.[3] There are different types of fuel cells like Alkaline Fuel cell (AFC), Phosphoric Acid Fuel Cell, Proton Exchange Membrane Fuel Cell (PEMFC), Molten Carbonate Fuel Cell (MCFC) and Solid Oxide Fuel Cell (SOFC). Among several types of fuel cells, the PEMFC is preferred due to its high electrical efficiency and simple design compared to others.[4] The PEMFC is an electrochemical device which employs hydrogen gas and oxygen gas as fuels along with a special proton exchange membrane (Nafion). The schematic diagram of PEMFC is shown in Figure 1. The outputs of the electrochemical reaction in PEMFC are water, electricity, and heat. The electrochemical reactions in PEMFC are given in Eq.(1–3).
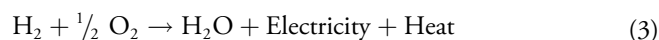
At anode catalyst layer:

$$H_2 \rightarrow 2H^+ + 2e^- \tag{1}$$

At cathode catalyst layer:

$$2H^+ + 2e^- + \tfrac{1}{2} O_2 \rightarrow H_2O + Heat \tag{2}$$

Overall reaction:

$$H_2 + \tfrac{1}{2} O_2 \rightarrow H_2O + Electricity + Heat \tag{3}$$

As the PEMFCs are having a high energy density[5] and operating at atmospheric pressure and temperature with zero emissions, they are widely used in Fuel Cell Electric Vehicles (FCEV).[6] As FCEV gives a lot of environmental benefits in urban regions, the major automakers like Toyota, General motors, Hyundai, Honda, Ford, Audi, Mercedes are majorly involving in the development of FCEV.[7] The need for hydrogen which used as a main fuel in PEMFC is also rising rapidly. The hydrogen demand for FCEV in 2030 at UK will be 254000 tons per annum as per the roadmap report.[8] The European Strategic Energy Technology commission targeted the fuel cell technology, and its allied new FCEV production will be increased by 40 % by 2030 for achieving zero-emission vehicles.[9] Figure 2 shows the fuel cell car market upto 2030.[10] Hence FCEV will contribute to the reduction of long period emissions and the pollution control worldwide.

The hydrogen storage and handling, high cost of the component (Platinum catalyst), instability during dynamic conditions, thermal and water handling issues in single-cell and stacks are some of the drawbacks of PEMFC. Many efforts have been carried out to solve the above problems like on-board generation of hydrogen, development of new catalysts at reduced cost[11–13] and the design modifications of components for thermal and water handling issues. The design parameters of components (flow field, MEA, current collectors, supporting plates) and the operating parameters of reactants (pressure, temperature, humidity and mass flow rate) are affecting the water management and performance of PEMFC[14–17] in addition to the material properties of the components.[18] The generated water at cathode side is to be maintained at optimum level to avoid flooding, dehydration, hotspot and drop in performance which are mainly affected by the flow field design. This can be overcome through effective flow field
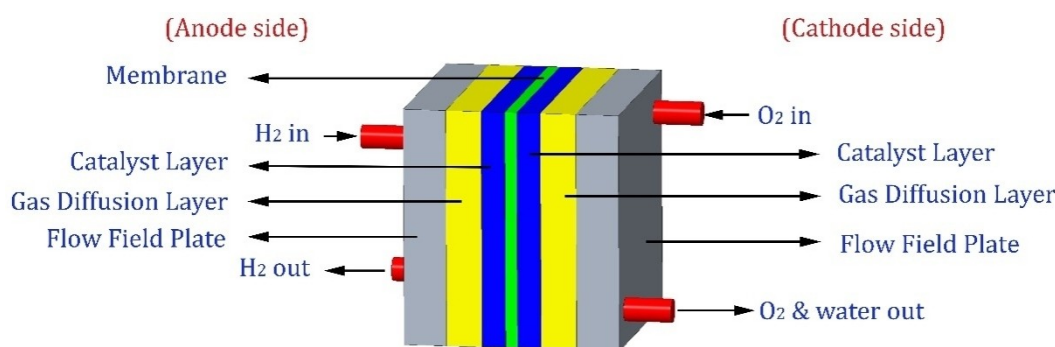

Figure 1. Schematic diagram of PEMFC with components.

Figure 2. Global scenario on Fuel Cell Passenger car market. (Adopted from Ref. [10])

design and this review is to focus on the flow field design aspects of the PEMFC.

1.2. Importance of Flow Field in PEMFC

The flow field is an important component which is designed and machined to supply the required amount of the oxygen and hydrogen to the Gas Diffusion Layer (GDL) and the Catalyst Layer (CL) with minimum pressure drop on cathode and anode sides respectively. In case of stack, the flow channels are machined on both sides of the plate which is called as a bipolar plate where one side is acting as anode and another side is cathode. The essential properties of flow field materials are high electric and thermal conductivities, high mechanical strength to withstand clamping pressure, non-toxic, water resistant and ease machinability. Usually plain graphite or stainless steel materials are used for this purpose and in which the graphite material is majorly used. The flow field plates perform several functions like carrying the electrons and water to and from the CL in addition to the supply of reactants on cathode and anode sides. The better design of the flow field will help to avoid the water flooding in the cathode and for better water management and higher performance.

1.3. Most Popular Flow Field Designs

In PEMFC, the single straight, parallel, serpentine, interdigitated, pin, spiral, cylindrical, radial, natural inspired, square tubular and fractal flow field designs are generally used. The most popular flow field designs of PEMFC are shown in

Figure 3. The design of flow field is highly affecting the performance of PEMFC which leads to many modifications to improve its performance further. This article is to review the effects of various conventional flow field designs, modified flow field designs, hybrid flow field designs, new flow field designs, channel tapering, channel bending, landing to channels width ratios, channel cross-sections and insertion of baffles/blockages/pin-fins/inserts on channel and ribs on the performance of PEMFC.

2. Effects of Different Flow Field Designs

The various design modifications have been made on the conventional flow fields (straight, parallel, serpentine, interdigitated, spiral, cylindrical, radial, bionic and square tubular flow fields) using grooves, blockages, sub channels, microdistributors, orientations, etc.

2.1. Straight Flow Field Design

The straight flow field is having only one channel with a straight path. It has uniform cross-section (normally square or rectangle) throughout the path. The provision of traps, open channels, and different shapes of blockages on the flow path are influencing the performance of straight flow fields.
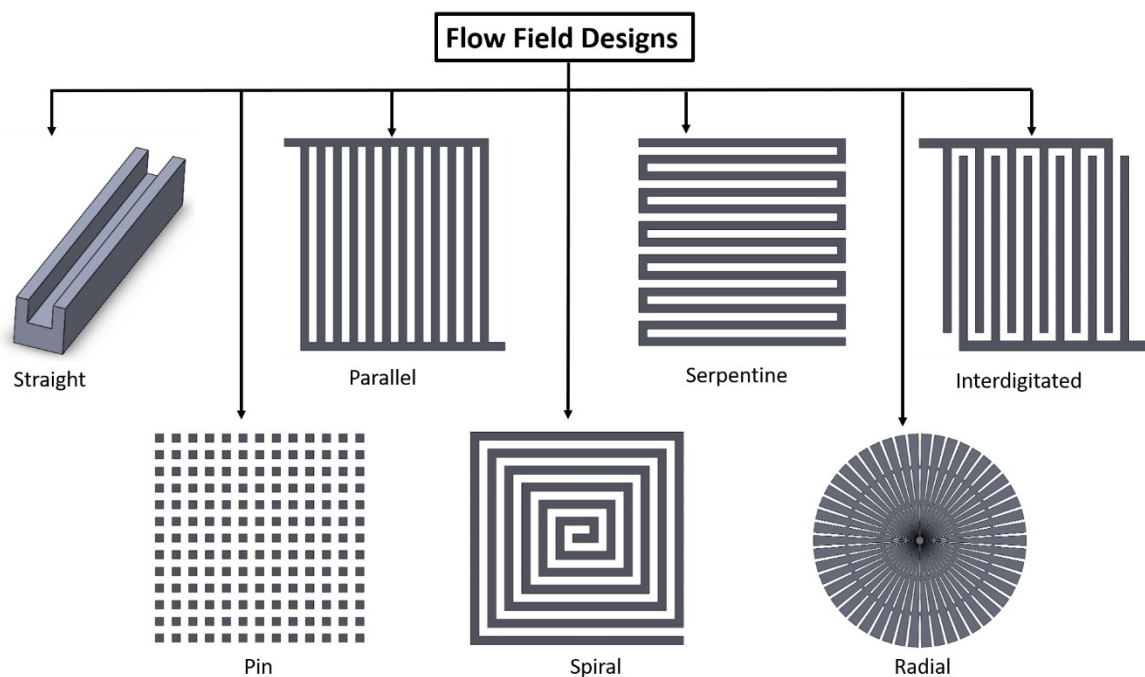
Figure 3. Most popular flow field designs used in the PEMFC.

2.1.1. Design Modifications in Straight Flow Field

By modifying the straight channel, the newest trap shaped flow channel (Figure 4a) was designed.[19] The channel with 8 mm long trap (among 2, 5, 8, 11, 14 mm traps) gave higher current densities and improved O_2 cum water distributions over CL. So, the trap shaped channel produced more power
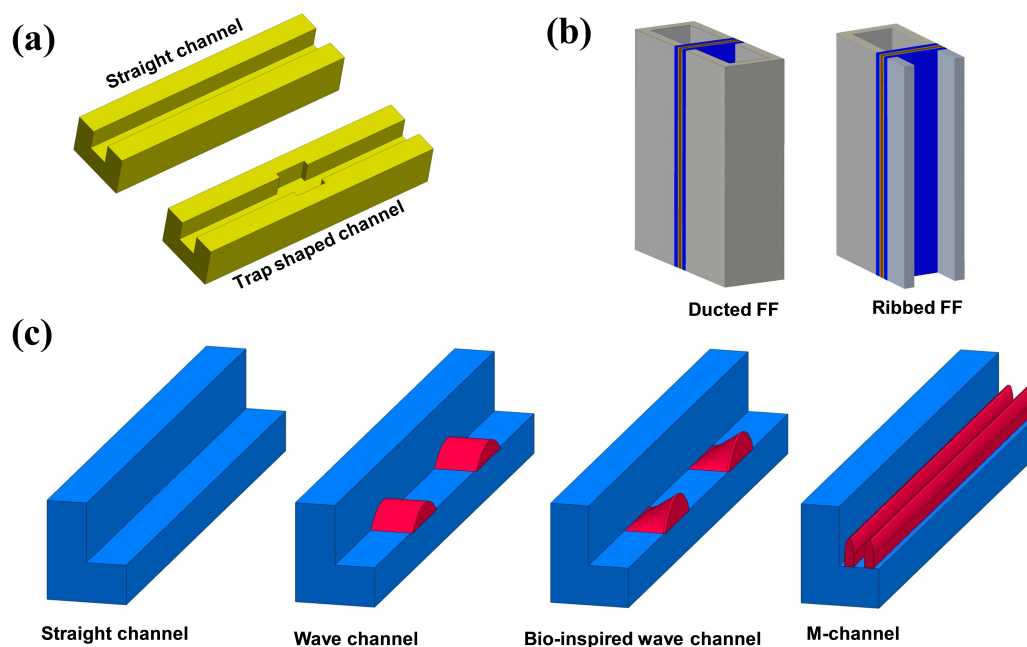

Figure 4. Straight flow field designs (a) Conventional straight channel and Trap shaped channel. Drawn from [19], (b) PEMFC with Ducted and Ribbed channels. Drawn from [20], (c) Cross-sectional views of straight, wave, bio-inspired wave, and M-flow channels. Drawn from [22, 23].

than the conventional straight channel. The cathode side channel is opened to atmosphere for breathing of air directly in Air Breathing Fuel Cell (ABFC) or Air Breathing-PEMFC (AB-PEMFC). This open channeled (or Ribbed) flow field and the conventional close channeled (or ducted) flow field as shown in Figure 4b were compared for vertical and horizontal orientations.[20] The ribbed design and vertical orientation of channels gave a better performance due to easy breathing of air and easy removal of water by the gravitational effects on water respectively.

2.1.2. Effects of Blockages in Straight Flow Field

In the wave channels, the wave shapes were formed along the straight channels to provide a uniform temperature distribution, high reactant velocity, an improved convective heat transfer, catalytic electrochemical reactions and power density compared to the straight channels.[21] The design of wave channels were further modified by using bioinspired wave form which was copied from the fins of cuttlefish.[22] The low resistance to reactant flow in the wavy channel improved the

performance compared to straight channel. Compared to the regular wave channel, the bioinspired wave channel reserved the flowing area of the channel with low flow resistance and high efficiency. The optimized wave channel with 3.05×10^{-5} m central amplitude and 3.52 wave cycles gave 2.2% improved power density.

The wave channels were further improved by the M-flow channels which generated lower entropy with same pumping energy and 21.3% high power density.[23] In M-flow channels, the thickness of blockage and height of obstacle increased the reactant flow in the direction of the wall along with higher mass and heat transfer rates. The cross-sectional views of straight, wave, bio-inspired wave and M-flow channels are shown in Figure 4c.

The various rectangular cylinders (N = 1, 3, 5, 7 as shown in Figure 5a) were transversely installed at the axis of flow channel to estimate the optimal parameters of PEMFC.[24] Among the four designs, the channel with five rectangular cylinders (N = 5) gave high performance and nominal pressure drop. Two transverse pin-fins with little hydraulic diameter along the transverse section of cathode channel (Figure 5b)
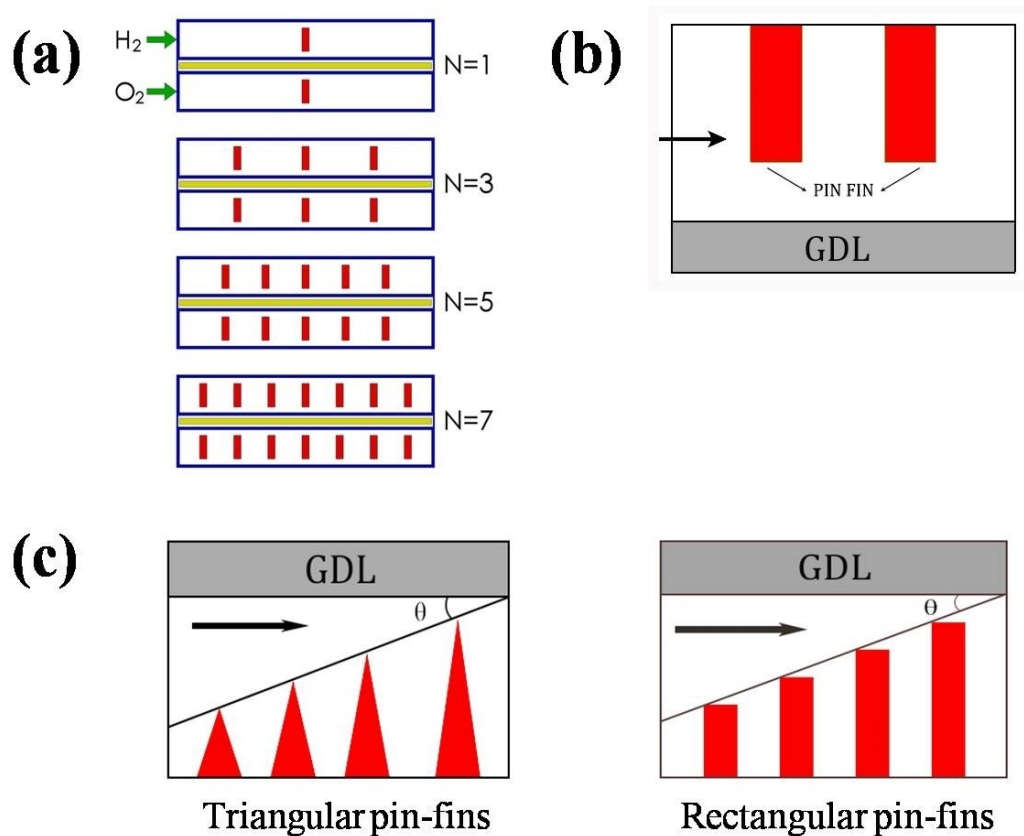

Figure 5. Blockages in straight flow field (a) Rectangular cylinders along the channels. Drawn from [24], (b) Two pin fins along the channel. Drawn from [25], (c) Triangular and Rectangular Pin-fins in channel. Drawn from [27].

were inserted.[25] The friction factor is changing in direct and indirect proportional to the clearance ratio (ratio of flow height below the fin and channel height) and GDL porosity, respectively. Further, increasing of Reynolds number increased the diffusion of gases through GDL. Use of Pin-fins with optimum design parameters increased the cell performance.

Six rectangular shaped obstacles (size: 0.4 mm × 0.8 mm) were placed close to the exit of both anode and cathode channels of 50 mm long.[26] Each obstacle was placed at 5 mm gap from the exit. These obstacles in channel increase the reactant distribution along the channel and GDL, thereby increasing the electrochemical reactions and performance of PEMFC at higher (more than 1.5 A/cm^2) current densities. The triangular and rectangular Pin-fins of different sizes and tilt angles (4°, 6° and 8°) were inserted in the single channel as shown in Figure 5c to improve the reactant distribution over GDL.[27] The increased radial velocity of reactant and the highest mixed flow created near the interfacial area of channel and GDL are developed by Pin-fins. Hence the reactants are forced towards the GDL. Further the reactant distribution over GDL and performance by rectangular fins were higher than triangular. The rectangular fins with 3 mm of both width and height and the H$_2$ velocity of 4.22 m/s were the optimum values.

2.2. Parallel Flow Field (PFF) Design

The PFF is one in which various straight channels are arranged parallel to each other with single/multiple inlet and outlet. This design is simple and easy to manufacture.

2.2.1. PFF with Varying Inlets

Based on the inlet and outlet positions, the PFF are categorized as U-type, Z-type, Multi Z-type (Multipass parallel), Mixed Z and U-type, 2 U-type and 4 U types as shown in Figure 6a. Though the pressure drop of reactants is reduced in PFF than Serpentine Flow Field (SFF), few of the channels are starved of the reactants due to the maldistribution of flow. The maldistribution is caused strongly due to the design parameters such as the header, channel, and rib dimensions. In the U-type, the flow distribution and flow rate are independent. So, the U-type configuration gave better performance than the Z-type at high flow rates. Both multiple U-type and multiple Z-type have a lower non-uniformity flow index, but multiple Z has much more pressure drop.[28,29] Mixed Z and U-type has better flow distribution than conventional PFF. Dividing the flow field into two halves and providing two inlets have reduced non-uniformity flow factor upto 50 %.[30]

The PFF was modified with single and double in/out and varying channel widths of 3 to 1 mm as shown in Figure 6b, where the width of the channel was decreased from entrance to middle and then increased up to exit for even distribution of reactant.[31] The single in/out PFF has equal channel length than double in/out PFF, which resulted in even distribution of reactants. The modified PFF with a single in/out showed high performance than the conventional PFF due to even distribution of reactant. Further the uniform reactant flow and uniform current generation in the modified PFF have reduced the hotspots.[32]

The PEMFCs having planar and ducted flow field designs of ABFC with different cathode open areas and different cell orientations (45° inclined cell with cathode upward/downward, horizontal and vertical) on cathode were analysed and found that the vertical orientation of cathode flow field was the best for both designs, due to better water removal characteristics and higher mass and heat transfer.[33]
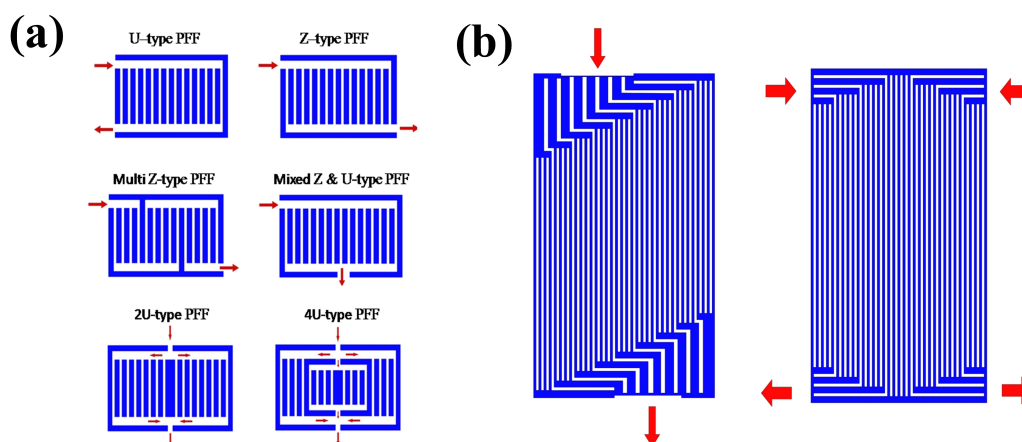

Figure 6. PFF designs (a) Various Z and U type PFFs, (b) Single and double in/out PFFs. Drawn from [31].

2.2.2. PFF with Baffles/Blockages

The baffles are the flow obstructing vanes used for increasing the efficiency of fluid flow systems. The different shapes of baffles/blockages and the use of high porous materials in flow channels instead of plain channels are influencing the performance. The various indentations with Trapezoidal, Semicircular and Square shapes were made along the cathode channel (6 dents at 10 mm distances along 80 mm cathode channel). These indentations increased the amount of reactant at CL and current due to synergy effect provoked by advection and diffusion mechanisms.[34] The variation of the dent height, dent locations (parallel and staggered) and rib sizes have increased upto 25 % of the net power. Further, the Trapezoidal indentation showed better performance than others.

The small rectangular baffles and a plain Nickel foam were introduced in the channels of PFF[35] as shown in Figure 7a. In this design, the Nickel metal foam (80 % porosity) was used as a flow distributing layer with total replacement of the channels and rib on the cathode. The current density and oxygen concentrations were increased by the addition of baffle plates and metal foam. The high porosity of metal foam enhanced the current density. Further, the current density was increased by decreasing the flow channel depth. The power density of porous Nickel foam (90 % porosity and 10^{-8} m^2 permeability) as flow field was higher upto 50 % than PFF and 10 % than SFF and Interdigitated Flow Field (IFF) at medium and higher humidity values.[36]

Instead of the rectangular blockages, the trapezoidal plates (4 Nos., 0.8 mm height and 45° slope angles) were located in parallel and staggered arrangements along the channels of PFF which in turn they named as parallel trapezoid baffle plate flow field (PTBPFF or FF:1) and staggered trapezoid baffle plate flow field (STBPFF or FF:2) respectively as shown in Figure 7b.[37] The cross flow of reactants (the over rib convection) between adjacent channels by staggered arrangement of trapezoidal plates, better water removal rate and lower pressure drop are the advantages of FF:2 than FF:1. This resulted in 2.54 % and 6.39 % higher net power density for FF:2 than FF:1 and PFF, respectively. The baffle plate flow
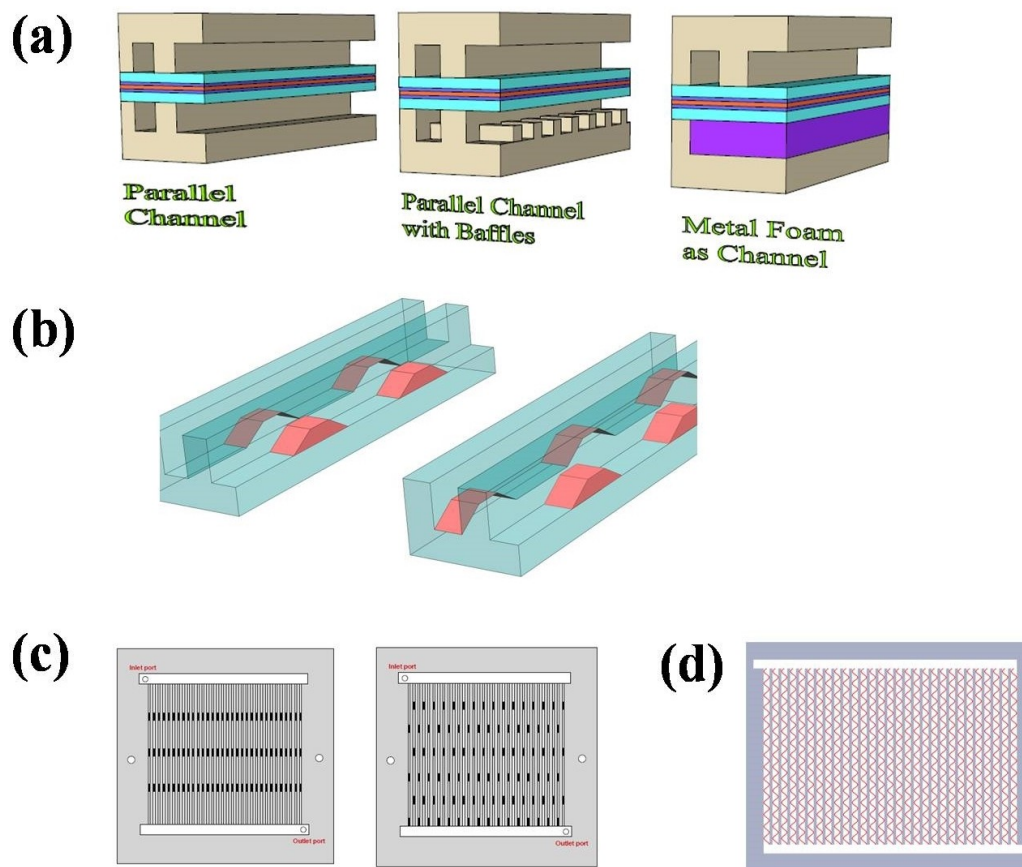

Figure 7. Blockages in PFF (a) Parallel channel, Baffle restricted channel and Metal foam as channel. Drawn from [35], (b) PFF with inline and staggered trapezoidal blockages. Drawn from [37], (c) PFF with inline and staggered rectangular blockages,[39] (d) PFF with wire coil inserts. Drawn from [42].

fields commonly result in larger flow resistance and pressure drop compared with the conventional PFF. The Eq. (4) shows the net power calculation of the PEMFC system.

$$\text{Net power } W_{NP} = W_{GP} - W_{PP}, \tag{4}$$

where W_{GP} is the gross power, W_{PP} is the pumping power.

For better water management, the first attempt to apply the carbon foams in channels of PEMFC was carried out.[38] So, the carbon foams (80 & 100 PPI pore sizes and 3% porosity) were inserted along two parallel micro channels. Here the carbon foam was selected than carbon cloth/paper, due to its high mechanical strength. Self-regulation of water content and very low flow maldistribution are the advantages, whereas the very high-pressure drop of reactants is the disadvantage of porous inserted channels compared to hollow channels.

The two PFF with inline and staggered blockages (3 blockages of rectangular shape in each channel) (Figure 7c) were analyzed.[39,40] These blockages induced the reactant velocity in the direction of GDL, thereby increasing the amount of reactant at CL, reaction rate and performance. Even though the pressure drop due to staggered blockages was high (160%) compared to conventional PFF, the additional pumping energy needed was very less. The parallel channel with staggered blockage gave the higher performance of 28% and 18% than the parallel channels without blockages and with inline blockages respectively due to both over rib and over block convections. The effect of wave gas channel (GC) on PFF, SFF and IFF were analyzed.[41] It was found that the wave GC on PFF improved the gas transport into GDL and performance, whereas the effect of wave GC on SFF and IFF was weakened by sub rib convection.

The wire coils (0.9 mm diameter, 1.3 mm pitch, Silver material, 28 coils) were inserted inside the cathode flow channels of PFF as shown in Figure 7d.[42] It has produced 41% more power density than the channel without coil due to the generation of circumferential flow of reactant near GDL, thereby forcing the reactants towards GDL and increasing the electrochemical reactions. The effect of inserting small cylindrical shaped obstacles (Each of 0.8 mm diameter in 9 rows with zigzag manner) inside the input header of PFF (having 32 channels) was analyzed.[43] These obstacles have reduced the maldistribution factor (MF) upto 3.8, thereby maintaining almost equal mass flow rates in all the channels.

2.2.3. PFF with Sub Channels and Microgrooves

The addition of sub channels, transition areas, micro distributors, and grooves in PFF is also affecting the performance of PFF. The SFR (Sub-channel Flow Rate) is the quantity of air from the sub channel entry as a percentage of the entire flow

rate in cathode. The performance of PFF with SFR and SIP (Sub-channel Inlet Position) on cathode (Figure 8a) was investigated.[44] The SFR with 70% and SIP at 30% (both among 30%, 50%, and 70% values) along the length of the main channel inlet had minimized 70% of water vapour which was used for humidification. The PFF with optimum SFR and SIP values gave a better performance and water removal than the conventional design at high current densities.

The effect of micro distributor of 0.2×0.2 mm^2 sectional area at the inlet of each channel on PFF was tested.[45] This modified PFF (Figure 8b) gave 22.8% higher performance than the conventional PFF and it showed a comparable output performance with the SFF. Further, the performance was increased by decreasing the size of the micro distributor. The reduction of uneven supply of O_2 in the interfacial area of GDL and CL can be achieved by the increased pressure drop between the main in and out channels.

The channel with microgrooves on rib walls and top of channels (Figure 8c) were designed.[46] The microgrooves (width and depth in mm of 0.2×0.2 and 0.3×0.2 with 20°, 30° and 45° inclinations along the flow direction) were made in two lateral sides and top of channel. Due to shear forces and capillarity of air flow, the water was taken away from GDL-Landing interfacial area along microgrooves to channel and 3.2% of power output was increased at 8 m/s air velocity. The Laser Induced Fluorescence method (LIF) was used to measure the water characteristics in the microgrooves. Further, 20° inclination of microgrooves showed better water removal characteristics.[47]

A novel 3D cathode flow field with Porous bottom landings, main channels, sub-channels, and transition areas was investigated.[48] The performance of the 3D flow fields was much better than the conventional PFF. Further, the species transport was better in this new flow field. Porous bottom landings increased the gas transfer to GDL/CL from the channel with minimum pressure drop, thereby improving the performance. The PFF with four main channels were cut with additional sub channels, inclinations, and transition areas for mixing and redistribution of reactant. This 4×3 structure of 3D flow field with 4 channels, 3 segments in each channel and height reduction in the linear axis is shown in Figure 8d.[49] This modified 3D flow field increased the Effective Mass Transfer Coefficient (EMTC) and cell performance compared to PFF.

2.2.4. PFF with Novel Designs

In PFF with conventional arrangement of inlet, the distribution of reactants is not uniform in all channels. To solve this issue and for the uniform supply of gases to all channels, the funnel shaped in/out was introduced on 225 cm^2 PEMFC.[50] Further the straight channels were bent to form a Zigzag PFF
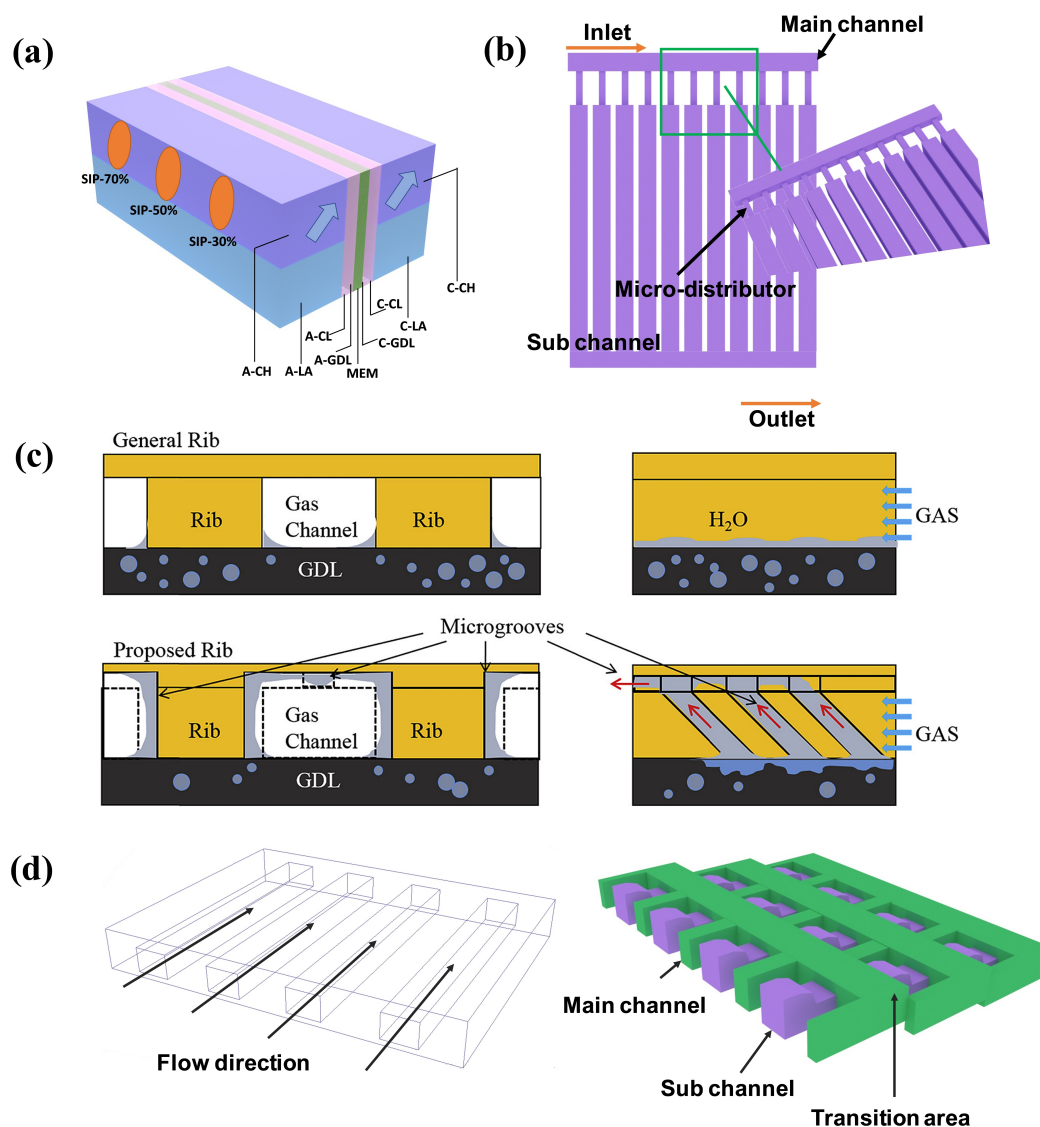
Figure 8. (a) PFF with sub channel. Drawn from [44], (b) Modified PFF with micro Distributors. Drawn from [45], (c) Channels with and without microgrooves,[46] (d) PFF and 3D flow field with 4×3 structure. Drawn from [49].

with single funnelled in/out. The current and power densities of zigzag PFF with single funnelled in/out are much more than the straight PFF with single funnelled in/out due to improved consumption of reactants, optimum distribution of water in the electrolyte and better removal of excess water from the cathode channels.

When the channel count is exceeding 13 in PFF with single inlet (with 500 ml/min flow rate), the uniform flow of reactants was disturbed. To improve the uniform supply of gases to all channels of zigzag PFF with larger active areas, the double funnelled inlet were introduced on 100 cm² PEMFC.[51] This zigzag PFF with funnelled in/out is also termed as sinuous flow field. The funnelled inlet and outlet

made the uniform distribution of reactants to all channels at entry and effective removal of generated water at exit of flow field. The sinuous FF has increased the power density by 7.7% than SFF. The various modifications in PFF with funnelled in/out are shown in Figure 9a.

In case of large sized PEMFC, the separate cooling flow channels are provided in bipolar plates. A new zigzag wavy cooling flow channel having the cooling plate with a pitch length of 4 mm and a channel width of 2 mm (Figure 9b) were analysed.[52] The performance of the zigzag channels was higher and about 23%, 5%, and 8% reductions were detected, in surface temperature difference, maximum surface temperatures, and uniformity indices respectively, compared to
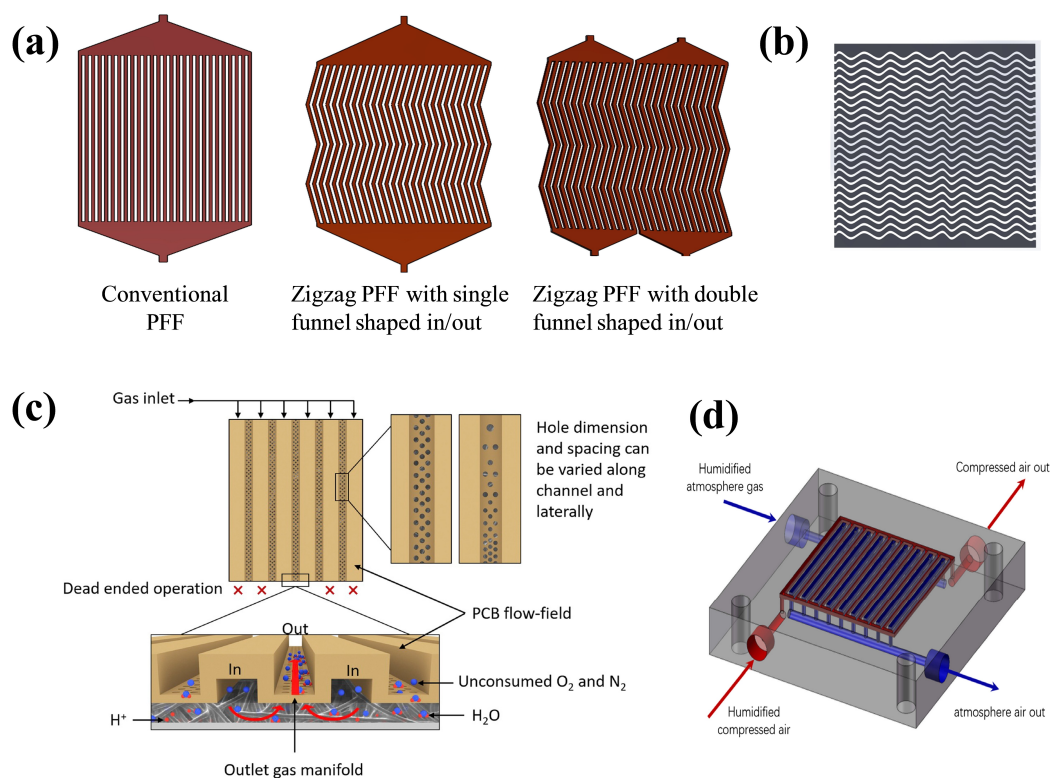
Figure 9. (a) Conventional PFF with single funnel shaped in/out, Zigzag PFF with single funnel shaped in/out and Zigzag PFF with double funnel shaped in/out. Drawn from [50,51], (b) Zigzag flow channel. Drawn from [52], (c) Novel flow field-TPA,[54] (d) Novel PFF having two sets of parallel channels.[55]

the straight channel. The thermal performance of PEMFC was improved with zigzag cooling flow channel.

The PFF and sinusoidal flow field (channels are same as zigzag flow channels) were compared.[53] Even though the pressure drop of sinusoidal flow field was 6 times more than PFF with more power consumption, this was helpful in the removal of water at higher current densities. Further, the performance of the sinusoidal flow field was better at concentration loss region, due to uniform reactant distribution and better water management.

A novel flow field-Through-Plane Array (TPA) (Figure 9c) was designed which had the advantages of high performance at high current density and low back pressure than PFF and SFF.[54] A construction of Printed Circuit Board (PCB) fuel cell was used without the need of end plates. In TPA design, the small holes of diameter less than 0.01 mm were incorporated on the landing areas of the PFF using laser beam. By forcing the oxygen to go into GDL in order to exit, the gas was exposed to under rib areas. This enhanced the easy removal of water and improved the performance.

A novel PFF (Figure 9d) was designed to have two sets of parallel channels which were run at different operating pressure.[55] The controlling pressure gradient in between the nearby channels, was obtained in this novel FF which

increased the reactant concentrations and water removal under the rib at cathode.

2.3. Serpentine Flow Field (SFF) Design

The serpentine flow field (SFF) is one in which the flow path is continuous from inlet to outlet and the channel arrangement resembles the form or movement of a serpent/snake. The pressure drop of reactants is increased in SFF than PFF. As SFF is efficient in distributing the reactant throughout the active area of PEMFC, this is majorly used in PEMFC. The SFF gave a better performance than the straight FF.[56]

2.3.1. Effects of Multi-passes in SFF

In general, SFF has a single channel path from inlet to outlet. The arrangement of two or more paths parallel to the first serpentine path is known as a multi path SFF (MPSFF or FF : 3). The single pass SFF (1-SFF), two pass SFF (2-SFF), cyclic 1-SFF and symmetric 1-SFF (Figure 10a) were analysed.[57] In Cyclic 1-SFF and Symmetric 1-SFF, the total length of single serpentine path of 1-SFF was split with five segments with separate in/out and varying flow directions. The performance of 2-SFF was higher at higher humidity than
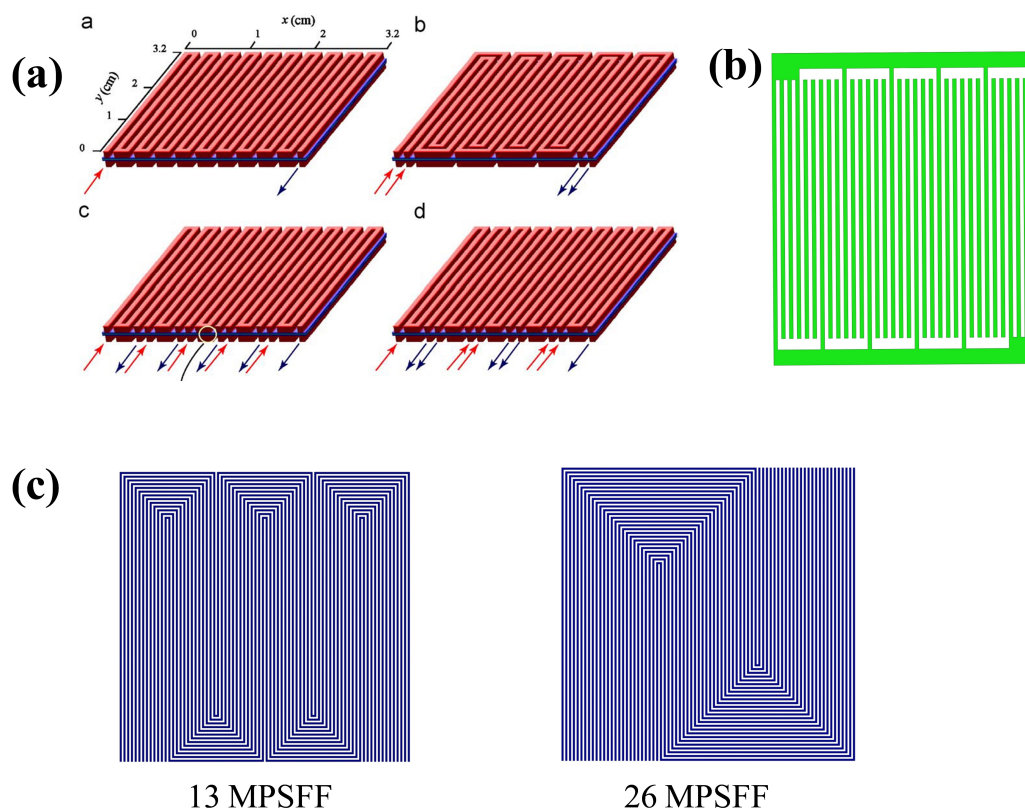
Figure 10. MPSFF (a) 1-SFF, 2-SFF, Cyclic 1-SFF and Symmetric 1-SFF,[57] (b) Triple mixed SFF. Drawn from [62], (c) 13 and 26 MPSFF. Drawn from [66].

other three designs, whereas the cyclic 1-SFF and symmetric 1-SFF produced lower pressure drop and higher performance at lower humidity.

From the comparison of 2, 3 and 4 pass SFF of same rib and channel size, it was found that the performance of 3 pass SFF was better compared to others.[58] Similarly from the comparison of 3, 6 and 9 pass SFF, it was found that the performance of 6 pass SFF was better compared to others.[59] The performance of 4-SFF and 1-SFF with parallel, counter and cross flows were investigated.[60] Compared to cross and counter flows, the parallel flow increased the performance of 4-SFF and 1-SFF at low and high voltages, respectively. However, the performance of 4-SFF was better than 1-SFF, when working under the same operating conditions.

The 3-SFF was analysed for evaluating the reactant humidification, water control and performance.[61] It was found that the humidity in the reactant gases was the major factor for increasing the cell performance. When the anode side humidity was increased, then the mass transfer of hydrogen, the chemical reaction and cell performance were increased in the triple-SFF. The FF:3 with common in/out header for each set flow channels is known as parallel-in-series (PIS) design. In this way, the 3-SFF with common mixed inlet

path, called Triple mixed SFF (Figure 10b) was analysed for High Temperature PEMFC (HTPEMFC) at various operating conditions.[62] Due to high proton conductivity and quick reaction kinetics, the performance of the fuel cell was improved with increase in temperature.

Due to higher flow velocity of reactants, the water management and performance of 3PIS and 5PIS designs were higher than FF:3.[63] The FF:3 with the effect of parameters like the channel width (w) and height (h), channel length (L), the numbers of parallel channels (n), the rib between two adjacent channels (d) and serpentine channel turns (s) were studied.[64] It was found that the most excellent possible SFF configuration for the running condition with geometrical specifications as 1, 1, 0.4, 249, 5, 4 for w, d, h, L, n, and s, respectively.

While comparing the PFF (17 channels), 1-SFF and 7-SFF, there was a considerable balance among the flow distribution and pressure drop in 7-SFF with robust operation of PEMFC.[65] The PEMFC with 3, 6, 13, 26 and symmetric 26 channelled MPSFF or FF:3 was analysed to find the effects of channel path length and more number of passes.[66] The shorter path length gave uniform current distributions and less condensed water and flooding, compared to the longer path

length. The 13-channel was better than 26-channel (Figure 10c), because of the differences in membrane hydration. Generally, the 90° bends are made on the channels of SFF. The single, double and triple SFF configurations namely 1-S, 2-S and 3-S respectively, having curved bends were studied.[67] When operated below 0.7 V only, the performance of the cell increased by decreasing the number of flow channel passes. This estimated the 1-S gave superior performance than the 2-S and 3-S.

2.3.2. Redesign of Serpentine Flow Path

2.3.2.1. SBFF

To enhance the under rib convection, the three pass serpentine flow field was redesigned with dead end which was named as a serpentine-baffle flow field (SBFF or FF:4).[68] The FF:4 design (Figure 11a) showed a higher performance than SFF at low cell voltages, whereas the same performance was obtained in both designs at high cell voltages. The baffles in SFF induced the higher-pressure differences between adjacent channels over the entire active area, thereby increasing the under-rib convection, mass transport, limiting current density and cell performance.

A Parallel Serpentine-Baffle Flow Field Plate (PSBFFP or FF:5) which was the modification of the FF:4 for improving the water management was proposed.[69] Refer Figure 11b–11c. The FF:5 design had the advantages of both Parallel Serpentine Flow Field Plate (PSFFP or FF:6) and IFF Plate. The FF:5 channels are the best suited for the operating temperature more than 100 °C because it avoids water loss from the flow channels. The FF:5 which is the FF:6 along with interdigitated features on anode side of DE-PEMFC was analysed.[70] The discontinuous path of channels in FF:5 improved the heat transfer between reagent and plate, thus increased the reactions and the performance.

2.3.2.2. CESFF

The continuous path of SFF is redesigned to enhance its performance. The under-rib convection is an important factor which is affecting the flow and distribution of reactants, water removal and performance of PEMFC. A Convection-Enhanced Serpentine Flow Field (CESFF or FF:7) as shown in Figure 11d for DMFC was analyzed.[71] In FF:7, the first and third paths carry the reactant from top to bottom of flow field, whereas the second and fourth paths carry reactants from bottom to top. Due to the large pressure difference between the nearby flow channels induced by FF:7, the mass flow rate of reactants to and from the CL has increased along with better water management. The under-rib convection in FF:7 removes the water from the active area by raising the local

pressure variation between adjacent pairs of channels. The FF:7 gave better performance than the conventional SFF.

Five different FF:7 designs are analysed and compared with SFF to enhance the under rib mass transport of SFF.[72] The CESFF or FF:7 are designated by its name followed by the number of paths and design number as CESFF 3-1, 3-2, 4-1, 4-2, and 4-3. The CESFF 4-3 configuration (Figure 11e) gave 22.6% increase in power when compared to the SFF. A cascade type of SFF (Figure 11f) with different channel widths of 0.8 mm, 1 mm, 1.2 mm, and 2.2 mm was designed.[73] The membrane flooding and drying problems are affecting the life of Membrane Electrode Assembly (MEA). The channel width, channel depth and rib width of 1.2 mm, 0.8 mm and 0.8 mm respectively, confirmed the best performance with uniform current density and better water management in cascade FF.

A Compensated SFF (Figure 11g) with 5 channels, 6 turns to have GDL area and electrode area of 49 cm^2 and 46 cm^2 respectively was proposed by the modification of SFF for HT-PEMFC.[74] The compensated SFF gave 27% higher current density at 0.57 V than SFF, due to more even distribution of current over the electrode area. A CDMD (Current density measurement device) was fabricated and used for current distribution. The simple design and low cost are the main features of CDMD compared to other devices.

2.3.2.3. MSFF

Nine different Modified Serpentine Flow Fields (MSFF or FF:8) were analysed based on number segments and channels.[75] The MSFF-1-7 and MSFF-3-7 (Figure 12a–12b) gave a better performance than PFF. The increased channel path number and the secondary flow in the channel (due to the serpentine path turn and the reactant transportation under the landing) have improved the performance of the MSFF-3-7 than parallel type.

2.3.2.4. ECSSFF

With the aim of reducing the pressure drop of reactants and parasitic losses of three pass SFF, the Enhanced Cross flow Split Serpentine Flow Field (ECSSFF or FF:9) was designed.[76] This FF:9 has three different serpentine flow channels arranged individually from a single inlet to reach a common outlet so that the same pressure drop is occurring between the entry and exit of each serpentine channel. This FF:9 was useful in the evacuation of water in U bends. Further, the pressure drop of FF:9 was reduced upto 30 times than Single Serpentine Flow Field (SSFF or FF:10).[77]

The FF:9 (Figure 12c) gave 7.51% of higher power density than Triple Serpentine Flow Field (TSFF or FF:11) due to better water management and less parasitic losses.[78] Further the scaling up studies of FF:9 with active areas of 50,
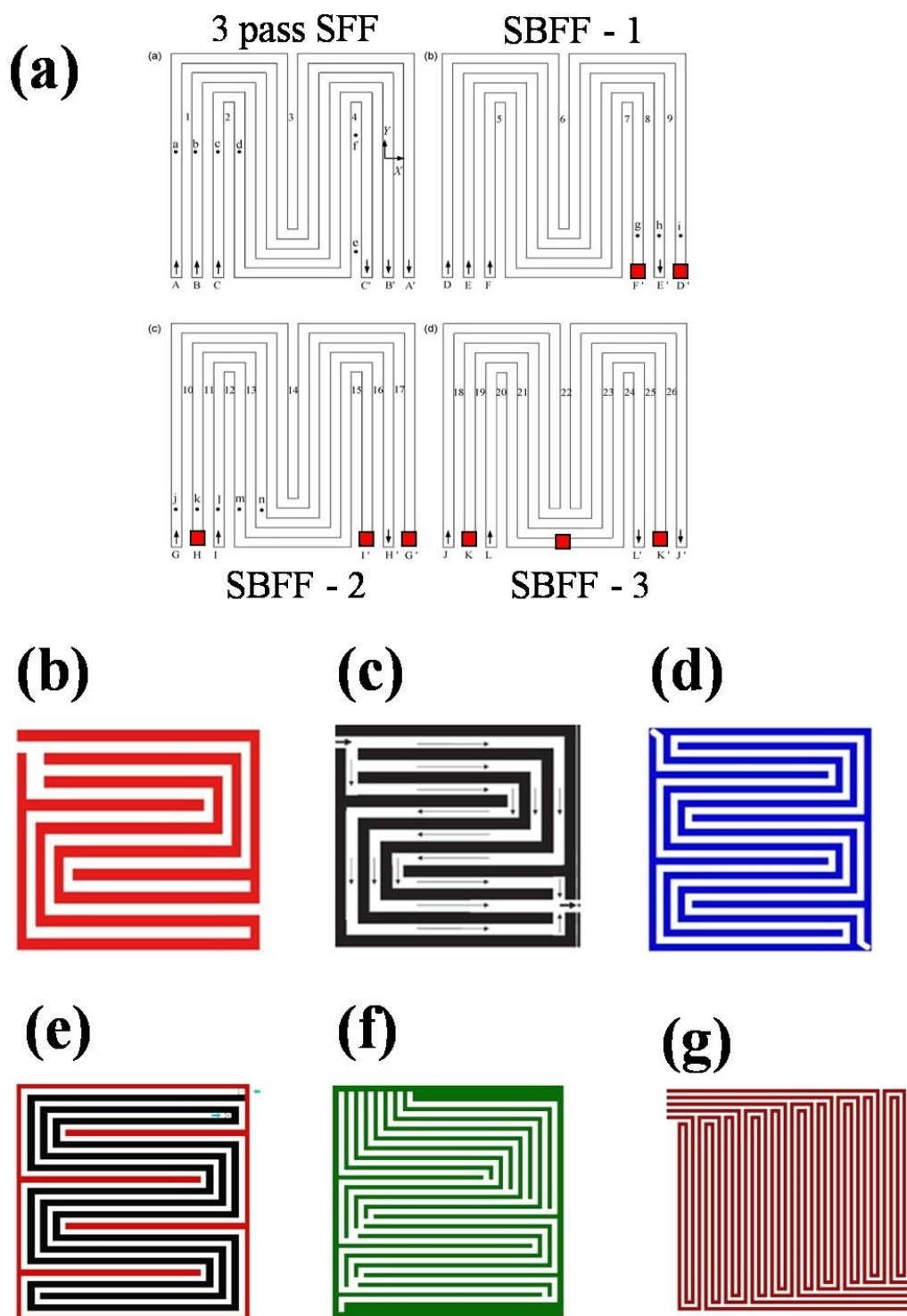
Figure 11. Redesigns of SFF (a) 3-SFF, SBFF-1, SBFF-2, SBFF-3,[68] (b) PSFFP. Drawn from [69] (c) PSBFFP. Drawn from [69], (d) CESFF. Drawn from [71], (e) CESFF 4-3 FF. Drawn from [72], (f) Cascade FF. Drawn from [73], (g) Compensated SFF. Drawn from [74].
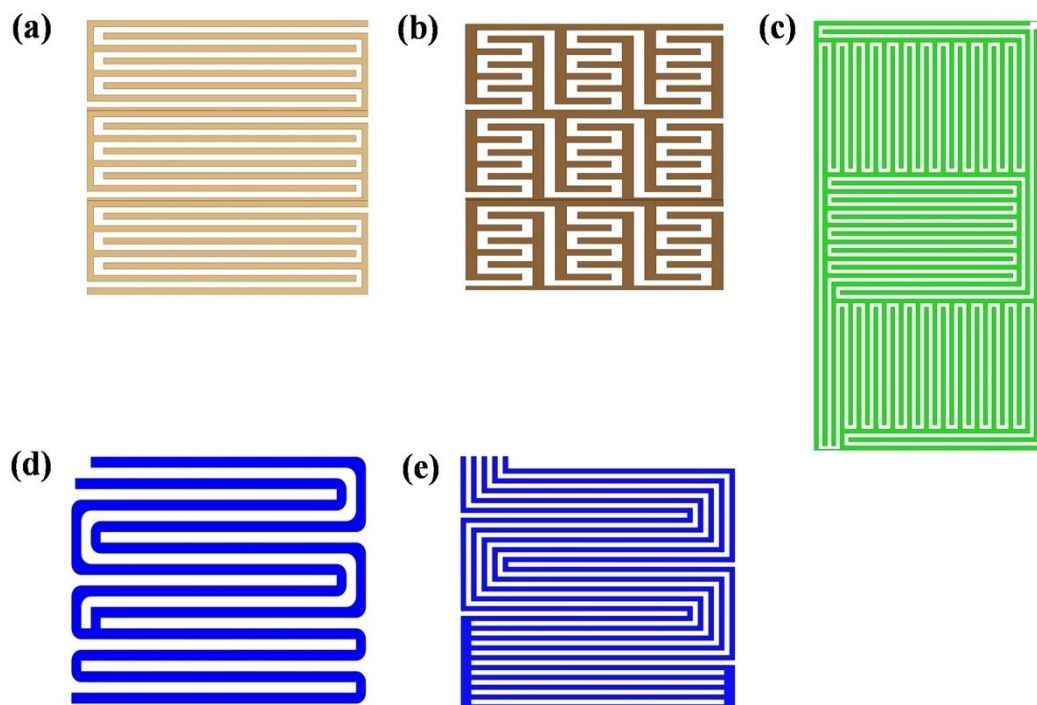
Figure 12. SFF designs (a) MSFF-1-7 (b) MSFF-3-7. Drawn from [75], (c) ECSSFF Drawn from [78], (d) 2 to 1 SFF. Drawn from [80], (e) Compound FF. Drawn from [81].

100, 150, 200 cm² were analysed.[79] While increasing the size of the active area from low to high, the power was increased 4.5 to 13.5% in FF:9 compared to FF:11.

The performance of Single Variable section Serpentine Flow Field (SVSFF or FF:12), Single Serpentine Flow Field (FF:10) and 2-1 SFF on cathode at cold start conditions were investigated.[80] In 2-1 SFF, two serpentine channels were combined into one channel at the mid of active area. The 3-SFF engraved on the PCB was used on anode side. The FF:12 showed better cold start performance below −5°C with higher pressure drop and lower outstanding water in the flow field. The 2-1 SFF (Figure 12d) showed the better performance at cold start above −5°C due to the most uniformity of current density.

The compound FF was designed which was the mixture of 5 pass SFF and PFF (Figure 12e).[81] Even though the performance of compound FF and SFF were approximately similar, the prevention of water flooding by compound FF was better than SFF.

2.3.3. SFF with Zigzag and Wavy Designs

A novel modified SFF called W flow field (Figure 13a) was developed and compared with seven Z and W types of flow fields.[82] As this novel design covered the maximum active surface and produced the uniform current, the performance was superior to other designs. The straight channel of SFF was bent to form a zigzag channel which was named as a Zigzag SFF as shown in Figure 13b. The straight zigzag channel showed better water removal and high performance with a minimum drop in the pressure when compared to the other three types namely PFF, Zigzag PFF and straight SFF.

Three sinusoidal wavy serpentine flow channels (Figure 13c) having the same wave length of 6.28 mm and three different amplitudes of 0.25 mm (C1), 0.5 mm (C2) and 0.75 mm (C3) were compared with the conventional serpentine channel (C4) for different cell temperature and H_2 flow rates.[83] The C1 showed higher results up to 20.15% than the base model (C4). At all flow rates, the C1 exhibited good performance than C2, C3 and C4. Further, the increase in reactant flow rates, have increased the diffusion and power.

The novel three pass Waved Serpentine Flow Fields (WSFF or FF:13) with bend radius of 0.5 mm and three different slope angles (Figure 13d) on channels were developed and compared with SFF of zero slope angle.[84] The wave channels affect the flow velocity, flow direction and pressure which cause the secondary and cross overflows thereby increasing the mass transfer in GDL and CL. Hence, the O_2 transport through GDL and the water management were better in FF:13 with 17.5% rise in power density than the
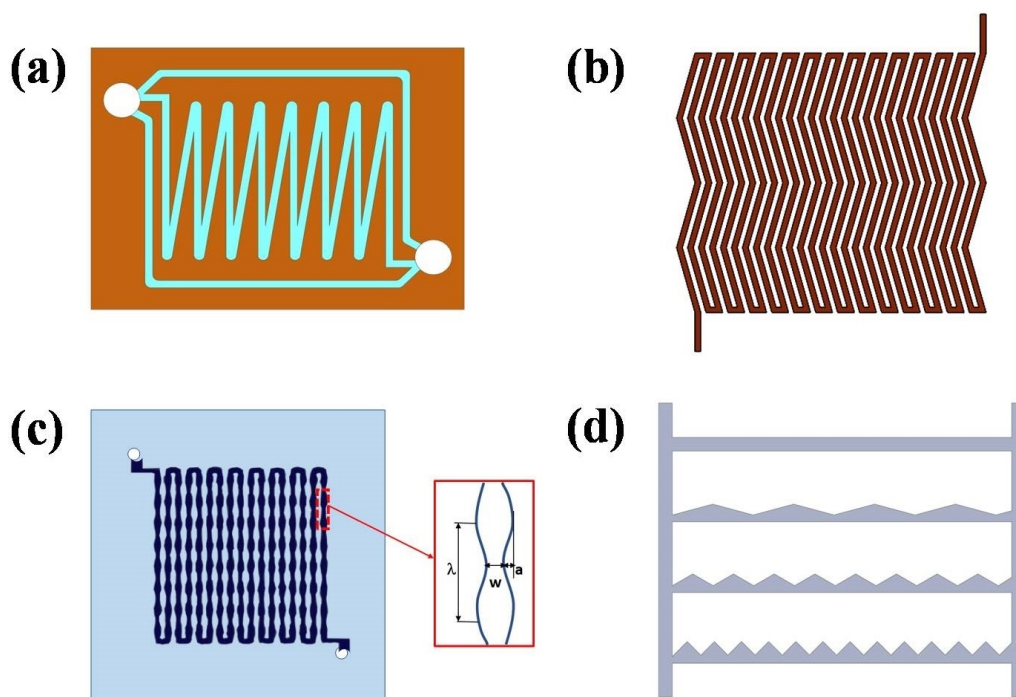
Figure 13. (a) Novel modified Serpentine-W flow field. Drawn from [81], (b) Zigzag SFF. Drawn from [82], (c) Wavy shape serpentine channel (a – amplitude). Drawn from [83], (d) Straight and waved flow channels of WSFF. Drawn from [84].

SFF (slope angle is zero). Further, the lower pressure drops over the entire current density range and better water removal are the important characterises of FF:13 over SFF.

2.3.4. SFF with Varying Channel Width/Height and Subchannels

The effects of changing the length and height of the serpentine channel (Figure 14a) was analyzed.[85] With the length reduction ratio of 0.3 and height reduction ratio of 0.4, the gas velocities, water removal and cell performance were increased. The effect of varying the channel width was analysed by designing four convergent serpentine flow slabs (TS28, TS36, TS44, TS52) and compared with One common-type (OS) design (Figure 14b).[86] Because of the proper mixing of fuels, the TS36 gave 1.35 times higher current density than OS.

The SFF of 5 passes and 4 turns without and with subchannels at landings (Figure 14c) were investigated.[87] Due to the easy removal of water, less power drop and uniform current density, the power output of the SFF having sub-channels was higher than the conventional SFF.

2.3.5. Effects of Orientations of Serpentine Channel

The different horizontal configurations (V–H–D, V–H–U, V–V–D, V–V–U) and vertical configurations (H–H–U,

H–H–D) of single SFF on two-phase flow were investigated to find the effects of orientations with different inlet/outlet.[88] The horizontally located channels along with upper side inlet manifolds showed the lowest pressure drop cum parasitic losses, easy water removal and higher performance. The serpentine multi-pass channels with horizontal and vertical orientations were investigated and found that the cell with horizontal orientation gave better performance (voltage gain of 20–35 mV at 10 A), superior membrane hydration and lower liquid blockages than the vertical orientation.[89]

2.3.6. Effects of Insert Technology in SFF

To enhance the performance of SFF with better water management, a specially made porous carbon inserts (PCI) were inserted along the cathode ribs[90,91] in uniform and staggered arrangements (Figure 15a,b). The PCI are made of Vulcan carbon. The water between the interfacial area of GDL and the rib was absorbed by the PCI and delivered through the lateral sides into the channel. Due to the globalized water absorption throughout the active area by PCI and better water management, the staggered arrangements of PCI along the rib of the cathode flow field increased the performance up to 11.56% compared to SFF. Further, the scaling up studies on PCI accommodated PEMFC[92] with three active areas 25, 36 and 70 cm^2 showed that the 36 cm^2 was the optimum active
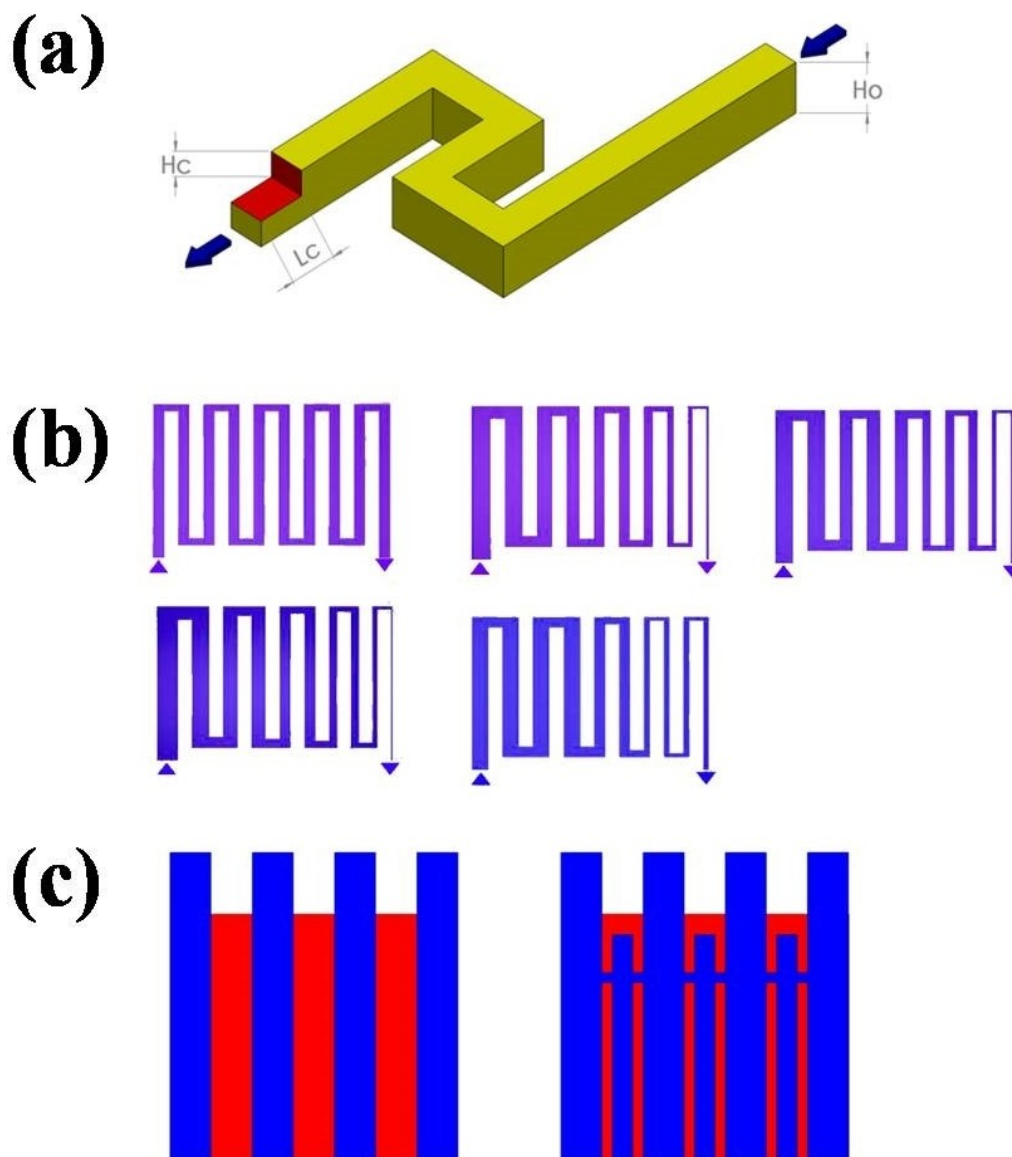
Figure 14. (a) SFF with outlet channel contraction. Drawn from [85], (b) Convergent serpentine flow slab. Drawn from [86], (c) SFF without and with sub channels. Drawn from [87].

area which produced higher power density than 25 and 70 cm^2.

To enhance the performance of SFF with better water management further, a specially made porous sponge inserts (PSI) were inserted along the cathode ribs in uniform and staggered arrangements. The PCI made of phenolic foam were inserted in uniform and staggered arrangements. The two flow fields namely Modified Serpentine flow field with Inline arrangement of porous inserts (MSI) and Modified Serpentine flow field with Staggered arrangement of porous inserts (MSS) with Porous Sponge Inserts were analysed.[93] Because of good

water absorption feature of PSI than PCI, the MSS with PSI yielded good performance than the MSI (Figure 15c).

When the nickel foams of 0.95 porosity, 110 PPI and different thicknesses (1 to 3 mm) were used to replace the cathode SFF, and keeping SFF on anode side, the performance was increased upto 6% and the internal impedance was reduced than graphite SFF.[94] Here the performance was analysed by Electrochemical Impedance and Electrochemical active surface area (EASA).
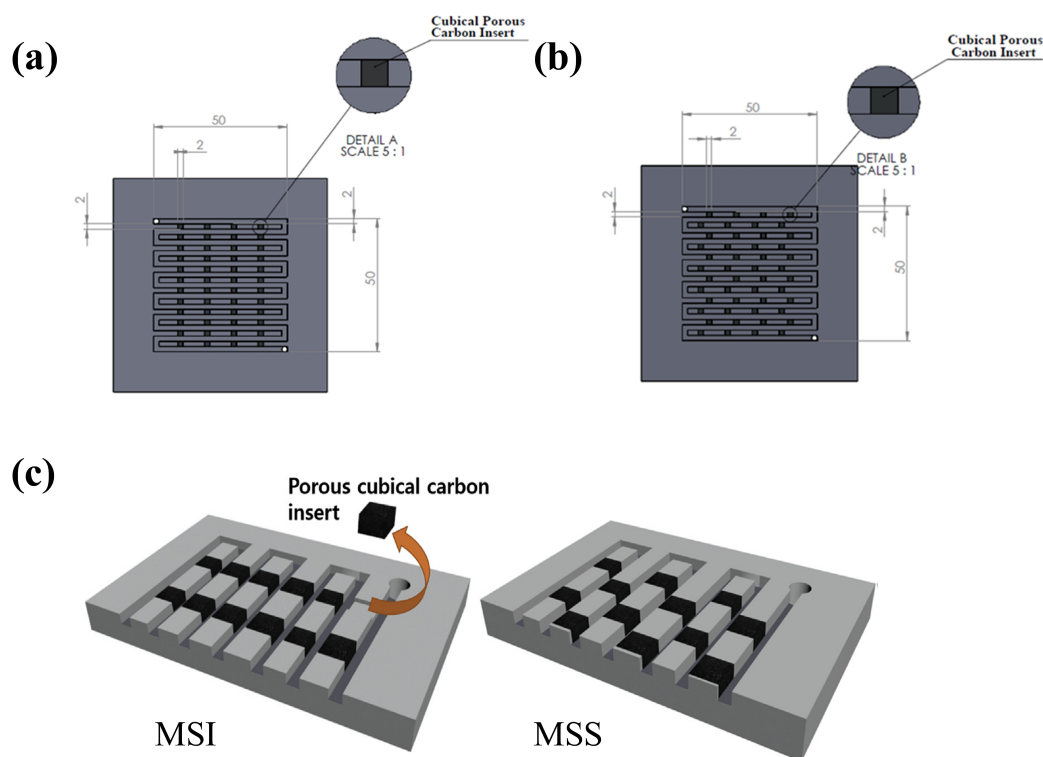
Figure 15. (a) Uniform pin type flow field with porous inserts, (b) Zigzag pin type flow field with porous inserts, (c) MSI and MSS.[93]

2.3.7. SFF with DEA

Sometimes the anodic flooding occurs in PEMFC, due to the back diffusion of water from cathode which causes voltage drop.[95] So periodic purging is necessary to avoid this. The H_2 pulsation is majorly affecting the performance of DEA-PEMFCs for portable applications.[96] The influence of Dead End Anode (DEA) on PFF, IFF and SFF in anode side was analysed. For SFF with anode exit reservoir and IFF without anode exit reservoir, the steady-state operation of PEMFC with DEA can be obtained. But the PFF with DEA was not fitted for PEMFC.[97]

2.4. Interdigitated Flow Field (IFF) Design

The flow field with dead ended channels, called interdigitated flow field (IFF) was proposed by Nguyen.[98] This design changed the diffusion transfer mechanism of the gases to/from CL into forced convection mechanism.[99] As the convection process is faster than diffusion process, the electrochemical reactions at CL of IFF are majorly increased. Further the water trapped inside the electrodes are taken away by the shear force of reactant flow.

2.4.1. Effects of Baffles in IFF

The insertions of baffles are changing the design parameters and performance of IFF. The PFF was modified into the IFF by using baffles at end of the path (Type I) and at the mid path (Type II) as shown in Figure 16a.[100] The blockage of channels increased the reactant flow transportation and cell performance. Further, the use of oxygen instead of air in the cathode side provided better results. A mid-baffle IFF gave 1.3 times more power output than the conventional IFF when air was used as reactant on the cathode.[101] When back pressure was raised from 1 to 2 bar, the power density of the mid-baffle IFF was improved by 24%.

The number of rectangular parallelepipeds of N = 1,3,5,7,8,9 and their different positions in inlet and outlet channels (Figure 16b) on the IFF were investigated.[102] The arrangement of rectangular parallelepipeds on outlet channels with the optimum combination of process parameters on the novel flow field gave 26% more power than the smooth-walled channel. The scaling up and stacking up studies on IFF and SFF with two C:L ratios (1:1, 2:2) showed that the IFF gave higher performance than SFF.[103] When back pressure was varied from 0 to 1.5 bar, the power density was raised by 65% for IFF with C:L ratios (1:1). The scaling up and stacking up
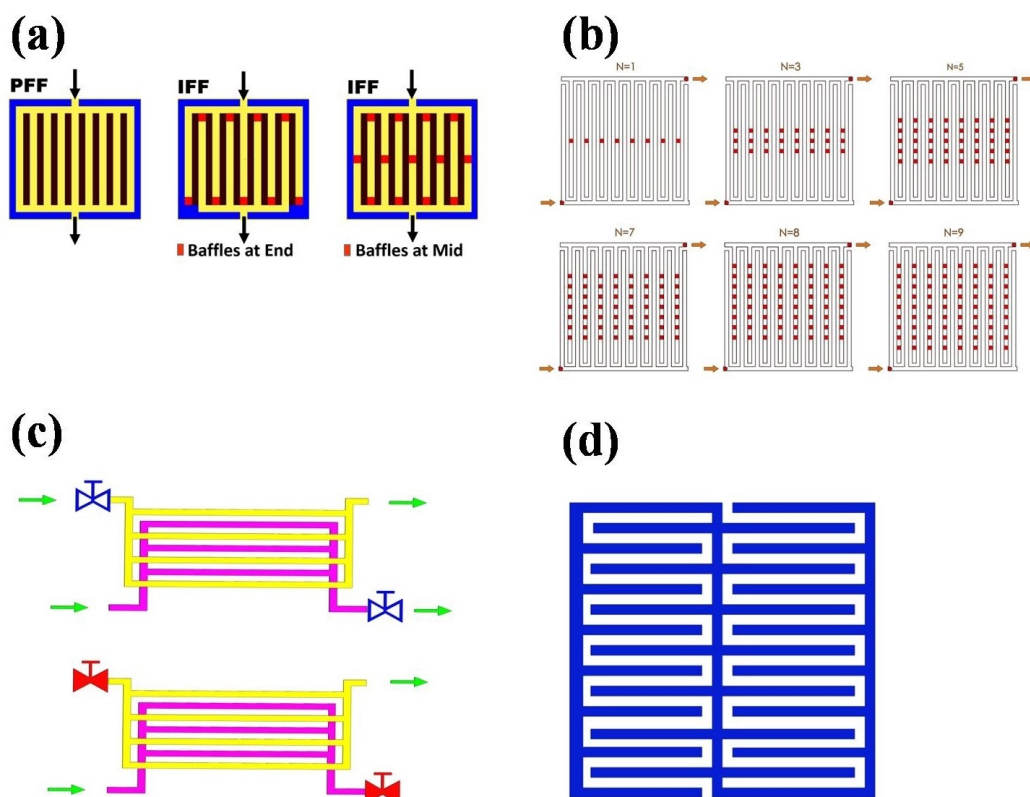
Figure 16. (a) PFF, IFF with baffles at end and IFF with baffles at mid. Drawn from [100], (b) Variations of the rectangular parallelepipeds number in IFF. Drawn from [102], (c) Common design for PFF and IFF. Drawn from [108], (d) Hybrid Serpentine Interdigitated FF (HSI). Drawn from [109].

of PEMFC has decreased the cell performance due to poor water management.

2.4.2. Design Modifications in IFF

The new slotted-IFF for stamped metal bipolar plates with uniform flow distribution and improved cell performance was proposed and optimized.[104] The two slots of each two adjacent channels in new slotted-IFF gave better performance due to uniform flow distributions.[105] The impacts of channel length on IFF was investigated and found that the fuel cell with 5 cm length gave better performance than 25 cm length. Further, there were a maldistribution in the longer cell and homogenous cross flow in the shorter cell.

The mass transport and electrochemical reactions of PEMFC were evaluated.[106] For the conventional straight flow channel, the least amount of current density was found beneath the land area. The current density of the IFF was comparatively higher than the straight flow field. The two pass IFF was analysed at various temperature and C:L values and found that the C:L of 2:1 yielded the maximum power density.[107]

2.4.3. Hybrid Designs in IFF

A novel flow field (Figure 16c) was developed which can be exchanged between PFF and IFF.[108] This FF has two flow paths with separate in/out and set of valves. By opening and closing of valves, the FF can be exchanged as PFF and IFF. The IFF gave higher current density and power at peak current density with low overvoltage.

The novel Hybrid Serpentine Interdigitated (HSI or FF:14) flow fields namely one inlet-one outlet (1-IO) FF:14, two inlets-two outlets (2-IO) FF:14 and one inlet-two outlets (1I-2O) FF:14 were developed and compared with one channel serpentine (1S).[109] The FF:14 flow field has the advantages of both SFF and IFF. At 0.6 V, the 2-IO FF:14 flow field (Figure 16d) showed better cell performance than other 1S and other two FF:14 flow fields due to uniform gas distributions, temperature and current.

2.5. Spiral, Cylindrical, and Radial flow fields

The multiple concentric spirals for the flow field with 1, 2, 3, 4, 6 and 8 concentric spirals channels were investigated.[110] The flow field with 3 and 4 channels (Figure 17a) gave better
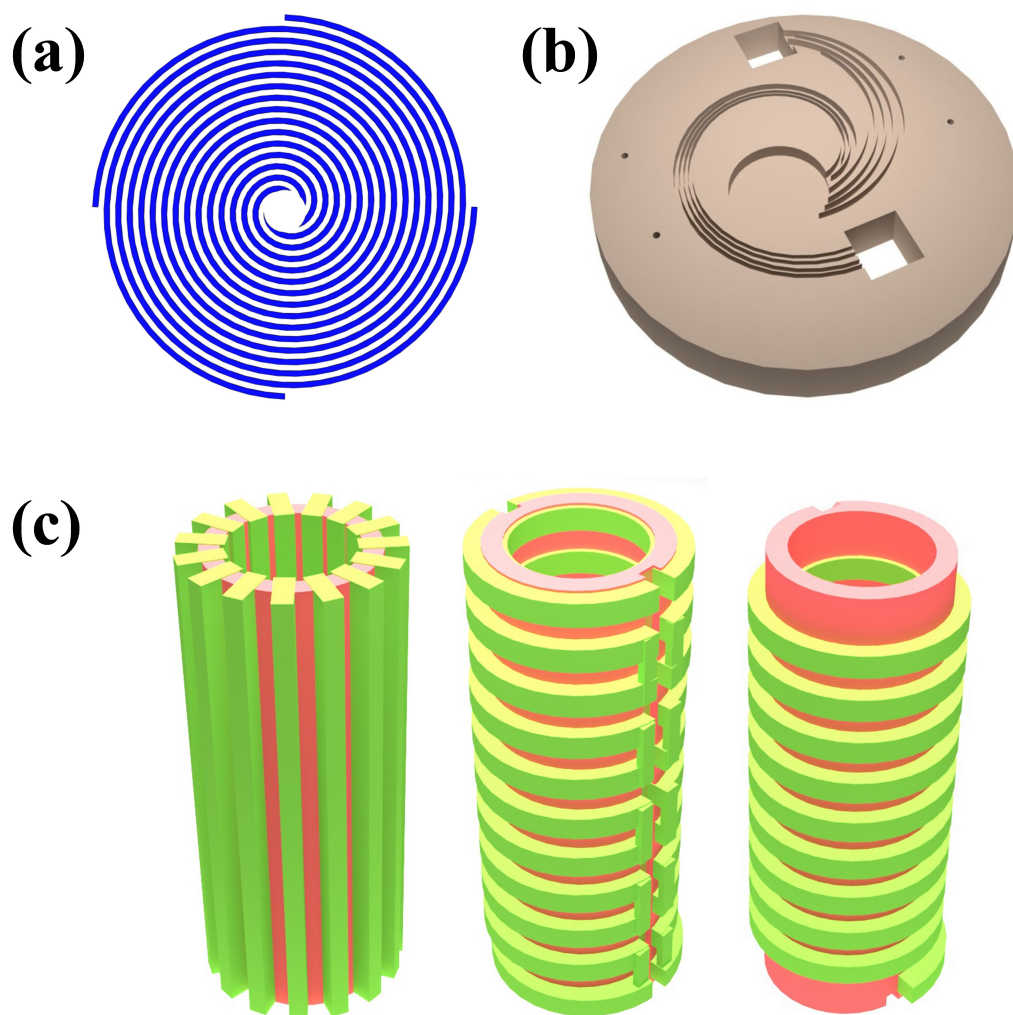
Figure 17. (a) Concentric spiral channels. Drawn from [111], (b) Spiral shaped flow channel. Drawn from [112], (c) Cylindrical designs of PFF, IFF and SFF. Drawn from [113].

performance, whereas the 6 and 8 channels gave the worst performance. Due to better distribution of gases, the 4-channel design was the best one. Five inlet and outlet spiral-shaped flow channels with radius of 28.2 mm (Figure 17b) were investigated.[111] The spiral flow field produced secondary vortices which led to the increased performance than the SFF. With the smaller outlet channel than the inlet channel, there was an improvement of water flooding on CL.

The designs of parallel, serpentine, and interdigitated in a cylindrical configuration (Figure 17c) were analysed.[112] The results showed that the cylindrical or tubular SFF had better performance than others. Because of twist and gradual declination of flow path angle in tubular SFF, there were a low-pressure drop along the channel designs, easy removal of water from GDL and high O_2 concentration at CL. The cylindrical PEMFCs are having high gravimetric and volumet-

ric power density compared to the planar PEMFC. Even though the design of cylindrical PEMFC is simple, its fabrication is complex. The 40% total power density was increased with the optimization of anode flow rate and cathode landing width.[113] An innovative radial flow field with control rings showed a superior flow distribution and water removal, better utilization of active area and lower pressure drop than parallel and serpentine types.[114]

2.6. Natural Inspired Flow Field Design

The flow field designs that are inspired from the nature like veins of plant leaves and human lungs are known as Natural inspired or Bio inspired flow fields. The various types of Natural inspired flow fields like bio-inspired with and without subchannels/obstacles, biomimetic, Ginkgo and Net leaf

designs were developed. The Bio-inspired (BI) flow field (Figure 18a) which was developed from the leaf flow patterns, showed the higher power densities of 26% and 56% at various current densities. when compared to SFF and PFF respectively,[115] due to more uniform flow and velocity distribution.

The impact of the bionic flow field (Figure 18b) using different branching structures through biomimetic analogy theory were investigated.[116] The location and number of branches played a vital role in exit velocity, which had impacts on the discharge of water. Due to secondary channels, more gas consumption ratio, even reactant distribution and low ohmic losses, the bionic flow field had high performance than the conventional flow field. A novel Biomimetic flow field with main, sub and third-level channels of varying width and height was designed based on Murray's Law as shown in Figure 18c.[117] When compared to serpentine and parallel types, the biomimetic flow field yielded higher power, uniform distribution of gases and easy removal of water.

Based on the human lungs and leaf veins of natural network system, the lung and two bio-inspired leaf flow fields were designed (Figure 18d) using Murray's law on DMFC.[118]

While testing the various combinations of flow fields on anode and cathode, the combinations of SFF on anode and second leaf design on cathode showed the highest performance. Further the leaf FF showed higher performance on cathode and the lung FF showed lower performance on both anode and cathode. The lung FF yielded 34% higher power than triple SFF.[119]

Three Bio-inspired IFF (Figure 19a) were designed based on Murray's law and these bio-inspired designs substantially improved the fuel cell performance by 25% compared to the conventional IFF and 5 channeled parallel-in-series designs.[120] The various biologically inspired IFF (Figure 19b) were designed using Murray's law and Pitchfork pattern.[121] The biologically inspired IFF with 9 entry channels had higher current density distributions and lower pressure drops.

The Ginkgo and Net leaf flow fields were analyzed (Figure 19c) and found that the water removal of the Ginkgo FF was better than PFF.[122] Further, the peak power density of Ginkgo FF was 40% higher than PFF and 7% lower than SFF. A semi cylindrical shaped obstacles along the daughter channels of natural inspired flow field which is called as a Nature inspired design with obstacle (NIDO) of PEMFC has
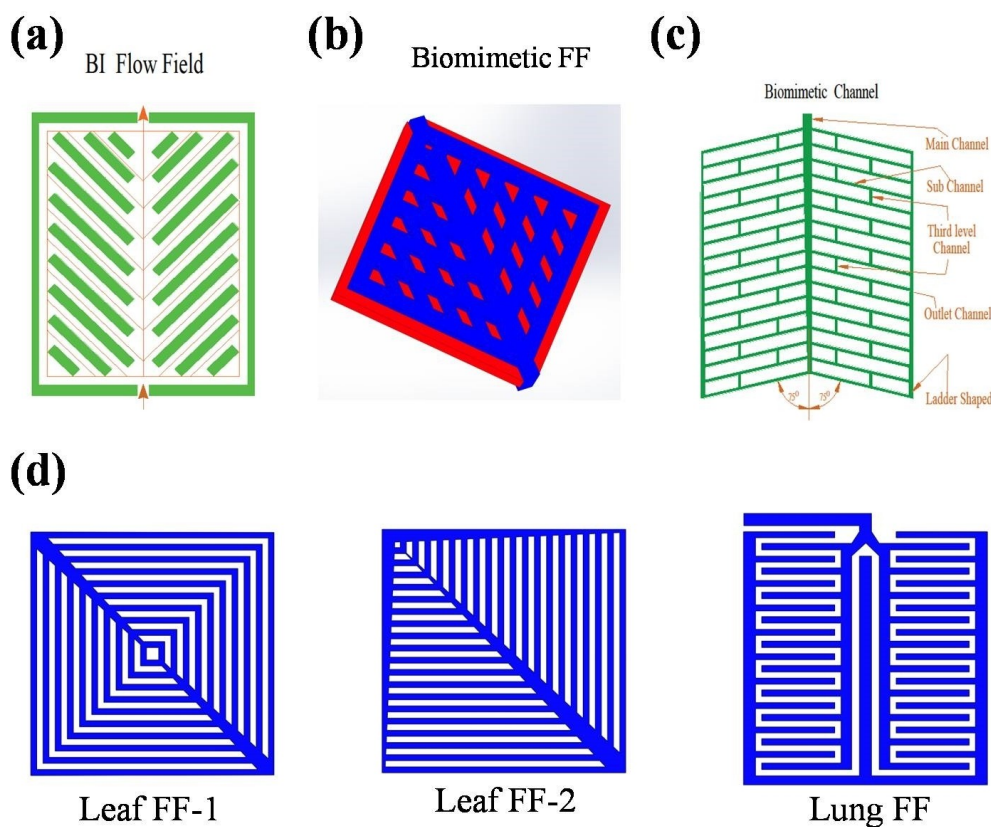
Figure 18. (a) Bio inspired (BI) flow field. Drawn from [115], (b) Biomimetic flow field. Drawn from [116], (c) New Bionic Flow fields. Drawn from [117], (d) Bio-inspired Leaf FF-1, Leaf FF-2 and Lung FF. Drawn from [118].
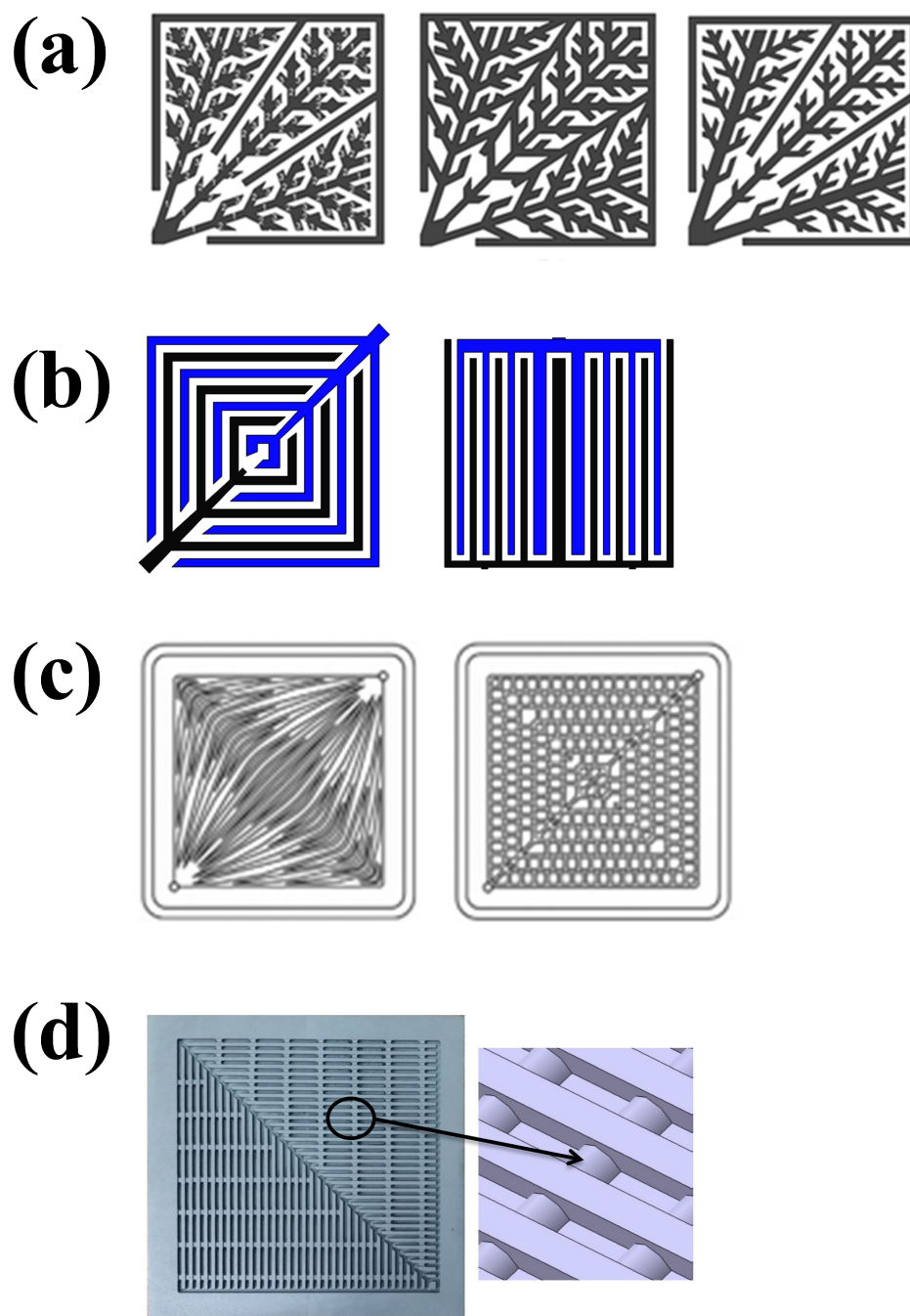
Figure 19. (a) Bio-inspired IFF with constant channel width, Bio-inspired Non-IFF with constant channel width, Bio-inspired IFF with varying channel width,[120] (b) Murray interdigitated-2 design (left) and Interdigitated pitchfork design (right). Drawn from [121], (c) Ginkgo and Net leaf FF,[122] (d) Obstacles along the daughter channels.[123]

improved the diffusion of reactant into the GDL and 41% higher performance than SFF (Figure 19d).[123]

2.7. Square Tubular Flow Field

The square tubular FF is having a squared cross-sectional area. Compared to the planar design, the tubular design is having the advantages of even pressure distribution on MEA. The effects of different architectures of GDL, membrane and CL

with square tubular PEMFC under the cases of Square Bisectors (SB), Square Chordal (SC) and Square Peripheral (SP) as shown in Figure 20a were investigated.[124] Among the three models, SC architecture had higher power density, and higher consumption of hydrogen and oxygen mass fractions. The results showed that the three-square architectures gave better performance than the conventional model.

Four square tubular flow fields namely simple square tubular (without intermediate electrode), Double Bisectors Intermediate Electrode (DBIE), Triple Parallel Intermediate Electrode (TPIE) and Double Parallel Intermediate Electrode (DPIE) were investigated.[125] DPIE and DBIE are shown in Figure 20b. Due to less mass transport losses in tubular flow fields and the additional intermediate electrode, the current density and cell performance were increased. Further, the performance of DPIE was greater than DBIE.

3. Mesh Type and Fractal FF Designs

The mesh-type designs (also known as pin or land-pillar or grid type) are made by two orthogonal sets of parallel flow channels. The intersectant FF (Figure 21a) with optimum porosity and channel depth of 0.5 and 0.3 mm respectively gave superior performance than the SFF.[126] The perforated FF consisting of 169 holes of each diameter 2 mm (Figure 21b) was analysed[127] and found that the perforated FF generated 5.2%, 6.5% and 5.8% of more power densities at 1, 0.5 and 0 bar pressure respectively on comparison with SFF.
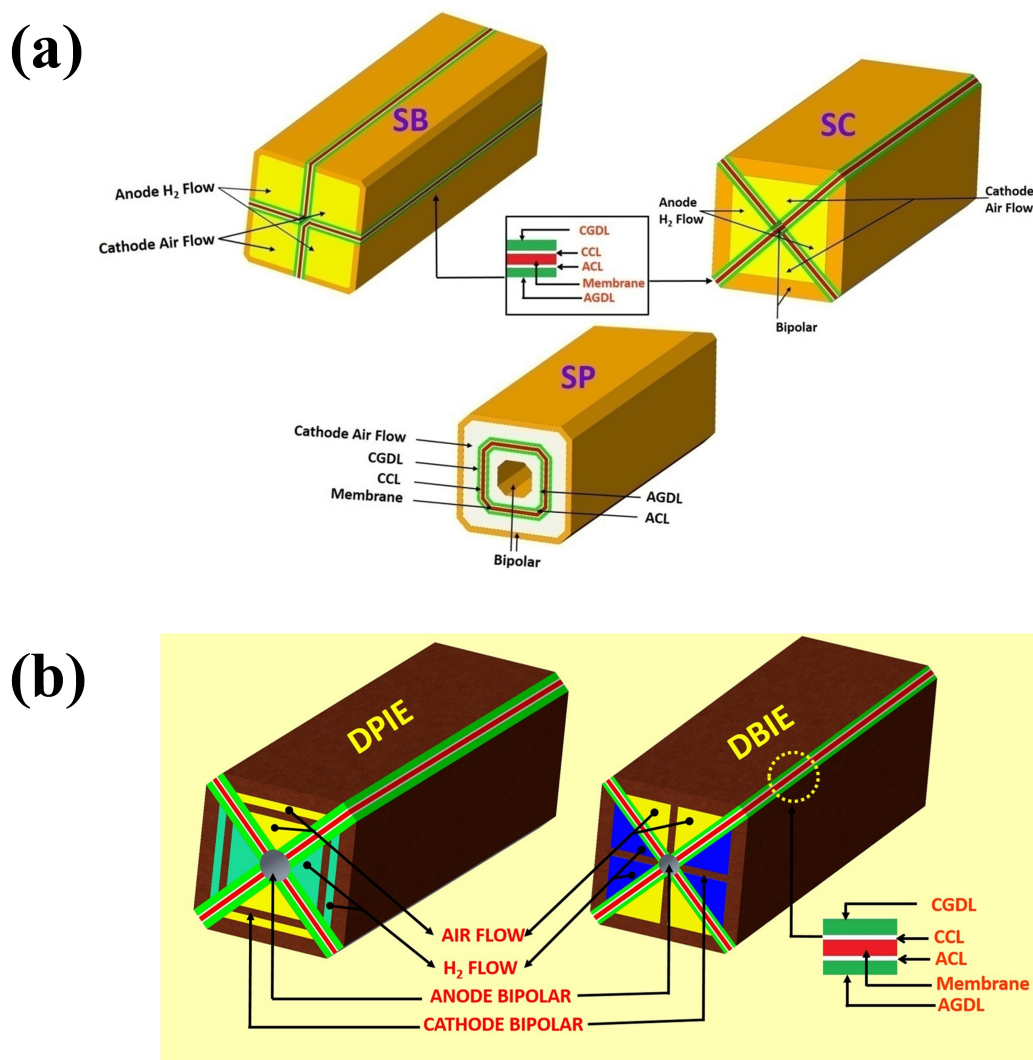
Figure 20. (a) SB, SC, and SP architectures. Drawn from [124], (b) DPIE and DBIE Drawn from [125].
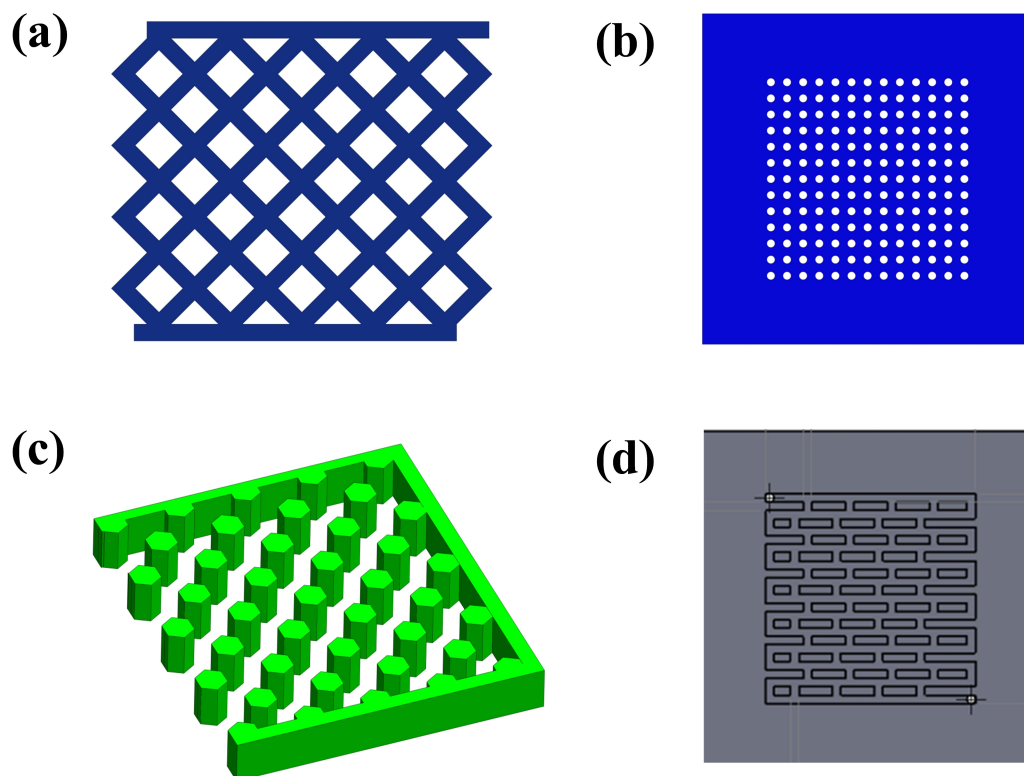
Figure 21. (a) Intersectant FF. Drawn from [126], (b) Perforated FF. Drawn from [127], (c) Honeycomb FF. Drawn from [128], (d) Zigzag pin type flow field.

The honeycomb FF (Figure 21c) having the hexagonal pins was analysed[128] and found that the hexagonal pins increased the diffusion rate of oxygen through GDL by 10 times. The land-pillar flow fields with different channel width (CW) of 2 and 3 mm and single/multiple inlets were optimized and it is found that the flow field with CW of 3 mm, single inlet and 76% flow area showed higher performance due to uniform reactant distributions.[129] When compared to the uniform pin type, the zigzag pin type flow field (Figure 21d) showed higher performance of up to 3% and 12% on 25 cm^2 and 70 cm^2 PEMFCs respectively, due to even distribution of reactant on active area.

The cascade FF with matching and crossed design configurations were analysed[130] and found that the large number of electrochemical reactions were carried out near the H$_2$ entry and thereby more water was formed. To improve the performance, it was suggested to give a greater number of H$_2$ inlets. Further, the area of catalyst under the rib was being unused, thereby it reduced the performance of PEMFC.

For the commercialization of PEMFC, the cost of the stack is to be reduced which is possible with large sized FF plates. So, the large-shaped branch channel with broad active area of 300 cm^2 and flow characteristics was proposed.[131] The branching factor (f) was ranged from 1 to 0.5 at the branch

outlet. Even though the performance of branch channel was 1.7% lower than SFF, its pressure drop was also 12.47% lower than SFF. So, the PEMFC with branch channel FF reduced the blower's power consumption and increased the system efficiency. The branched channel with f=0.5 gave 3.55% higher performance than the serpentine channel due to less electric power consumption of blower.

In the air-breathing cathode with three-channel widths and fixed rib width of 1 mm, the air was brought into the channels by a natural convection.[132] It was found that the 3 mm channel width and 75.9% open ratio gave the best performance from the open ratios of 67.5, 75.9 and 80% and channel widths of 2, 3 and 4 mm. The three dimensional flow field (3DFF) with trapezoidal baffles of different inclination angles (90°, 15°, 10° and 5°) increased the reactant transport and the power (upto 15%) than PFF.[133] Further, the baffles with small inclination angle were the best for the high water and high relative humidity conditions.

The performance of a fractal design (Figure 22a) was higher than the PFF, but lower than the SFF.[134] The constructal flow distributor with 16 and 64 outlets using fractal structure (Figure 22b) had a good hydrodynamic performance.[135]

Figure 22. (a) Parallel fractal branching design. Drawn from [134], (b) Fractal structure with 64 outlets. Drawn from [135].

4. Effects of Different Landing and Channels Width Ratios of Channels

The channel in FF is the flow path for the reactants and the landing is the wall separating the channels. The landing and channels width ratios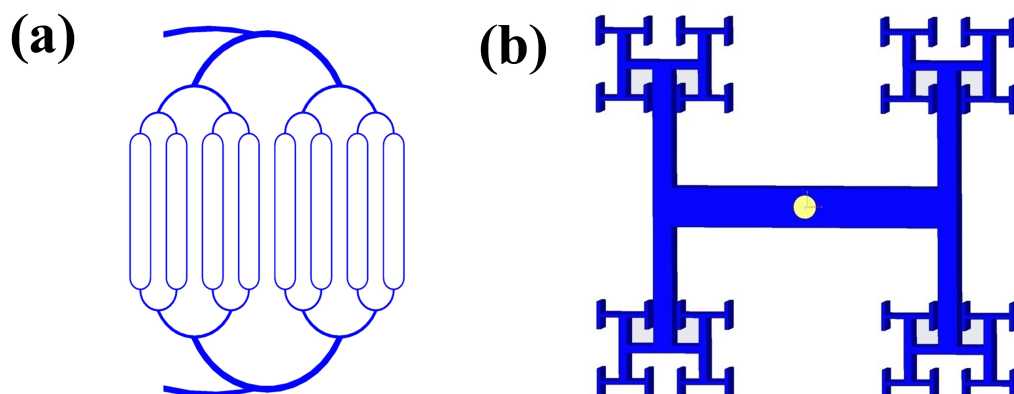 are influencing the reactant flow, current conduction and performance of PEMFC. The performance of a fixed channel height (0.55 mm) and varying channel/rib ratios (0.9/0.9, 1/0.7, 0.7/1) were investigated for different flow channel designs (Figure 23a).[136] The channel with high rib ratios showed high performance and better heat transfer. The six Channel to Rib width ratios (η) (Figure 23b) for SFF, IFF and PFF having 25 channels were investigated.[137] While increasing the rib width and decreasing the channel width, the performance of the cell was improved. At $\eta = 0.25$ than 2.66, the performance was increased as 120%, 45% and 23% for SFF, IFF and PFF respectively.

SFF with different (horizontal and vertical) cross-section aspect ratio of the channel as shown in Figure 23c was investigated.[138] The ratio between the height and width is known as the aspect ratio. The cell was operated under aspect ratios ranging from 0.07 to 15. The channel with a high cross-section aspect ratio gave better performance than the channel with low cross section aspect ratio. The aspect ratios of 10:06 and 12:05 gave the best results.

The various Channel to Landing (C:L) width ratios of 0.5:0.5, 1:1, 1.5:1.5 and 2:2 on straight flow field were analysed and found that 0.5:0.5 gave the highest power density.[139] The optimum C:L ratio was found as 2:1 among 2:1, 1:1 and 0.5:1 for SFF.[140] The four C:L ratios of 1:1, 2:1, 1:2 and 2:2 on SFF and IFF were analyzed and found that 2:1 gave the highest power density.[141] Six different aspect ratios (width to depth ratio of 1.26/1.58, 1.58/1.26, 2/2.5, 2.5/2, 2.53/3.16, 3.16/2.53) on the cathode side were investigated.[142] The high aspect ratio of the channel greatly increased the performance of the open cathode, due to good

dissolving capacity of air with MEA. Further, too high aspect ratio also increased the mechanical stress.

The different aspect ratios (0.8 and 1.25) and cross-sectional areas (2, 5 and 8 mm^2) of flow channels were investigated.[143] The cell performance is directly proportional to the aspect ratio and inversely proportional to the cross-sectional area. The reduction of the rib area has increased the oxygen molar concentrations between GDL and CL. The 5 pass SFF with different channel widths (1, 1.25, 1.5 and 1.75 mm) and different channel heights (0.34, 0.5, 0.67 and 0.83 mm) were investigated.[144] Increasing the channel height has increased the area and water accumulation; and has decreased the cell performance. Further, increasing of channel width caused the membrane dehydration.

5. Effects Of Different Shapes of the Channel

The cross-sections of the flow channels are also influencing the performance of PEMFC. The various cross-sectional shapes like rectangular, trapezoidal and parallelogram, triangular, stepped, semi-circular, hemisphere, slanted, parallelogram and combinations of above were developed and analysed.

From the analysis of three channel shapes (rectangular, trapezoidal and parallelogram) as shown in Figure 24a, the rectangular channel gave higher cell voltage than other channels.[145] The rectangular channel offered elevated cell potentials, but the trapezoidal channel offered uniform current density distributions. The triangular and rectangular cross-sections (Figure 24b) were used with and without PTFE coating to increase the surface static contact angle.[146] The water accumulation in the channel was largely affected the performance of the cell. With the use of PTFE coated membrane, the water clogging was reduced to an optimal level. Further, the triangle channel kept low water than rectangular.
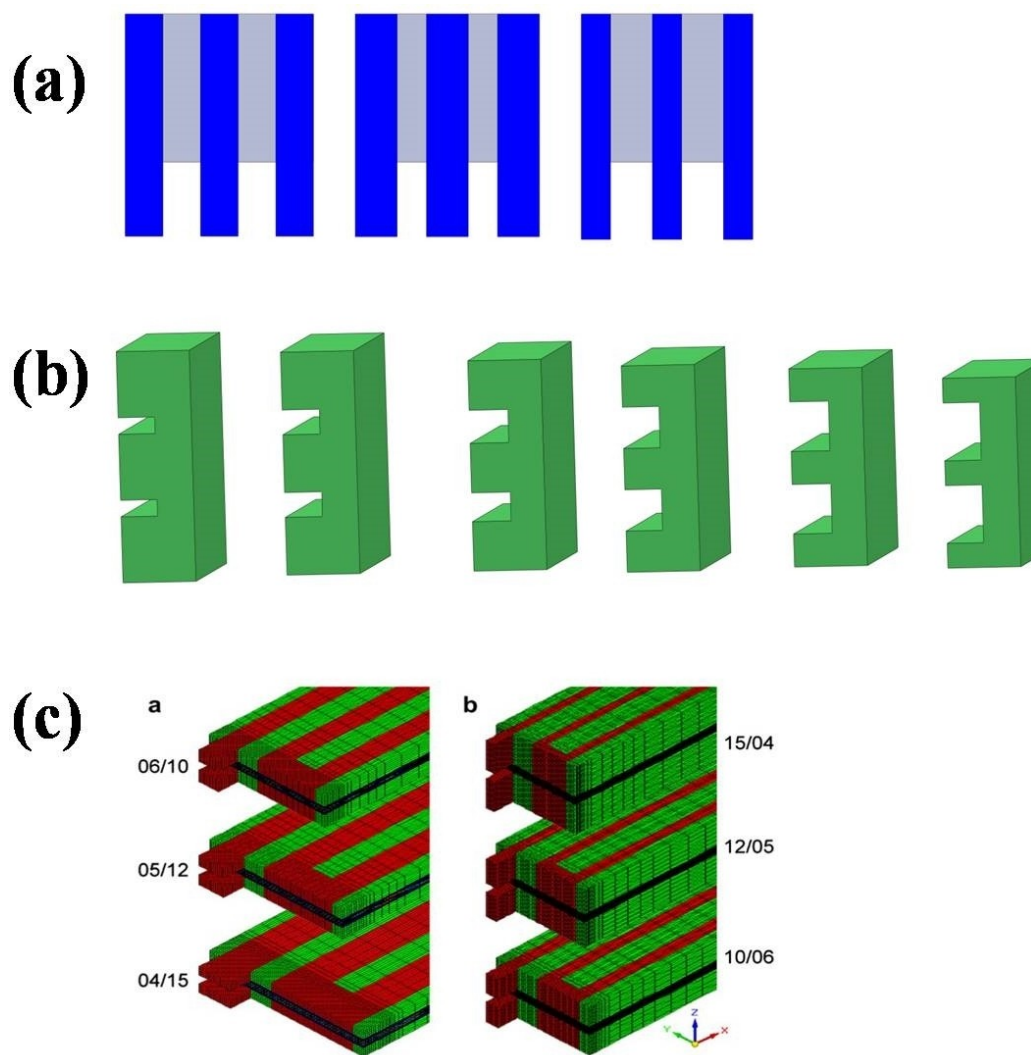
Figure 23. (a) Three channels to rib ratios (0.9/0.9, 1/0.7, 0.7/1 from left to right). Drawn from [136], (b) Various channel to rib width ratios ($\eta = 0.25$, 0.43, 0.66, 1.0, 1.5, 2.66 from left to right). Drawn from [137], (c) Horizontal and vertical cross section models.[138]

The square, trapezoidal and stepped channels (Figure 24c) were investigated.[147] The square channel exhibited better electric performance than the trapezoidal and stepped channels, whereas the trapezoidal and stepped channels showed better water management than the square channel. The semicircular, trapezoidal and triangular channels and rectangular channel were analyzed.[148] Based on cell performance, the channel cross-sections can be ordered from high to low range as triangular, semi-circular, trapezoidal and rectangular (Figure 24d). At low cell voltages, the rate of electrochemical reactions and water formation were more. So, there was the effect of channel cross-sections only in low voltages, not in high voltages.

The effect of shape and channel dimensions were analyzed.[149] The triangle and hemisphere shapes gave 9% more H_2 consumption than rectangular shape. The optimum values of the channel depth, channel width and land width were found as 1.5, 1.5 and 0.5 mm respectively at 80% H_2 consumption. It also showed that the H_2 consumption at the anode was increased with decreasing of land width. The increase in the H_2 consumption has increased the performance.

The different channel shapes namely trapezium, parallelogram, inverted trapezium, and square of same area (0.01 cm^2) were analyzed.[150] It is found that the square channel offered elevated cell performance compared to others. The different channel shapes namely the semicircular, trapezoidal and
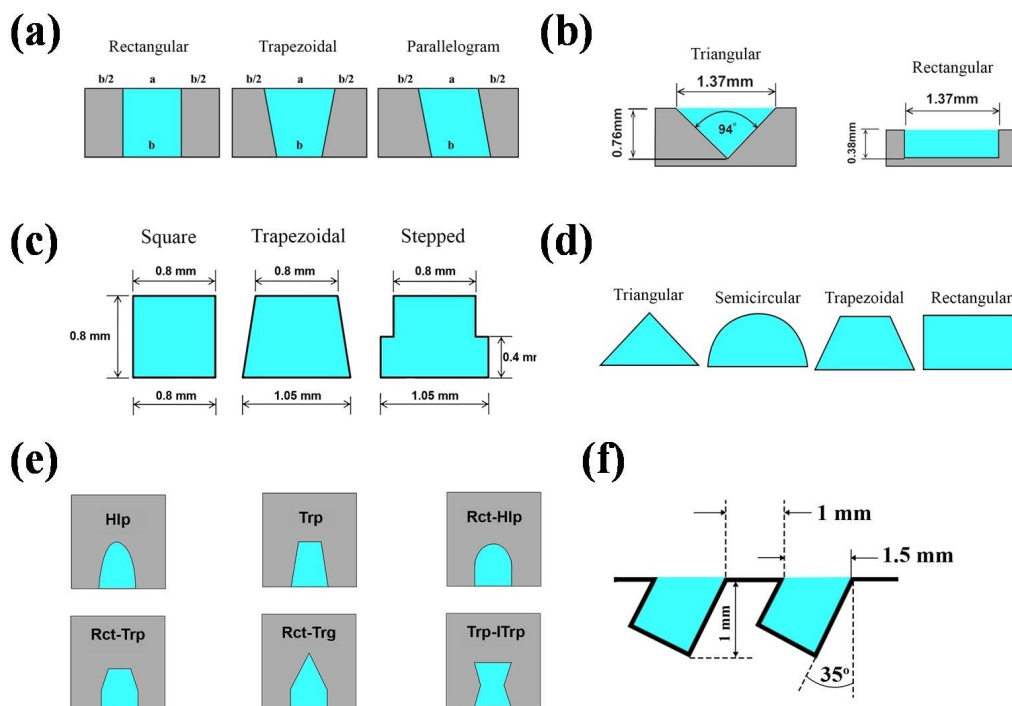
Figure 24. Different channel cross-sections (a) Rectangular, Trapezoidal and Parallelogram cross-sections. Drawn from [145], (b) Rectangular and Triangular cross-sections. Drawn from [146], (c) Square, Trapezoidal and Stepped cross-sections. Drawn from [147], (d) Triangular, Semicircular, Trapezoidal and Rectangular cross-sections. Drawn from [148], (e) New channel cross-sections. Drawn from [152], (f) Slanted channels. Drawn from [153].

triangular and rectangular of same area (3 cm^2) were analyzed.[151] It is found that the rectangular channel offered higher cell performance compared to others.

The 25 new channel cross-sections with the combinations of Rectangular (Rct), Trapezoidal (Trp), Half elliptical (Hlp) and Triangular (Trg) shapes in straight and inverted positions were designed and analysed.[152] The Half elliptical, Trapezoidal, Rectangular-Half elliptical, Rectangular-Trapezoidal, Rectangular-Triangular and Trapezoidal-Inverted Trapezoidal shapes (Figure 24e) produced more power density than a rectangular shape. Among 25 new channels and 5 conventional channels, the Trapezoidal-Inverted Trapezoidal shape gave higher power density up to 4.65%.

A channel with 35° inclined slanted grooves (Figure 24f) were designed and analysed and it is found that the downward slanting of the channel on anode stimulated the back diffusion of water from cathode to anode.[153] This increased the membrane conductivity, hydration, and performance.

6. Effects of Taper in Flow Fields

The tapering in channel width/height, inlet header of various flow fields is affecting its performance.

6.1. Taper in Straight Flow Field and PFF

Two novel PFF with channels tapered in height and width (Figure 25a) were proposed.[154] The reduction on the height of the cathode channel outlet increased the fuel consumption efficiency and performance. Further, increasing the width of the tapered channel has increased the contact area between GDL and channel, thereby giving better performance. The highest performance was obtained for 0.5 and 1.8 values of the height and width taper ratios, respectively. The channel taper angle of 0.75° (among 0°, 0.5°, 0.75° on 50 mm long channel) increased the power density by 8% due to better O$_2$ distributions and heat transfer along the taper channels.[155] The increase in taper is directly increasing the pressure drop factor in straight flow field.

The converging-diverging flow channels having convergence angle of 0.2° and divergence angle of 0.3° as shown in Figure 25b were designed.[156] At the channel angle of 0.3°, the electrical power output was increased by 16% in comparison with the conventional parallel flow channels. Due to the pressure variations between adjacent channels, a transverse over rib velocity was produced which in turn increased the O$_2$ distribution over the CL and increased the cell performance. The inlet header with reducing width (PFF with tapered inlet manifold as shown in Figure 25c) has greatly increased the
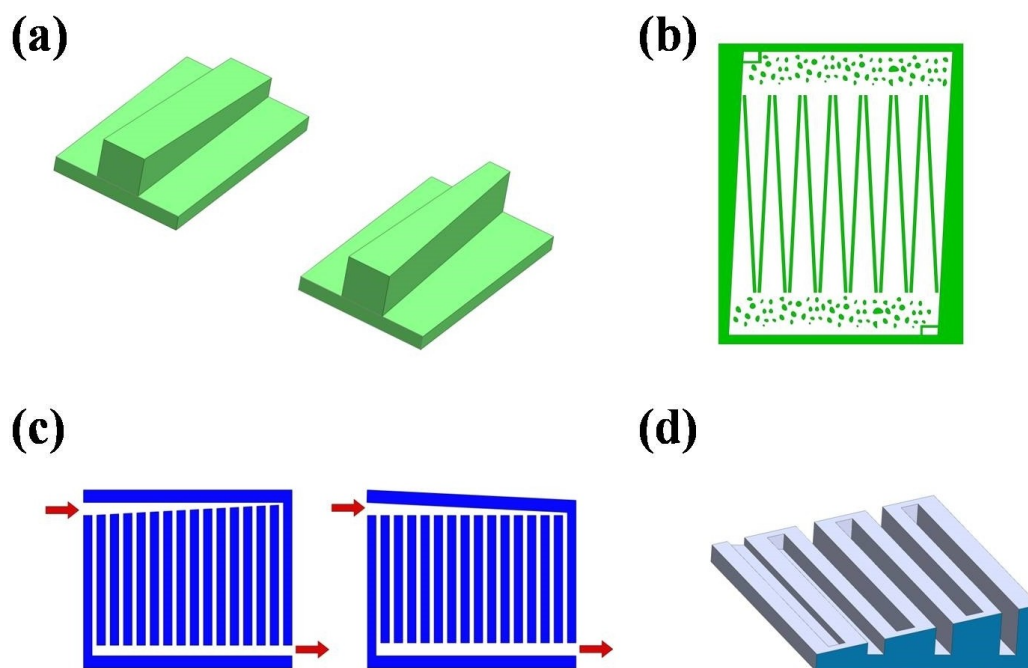
Figure 25. (a) Channels tapered in height and in width. Drawn from [156], (b) Converging-Diverging flow channels. Drawn from [158], (c) PFF with tapered inlet manifold. Drawn from [30] (d) Convergent Serpentine (SC) flow field. Drawn from [161]

reactant flow. In this design, 70% of gas is flowing through 80% of the active area, whereas in the conventional PFF, 80% of gas is flowing through only 20% of the active area.[30]

An innovative cathode flow field was designed which showed a greater water maintaining capability on the membrane compared to conventional PFF.[157] This design supplied an additional air to the cooling channels. Further, it decelerated the air in the gas channels and accelerated the coolant air in the cooling channels at the same time.

6.2. Taper in SFF and IFF

In the converging-diverging flow channels, the depth of the channel was varied from inlet to outlet by varying the angle of inclination.[158] The different depths of channels used in Inlet-Outlet were 3.5–0.5 mm, 3–1 mm, 2.5–1.5 mm and 1.5–0.5 mm. The high-power density was obtained for the design having less channel width between the inlet and outlet. Further, the current density and water management were better in a convergent flow channel. The transport phenomena of Convergent Serpentine (SC) and Divergent Serpentine (SD) flow fields with variable channel depth were compared with a conventional serpentine flow field (S).[159] Due to low concentration of water and high O_2 transport over the active surface on the cathode; and high-pressure distribution along the channel, the SC (Figure 25d) gave higher performance than the S and SD.

A taper SFF was designed with starting and ending height of 1 mm and 0.5 mm respectively in each channel.[160] With continuous loading of 5 hours, the tapered SFF resulted in 15% of higher current at 0.5 V than conventional SFF. The tapered arrangement induced the reactant velocity in the direction of GDL, thereby increasing the amount of reactant at CL, reaction rate and performance. Bode and Nyquist plots were used to confirm the performance. The width of the outlet channel was made narrower than the conventional channel in taper IFF.[161] The results showed that there was better oxygen transport and higher performance in the narrower channels than the conventional ones.

7. Effects of Channel Bending

The performance of serpentine channels without slope and with different slope turns of normal, small and large sectional areas (Figure 26a) were investigated and found that the slope and contact angle of 120° and 160° respectively gave better water removal for the given condition.[162] Due to the hydrophobic of slope turns, the water particles were removed effectively from the MEA surface. From the analysis of the SFF with 1, 2, 3, 4, 5, 6 channels and different channel curvatures (Figure 26b), it was found that the 6-channel flow field with a sharp channel curve had 25% of more perform-
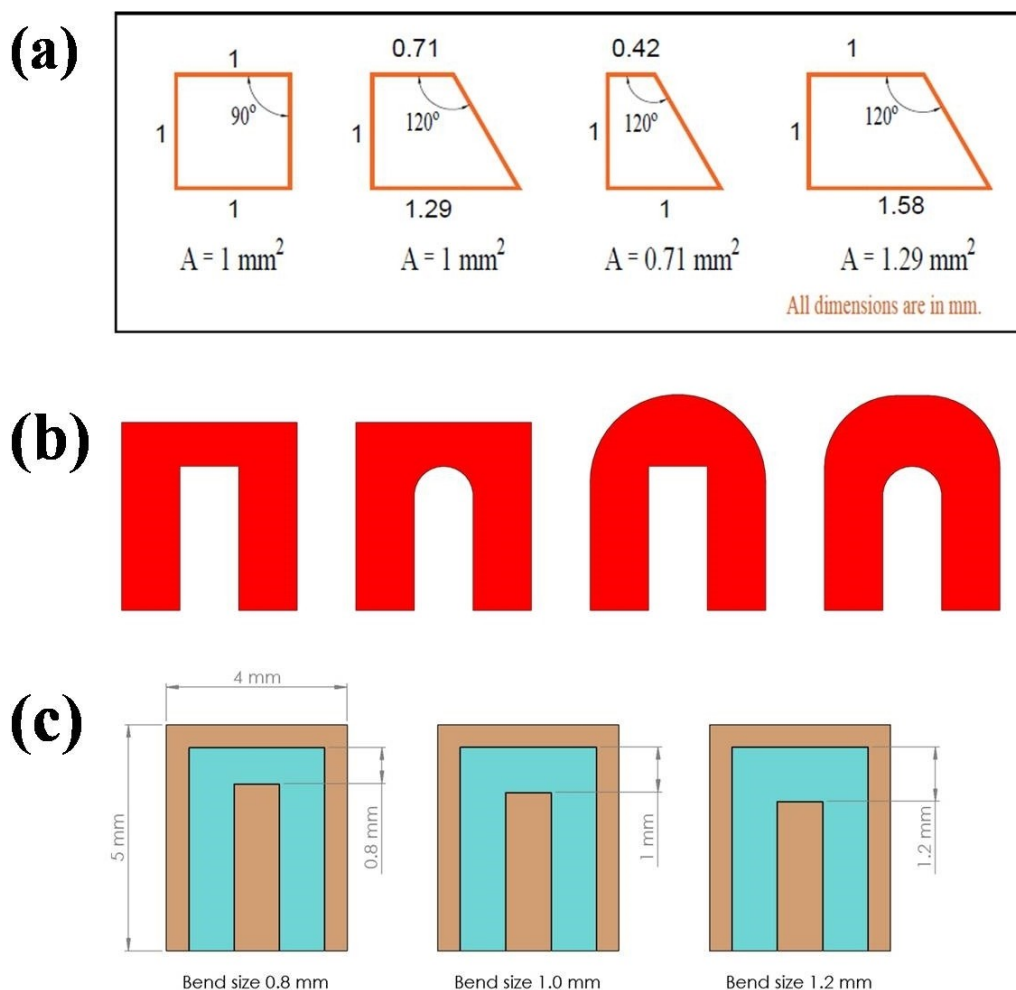
Figure 26. (a) Cross-sections of serpentine channels without and with different slope turns. Drawn from [164], (b) Sharp, Radius in, Radius out and Smooth curves. Drawn from [165], (c) Different bend sizes. Drawn from [166].

ance than the 4-channel flow field, as it contained larger areas of gas flow, high secondary flow and velocity.[163]

The effects of the single sharp bend, 180° bend, curved bends and serpentine channels were investigated.[164] The various curvature ratios of channel bend (C=0, 1.41, 2.82 and 5.66) were studied. In the fuel cell stacks, the pressure losses of reactants are key factors for overall fuel cell efficiency. The optimization of the channel configurations (i.e. height, width, and gap) can improve the water management and the cell performance through a desired pressure drop. From the analysis of three bend sizes of 0.8, 1 and 1.2 mm on serpentine channels (Figure 26c), it was found that the 1.2 mm bend size had less pressure drop and uniform temperature distribution.[165] So the current density was more uniform at this channel which increased the power density.

8. Effects of Compression on the Performance

The clamping pressure of the fuel cell is also affecting the performance of a single cell assembly. Chang et al.[167] studied the contact resistance among the GDL, and the flow field was measured under different clamping pressures for a 25 cm² active area. While increasing the clamping pressure, the interfacial resistance was reduced between them, and it improved the electrochemical performances of the single cell. The optimal clamping pressure of carbon paper was found between 10 and 20 bar, and it was reduced up to 20–30 % in thickness in that pressure range. Meanwhile, a higher clamping pressure reduced the ohmic resistance and caused harmful effects such as GDL damage, loss of porosity, and tenting.[168–171] Wang et al.[172] designed a pair of fixture plates to study the pressure distribution in a single cell and fuel cell stack and concluded that the optimum pressure was delivered

better. PEMFC with an active area of 25 cm^2 and the clamping pressure of about 1.38 MPa showed higher current density for the new end plates. When the flow path was partially blocked during non-uniform clamping, the membrane got deflected and extended. The high interfacial contact area between the channel surface and the carbon paper (GDL) ending with an exponential increase in the contact at higher compression. These will significantly affect the relationship between the contact resistance and cell performance.[173] Xing et al. numerically evaluated the clamping pressure on GDL's porosity, conductivity, and the contact resistance between flow field and GDL. When the clamping pressure was raised from 0 to 3 MPa, the plane conductivity increased by 52.9% and 71.3%, whereas the permeability non-linearly decreased by 69.5% and 87.5% for SGL-10-BB and SGL-10-BA, correspondingly.[174] Chen et al.[175] conducted experimental studies to find the cell's optimum clamping pressure and concluded that 1 MPa was optimum. The clamping pressure of 0.5 MPa showed the least performance, whereas, in 3.5 MPa, GDL thickness was reduced by 31.6% from the original state. There is a linear variation (resistance and conductivity) in cell performance due to the increased clamping pressure (above 3 MPa) from the overall observations. Low clamping pressure (below 1 MPa) leads to rectants

leakage, and High clamping pressure reduces the thickness and porosity of the GDL.

9. Performance Comparison of Various Flow Fields by using Numerical Analysis and Experimental Evaluation

The performance evaluation by using Numerical analysis for Trap channel, straight channel, bio inspired, wave and M channels is shown in Figure 27. Trap shaped straight channel had the maximum power density of 0.82 W/cm^2 compared with straight channel having 0.7 W/cm^2 (Figure 27a). Similarly, the wave channel (Figure 27b) had the maximum power density of 0.73 W/cm^2 due to the improved convective heat transfer, catalytic electrochemical reactions. Bio-inspired wavy channel (Figure 27c) had the maximum power density of 0.562 W/cm^2. M-flow channel (Figure 27d) had generated 21.3% high power density than the wave flow channels.

Similarly, the performance comparison by using Numerical analysis and Experimental evaluation for Metal foam and PFF; FF:1 (PTBPFF) and FF:2 (STBPFF); and PFF with and without blockages is shown in Figure 28. PFF with rectangular baffles and plain Nickel foam had maximum power density of
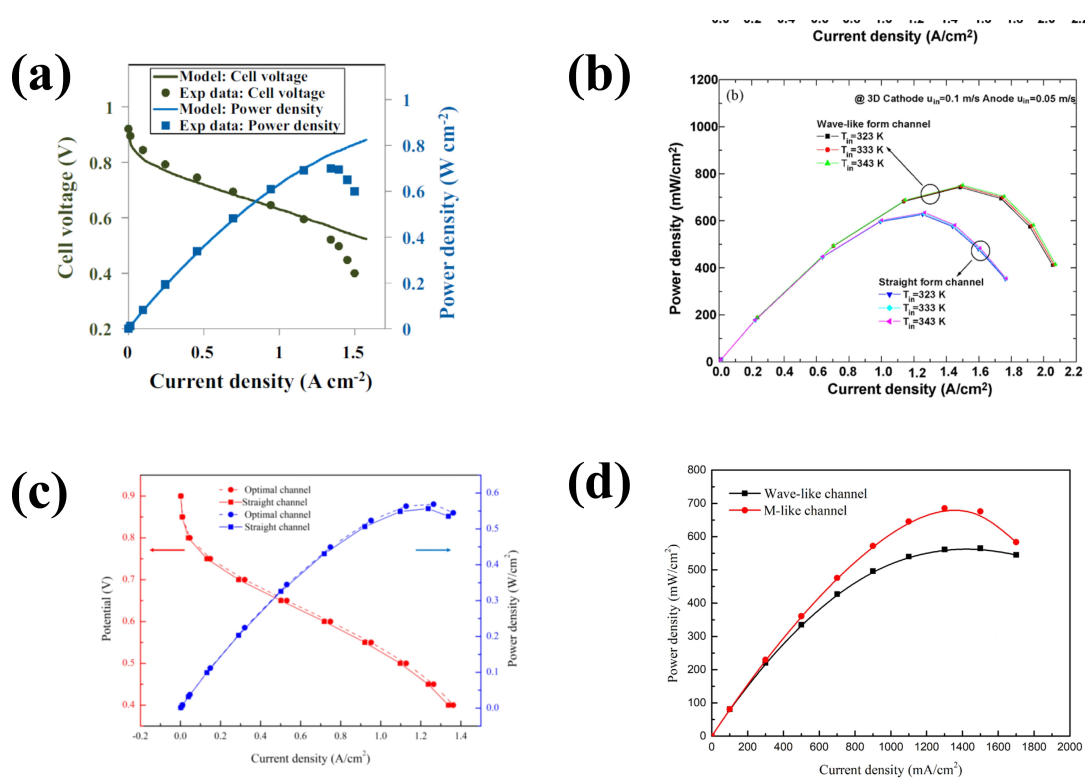
Figure 27. Power density curves of (a) Trap channel (blue line) and straight channel (square shaped curve),[19] (b) Wave and straight channels,[21] (c) Bio inspired wavy (optimal channel) and straight channel,[22] (d) Wave and M channels.[23]
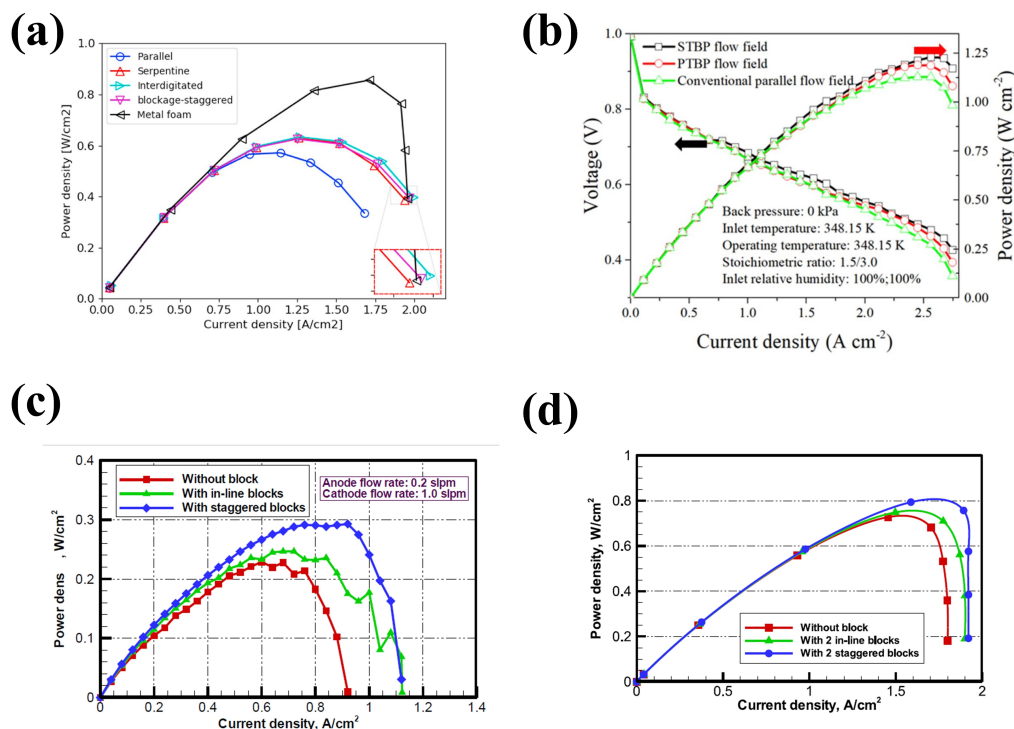
Figure 28. Power density curves of (a) Metal foam and PFF,[36] (b) STBPFF and PTBPFF,[37] (c) PFF with and without blockages,[39] (d) PFF with 2 blockages and without blockages.[40]

$0.87\,W/cm^2$ compared with PFF having $0.58\,W/cm^2$ (Figure 28a). Similarly, PFF with trapezoidal plates (FF:1 and FF:2) had the maximum power density of $0.25\,W/cm^2$ due to the better water removal rate and lower pressure drop (Figure 28b). PFF with blockages (Figure 28c-d) yielded the maximum power density due to the enhanced under-rib convection of the staggered design.

Similarly, the performance comparison by using Numerical analysis and Experimental evaluation for PFF with subchannels and micro distributor, Serpentine/Straight zigzag FF and Sinuous FF is shown in Figure 29. PFF with subchannels and micro distributer (Figure 29a-b) yielded a higher performance due to the influence of sub channels and the reduced size of the micro distributor respectively. The performance of straight zigzag FF was higher than serpentine zigzag FF as shown in Figure 29c. Similarly, the Serpentine-Sinuous FF combinations on anode and cathode respectively showed a higher performance (Figure 29d) than Sinuous-Sinuous and Serpentine-Serpentine combinations due to the enhanced under rib convection and better water removal.

The performance comparison by using Numerical analysis and Experimental evaluation for Sinusoidal and PFF; TPA, PFF and SFF; PIS; and FF:4 (SBFF) flow fields ise shown in Figure 30. Sinusoidal FF showed the enhanced performance due to the uniform reactant distribution (Figure 30a). The

performance of TPA was higher than PFF and SFF (Figure 30b). Similarly, PIS increased the performance of cell with the increase of temperature (Figure 30c). Increasing the number of Baffles in FF:4 induced the higher pressure differences between the adjacent channels than SFF (Figure 30d).

The performance comparison by using Numerical analysis and Experimental evaluation for FF:5 (PSBFFP), FF:6 (PSFFP), FF:7 (CESFF), Cascade FF and Compensated SFF si shown in Figure 31. Discontinuous path of channels in FF:5 gave better performance with good membrane hydration, and enhanced heat transfer (Figure 31a). FF:7 had the enhanced performance compared with SFF due to the under-rib convection which removed the water from the active area (Figure 31b). Also, Cascade FF showed better performance due to the optimum values of channel width, channel depth and rib width (Figure 31c). Compensated SFF showed 27% higher performance than SFF (Figure 30d).

10. Conclusion

Use of the fuel cell technology is playing a vital role in pollution control for the benefit of people throughout the world. Even though the PEMFCs are majorly used in Fuel
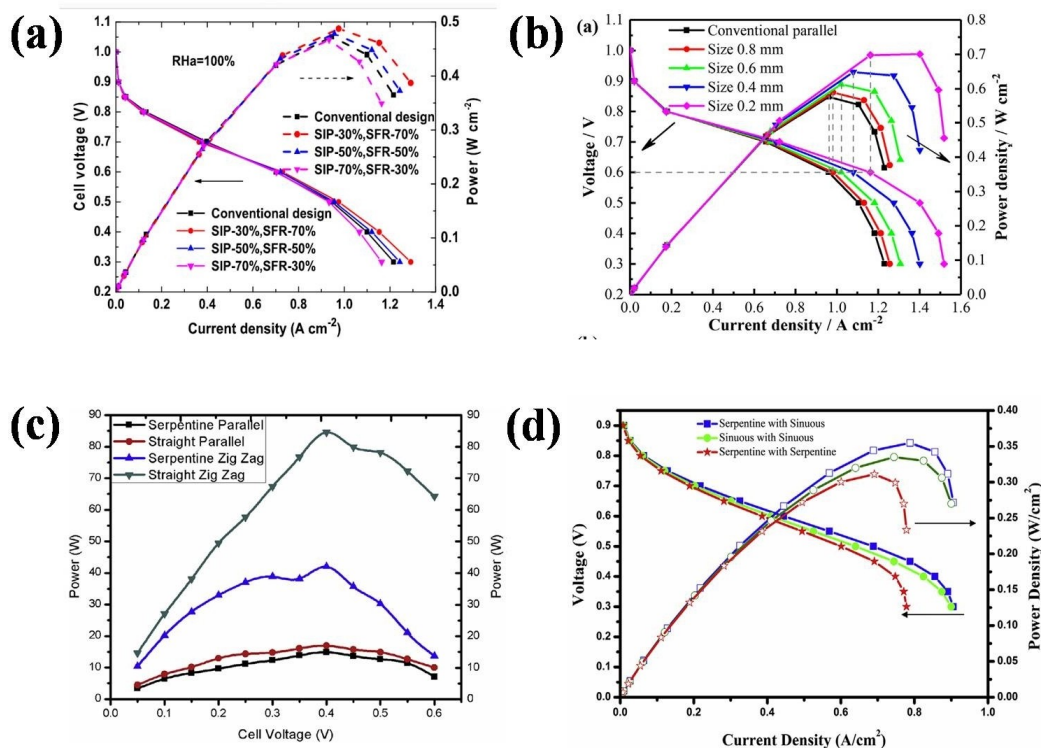
Figure 29. Power density curves of (a) PFF with and without subchannels,[44] (b) PFF with and without micro distributor,[45] (c) Serpentine zigzag and Straight zigzag FF,[50] (d) Sinuous FF and SFF.[51]
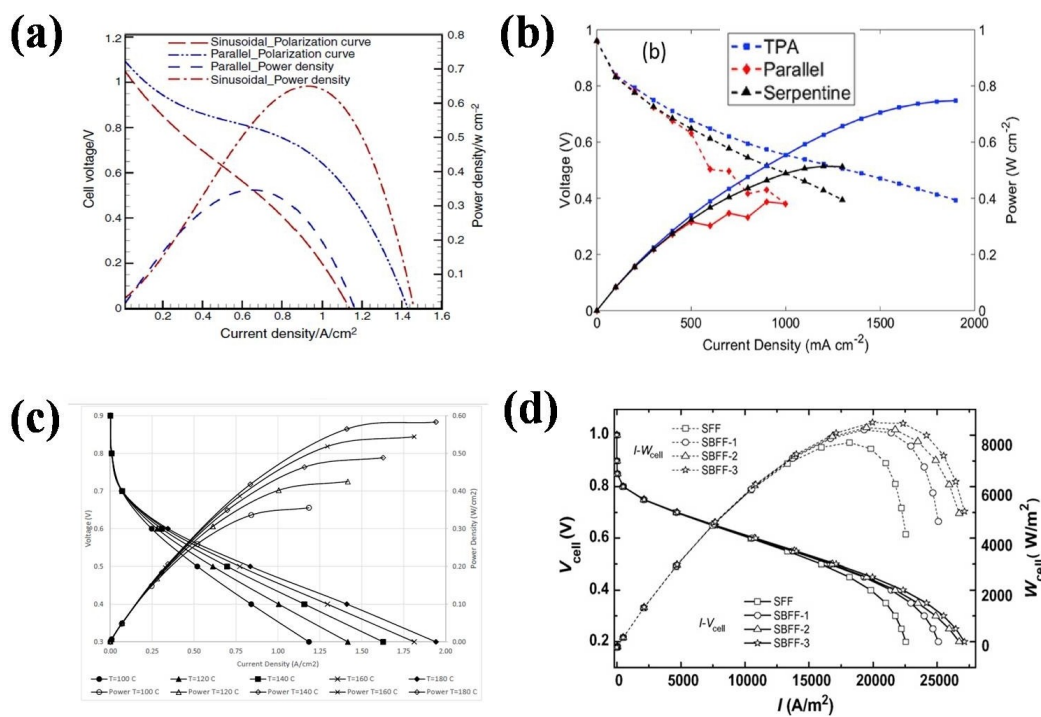
Figure 30. Power density curves of (a) Sinusoidal and PFF,[53] (b) TPA, SFF and PFF,[54] (c) PIS at different temperature,[62] (d) FF:4 (SBFF) and SFF.[68]
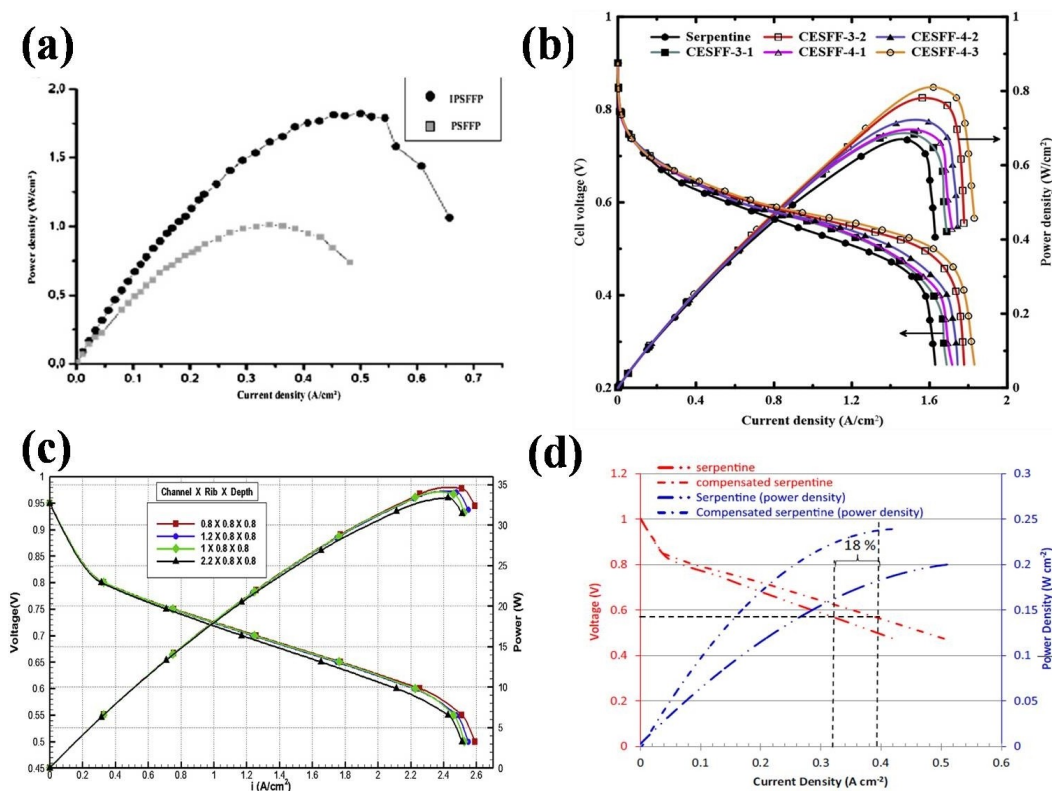
Figure 31. Power density curves of (a) PSBFFP and PSFFP,[69] (b) CESFF and SFF,[72] (c) Cascade SFF at different channel width,[73] (d) Compensated SFF and SFF.[74]

Cell Vehicles like cars and buses, still many research works are being carried out to rectify the major issues in it. In this regard, the design of the flow field of fuel cell is also highly affecting the water control on the interfacial between the GDL and catalyst layer of the cathode side and the performance of PEMFC. Each flow field design has pros and cons which in turn make it for different applications. The design and operating parameters along with the power density values of various flow field designs which are analysed experimentally and numerically are given in Table 1 and Table 2 respectively. From the wide literature, the following important points are derived.

1. As the trap shaped flow channel is simple, inexpensive, and having high performance, it will be one of the potential designs for the coming generations. Further the vertical orientations of AB-PEMFC are the best due to easy removal of water at cathode side. The wave, bio-inspired wave and M-shaped blockages and the arrangement of pin-fins and cylinders in flow channel have improved the performance.

2. The PFF design is simple and easy to manufacture. Though the pressure drop of reactants is reduced in PFF than SFF, few of the channels are starved of the gases due to the maldistribution of flow. The performance of PFF can be improved by the following ways;

- The staggered arrangement of rectangular and trapezoidal blockages along the channel (due to the cross flow of reactants and over rib convection)
- The use of metal foams with high porosity
- Provision of sub channels, transition areas, inclinations, microgrooves in rib walls and micro distributor
- Provision of bends and curves in channels, number of funnelled in/out, small holes in landing/rib areas of the flow field and two sets of parallel channels operating at different pressures
- Generation of circumferential flow of reactant near GDL by the insertion of wire coils in channels

3. Due to the high cell performance, reliability and durability, the SFF is widely used for many applications and it is considered as the "Industry standard".[176] Hence many design modifications are being made on serpentine design for further enhancement of fuel cell performance. The FF:3, FF:4, FF:5, FF:6, FF:7, FF:8, FF:9, FF:13, FF:14 Cascade type, Compensated SFF, W and Z type SFF, 2 to 1 SFF, zigzag SFF,

Table 1. Design and operating parameters of various flow field designs with Experimental analysis.

Type of Flow channel/Flow field design	Active area cm²	Channel width (CW) W_c mm	Landing or Rib width (RW) W_r mm	Channel height or depth D_c mm	Number of channels N_{ch} –	Pressure P kPa	Temperature T K	Power density W/cm²	Type of study	Remarks	Ref.
PFF with trapezoidal plates – FF:1 (PTBPFF) and FF:2 (STBPFF)	26.95 (5.5 × 4.9)	1	NA	1	2	NA	348	0.250 (FF:2), 0.125 (PFF) (approx.)	Experimental & Numerical	Better water removal rate and lower pressure drop are the advantages of FF:2 than FF:1	[37]
PFF with porous inserts	4	1.5	1.2	1.5	2	NA	NA	NA	Experimental	Self-regulation of water content and very low flow mal distribution are the advantages.	[38]
PFF with blockages	5.1	0.8	0.8	0.8	32	101.3	333	0.300 (with staggered block), 0.235 (without block) (approx.)	Experimental	The under-rib convection of the staggered design on parallel channels reduced 18% of the pressure drop, thereby increasing 28% of power density.	[39]
PFF with wire coil inserts	25	1	0.5	1	28	NA	333	0.146 (modified design), 0.106 (plain design) (approx.)	Experimental & Numerical	Produced 41% more power density due to the circumferential flow of reactant.	[42]
PFF with microgrooves	42 (2.1 × 20)	1	1	1	11	1230 clamp pressure	323, 343, 353, 363	0.591 (PFF with micro grooves), 0.585 (without micro grooves) (approx.)	Experimental	Water was taken away from GDL-Landing interfacial area along microgrooves to channel. 16% of current density and 3% of power density were increased.	[46]
Zigzag PFF with single funnelled in/out	225	2	2	2	28	200	353	0.3758 (Straight zigzag), 0.1865 (Serpentine zigzag), 0.0753 (Straight parallel)	Experimental	Straight zigzag channel showed the better water removal and high performance	[50]
Zigzag PFF with double funnelled inlet (OR) Sinuous FF	25, 100	2	2	2	12	200	333	0.3476 (25 cm²), 0.2628 (100 cm²) on Serpentine-Sinuous FF combinations	Experimental & Numerical	Serpentine-Sinuous FF combinations on anode and cathode respectively showed higher performance. Sinuous flow field has increased the power density by 7.7%.	[51]
Parallel-TPA	6.25	NA	NA	NA	6	NA	343	0.775 (TPA), 0.500 (SFF), 0.400 (PFF)	Experimental	The small holes incorporated on the landing areas improved the performance	[54]

Table 1. continued

Type of Flow channel/Flow field design –	Active area cm²	Channel width (CW) W_c mm	Landing or Rib width (RW) W_r mm	Channel height or depth D_c mm	Number of channels N_{ch} –	Pressure P kPa	Temperature T K	Power density – W/cm²	Type of study –	Remarks	Ref.
PFF with two sets of channels	NA	Channel to rib ratio = 0.5, 1, 2	–	1.5	13,19,25	101.3, 202.6	353	NA	Experimental & Numerical	Controlling pressure gradient was obtained in between the nearby channels.	[55]
1-S, 2-S and 3-S	49 (7×7)	0.1	NA	0.5	1,2,3	100	323	0.370(1-S), 0.330 (2-S), 0.295 (3-S)	Experimental & Numerical	Performance of the cell increased by decreasing the number of flow channel passes.	[67]
FF:5 (PSBFFP), FF:6 (PSFFP),	8.41	2	2	1	3	NA	343–363	1.8 (FF:5), 0.9 (FF:6)	Experimental	FF:5 gave better performance with good membrane hydration.	[69]
FF:5 (PSBFFP)	8.41 (2.9×2.9)	2	1.37	1	3	NA	353	NA	Experimental	Discontinuous path of channels in FF:5 improved the heat transfer and cell performance	[70]
FF:7 (CESFF)	9 (3×3)	1	1	1	1	101.3	343, 348	NA	Experimental	FF:7 gave better performance than SFF	[71]
Cascade	25	1.2	0.8	0.8	8 (Inlet)	101.3	343	1.40 (at Channel, Rib and Depth of 0.8 mm)	Experimental & Numerical	Optimum values of channel width, channel depth and rib were found	[73]
Compensated SFF	46	1	1	1	5	101.3	433	0.220 (Compensated SFF), 0.180 (SFF)	Experimental & Numerical	Compensated SFF gave 27% higher performance than SFF.	[74]
FF:9 (ECSSFF)	36.6 (3.7×9.9)	1	1	1	3	NA	318	NA	Experimental & Numerical	FF:9 was evacuating water in U bends.	[76]
FF:9 (ECSSFF), FF:10 (SSFF)	55	2	1	1	3	100, 200, 300	323, 333, 343	1.6 (FF:9), 1.3 (FF:10) (approx.)	Experimental & Numerical	FF:9 has 30 times lower pressure drop than FF:10. If it is maintained, a 100% more maximum current density can be obtained in FF:9 than SFF	[77]
Modified W-FF	NA	1.1	NA	0.4	3	70	313	4 W (Modified W), 2.6 (Serpentine-Z)	Experimental	Novel design covered the maximum active surface and produced uniform reactant gases and current.	[82]
Wavy serpentine FF	25	1	1	1	1	NA	298, 313, 333	0.446 (C1), 0.346 (C2), 0.307 (C3), 0.371 (C4)	Experimental & Numerical	Wavy serpentine was better than SFF	[83]
FF:13 (WSFF)	49 (7×7)	1	1	0.4 (min), 1 (max)	3	NA	353	0.685 (FF:13), 0.615 (SFF)	Experimental & Numerical	Water management was better in FF:13 with a 17.5% rise in power density.	[84]
Hybrid between parallel and serpen-	50	NA	NA	NA	5 ch	200	333	NA	Experimental	Cell with horizontal orientation gave better performance.	[89]

Table 1. continued

Type of Flow channel/Flow field design	Active area cm²	Channel width (CW) W_c mm	Landing or Rib width (RW) W_r mm	Channel height or depth D_c mm	Number of channels N_{ch} —	Pressure P kPa	Temperature T K	Power density W/cm²	Type of study —	Remarks —	Ref.
tine (or) Serpentine multi pass FF (Vertical and Horizontal)											
SFF with zigzag and uniform placed PCI	25	2	2	2	1	101	323	0.270 (Zigzag PCI), 0.265 (Uniform PCI), 0.242 (SFF)	Experimental	Zigzag placed porous inserts increased the performance due to better water management.	[90]
SFF with zigzag and uniform placed PCI	25 & 70	2	2	2	1	101	323	0.170 (Zigzag PCI), 0.158 (Uniform PCI), 0.141 (SFF)	Experimental	Performance of 25 cm² was better than 70 cm².	[91]
SFF with zigzag and uniform placed PCI	25, 36 & 70	2	2	2	1	101	313	0.338 (36 cm²), 0.270 (25 cm²), 0.170 (70 cm²),	Experimental	36 cm² is the optimum active area which produced higher power density.	[92]
MSS and MSI	25	2	2	2	1	101	313	0.420 (MSS 4 mm PSI), 0.345 (MSS 4 mm PCI), 0.242 (SFF)	Experimental	Increasing the size of the porous insert increased the performance.	[93]
SFF with DEA	53	0.686	0.762	0.991	5	123	313,323, 333	NA	Experimental	H₂ pulsation on anode affected the performance.	[95]
Nickel foam	25	NA	NA	NA	NA	110, 120, 130	338	NA	Experimental	Performance of Nickel foam channel was increased upto 6%.	[96]
PFF, SFF, IFF	16 (4×4)	2	1	2	10	20 (anode)	333	NA	Experimental	DEA suitability for steady state operation was found.	[97]
IFF	100	NA	NA	NA	1	101	298	0.25 (IFF), 0.15 (conventional)	Experimental	IFF changed the diffusion transfer mechanism of the gases to/from CL into forced convection.	[98]
PFF/IFF	198.81	0.8, 1, 1.2	1.2, 1, 0.8	1	69	97.272 Back pressure	323	NA	Experimental	The blockage of channels increased the reactant flow and cell performance upto 1.4 times.	[100]
Mid-baffled IFF	50.4 (7.1×7.1)	1	1	1	1	100, 200	353	0.27 (FF with O₂), 0.18 (FF with air),	Experimental	Mid-baffled IFF gave better performance than the conventional	[101]
SFF, IFF	25,70	1,2	1,2	1,2	1	0, 50, 100, 150 (back pressure)	323	0.334 (25 cm²), 0.199 (70 cm²)	Experimental	IFF gave higher performance than SFF. The scaling up and stacking up of PEMFC has decreased the cell performance.	[103]

Table 1. continued

Type of Flow channel/Flow field design	Active area cm²	Channel width (CW) W_c mm	Landing or Rib width (RW) W_r mm	Channel height or depth D_c mm	Number of channels N_{ch} –	Pressure P kPa	Temperature T K	Power density W/cm²	Type of study	Remarks	Ref.
IFF	8.5 & 42.5 (1.7×5, 1.7×25)	1	1	1	8	NA	343	0.436 (IFF-short), 0.387 (IFF-long), 0.278 (PFF-short)	Experimental/ Numerical	Shorter length of channel was better with 12.7% more power density than long length channels.	[105]
PFF/IFF with valves	30.5	1	1	1	7	NA	NA	0.325 (IFF), 0.300 (PFF)	Experimental	By using valves, the PFF can be exchanged as IFF.	[108]
Spiral	25	1	1	1	5	NA	343	NA	Experimental/ Numerical	Spiral flow fields produced secondary vortices which lead to the increased performance than SFF. The increase in current density was 11.9%.	[111]
Lung	49	1	1	1	2	100	333	Power of 25.62 W (Lung), 18.5 W (Triple pass SFF).	Experimental	Lung type yielded 34% higher power than triple pass SFF.	[119]
BI –Interdigitated & Non interdigitated	25	Middle branch width=1, 1.14, 1.78.	variable	1.5	3	101.3	348	Above 0.5	Experimental & Numerical	Bio-inspired designs substantially improved the fuel cell performance by 20–25% than conventional designs.	[120]
Murray-interdigitated	5	0.6 to 1.4 mm	variable	0.8	6	NA	353	NA	Numerical & Experimental	Murray Interdigitated design with pitchfork showed good performance.	[121]
Ginkgo and Net leaf	25	NA	0.8	NA	38 (Ginkgo), 251 (Leaf)	101.3	353	0.55 (Ginkgo), 0.43 (Net Leaf) (approx.)	Experimental & Numerical	Peak power density of ginkgo was 40% more than parallel and 7% lower than serpentine.	[122]
NIDO, SFF	50	1	1	1	34	150 (back pressure)	333	0.51 (NIDO), 0.4 (NID & Murray) 0.36 (SFF) (approx.)	Experimental & Numerical	41% higher performance in NIDO than SFF	[123]
Intersectant FF, SFF	2.25 (1.5×1.5)	0.6	NA	0.2, 0.3, 0.4, 0.5	1	200	353	0.28 (Intersectant), 0.25 (SFF). (approx.)	Experimental & Numerical	Intersectant FF was better than SFF. H₂ flow rate and temperature were optimized.	[126]
Perforated FF, SFF	25	2	2	2	NA	0, 50,100	313	0.242 (Perforated), 0.230 (SFF)	Experimental	More power densities in Perforated FF than SFF.	[127]
PFF, SFF, Branch type	300	0.8, 0.8, 1.6	0.8, 0.8, 0.8	0.5, 0.5, 1.0	NA	NA	338	0.451 (Branch f=0.5), 0.4356 (SFF)	Experimental	The branched channel with f=0.5 gave higher performance	[131]

Table 1. continued

Type of Flow channel/Flow field design	Active area	Channel width (CW)	Landing or Rib width (RW)	Channel height or depth	Number of channels	Pressure	Temperature	Power density	Type of study	Remarks	Ref.
–	– cm²	W_c mm	W_r mm	D_c mm	N_{ch} –	P kPa	T K	– W/cm²	–	–	
								(SFF) – Net output		due to the less power consumption tion	
3DFF with trapezoidal baffles	50	1	1	0.4	Variable	200 Back pressure	353	0.9 (3DFF3, 0.79 (PFF) Net power density	Experimental & Numerical	High reactant transport and 15% more power than PFF	[133]
Fractal	109.5	1	Variable	1 (variable)	Variable	101	323	NA	Experimental	Performance of a fractal design was higher than PFF	[134]
SFF	25	2,1,0.5	1	variable	1	121.6	353	NA	Numerical & Experimental	Optimum C:L ratio was found as 2:1	[140]
SFF, IFF	25	1,2	1,2	1	1	200	323	0.266 (SFF), 0.260 (IFF)	Experimental & Numerical	2:1 (C:L) gave the highest power density	[141]
Parallel-Serpentine	100	1.26, 1.58, 2.00, 2.50, 2.53, 3.16	NA	1.50, 1.26, 2.50, 2.00, 3.16, 2.53	40, 25, 20	13.79 (H_2)	298	0.154 (Aspect ratio 1.25), 0.138 (Aspect ratio 0.8).(approx.)	Experimental	Increase in aspect ratio increased the performance	[142]
Parallel in series with slanted channels	150 (17.34×8.65)	1.5	1	1	5	NA	353	Power: 0.40 W (Anode slanted), 0.35 W (Cathode slanted)	Experimental	Downward slanting of channel on anode stimulated the back diffusion of water from cathode to anode.	[153]
Novel convergent divergent SFF	4.7	1.5	1	variable	1	na	318	0.29 (C1) 0.285 (C2) 0.275 (C3) 0.265 (C4) 0.275 (D1) 0.275 (D2) 0.26 (D3) 0.25 (D4) 0.249 (S1) 0.23 (S2)	Experimental	Design with less channel width gave superior performance	[158]
Taper SFF	25	1	NA	1 to 0.5	1	NA	323	0.22 (Taper SFF) 0.18 (SFF without taper)	Experimental	Tapered SFF resulted in 15% of higher current at 0.5 V than conventional SFF	[160]

NA – Not Available

Table 2. Design and operating parameters of various flow field designs with Numerical analysis.

Type of Flow channel/Flow field design	Active area cm²	Channel width (CW) W_c mm	Landing or Rib width (RW) W_r mm	Channel height or depth D_c mm	Number of channels N_{ch}	Pressure P kPa	Temperature T K	Power density W/cm²	Type of study	Remarks	Ref.
Trap shaped straight channel	1	1	1	1	1	304	353	0.820 (Trap design), 0.700 (Straight design) (approx.)	Numerical	The channel with 8 mm long traps gave higher current densities.	[19]
Single straight channel	1.8	2	1	6	1	101.3	293	0.232 (Rib design), 0.205 (Duct design)	Numerical	The ribbed design and vertical orientation of channels gave better performance.	[20]
Wavy channel	NA	0.5	NA	0.5	NA	101.3	323, 333 and 343	0.730 (Wave design), 0.620 (straight design) (approx.)	Numerical	The wave form channel provided an improved convective heat transfer, catalytic electrochemical reactions, and power density	[21]
Bio-inspired wavy channel	0.6	1	1	1	1	101.3	343.15	0.562 (Wave design), 0.550 (Straight design) (approx.)	Numerical	Low resistance to reactant flow improved the power density upto 2.2%.	[22]
M-flow channel	0.9 (approx.)	1	1	1	1	101.3	343	0.675 (M-design), 0.556 (Straight design) (approx.)	Numerical	M-flow channel generated 21.3% high power density than the wave flow channel.	[23]
Single serpentine channel	25	1.5	1.5	0.5	1	101.3	313	0.760 (N=7), 0.740 (N=5, 0.69 (N=0) (approx.)	Numerical	Though the cell with 7 rectangular cylinders showed maximum power density, the performance. of the cell with 5 rectangular cylinders was good due to reasonable pressure drop.	[24]
Single straight channel	NA	1	NA	1.2	1	304	343	NA	Numerical	Use of Pin-fins with optimum design parameters increased the cell performance.	[25]
Single straight channel	1.5	1	1	1	1	202	338, 358	0.755 (Channel with obstacle), 0.711 (straight channel)	Numerical	Obstacles in channels increase the reactant distribution along the channel and GDL	[26]
PFF (Z and U types)	300 (15×20)	2	2	0.72	39	NA	NA	NA	Numerical	U-type configuration gave better performance than the Z-type at high flow rates	[28]
PFF with single and double in/out	393.45 (12.9×30.5)	3 to 1 tapered	1 (varying)	1	65	101.3	NA	NA	Numerical	Single inlet channel having same channel length made uniform gas distributions	[31]

Table 2. continued

Type of Flow channel/Flow field design	Active area cm²	Channel width (CW) W_c mm	Landing or Rib width (RW) W_r mm	Channel height or depth D_c mm	Number of channels N_{ch}	Pressure P kPa	Temperature T K	Power density W/cm²	Type of study	Remarks	Ref.
PFF with single and double in/out	393.45 (12.9×30.5)	1	1	0.8	65	101.3	353	NA	Numerical	Uniform reactant flow and uniform current generation have reduced the hotspots	[32]
PFF with trapezoidal, semi-circular and square dents	1.2	0.5	1	0.6	1	100	333	0.381 (trapezoidal), 0.369 (Straight)	Numerical	Trapezoidal dent showed better performance	[34]
PFF with partial restricted channel and Metal foam as channel	NA	1	1	1	NA	101.3	353	NA	Numerical	Current density and oxygen concentration were increased by the addition of baffle plates and metal foam.	[35]
PFF with rectangular baffles and a plain Nickel foam	3.6 (approx)	1	1	1	4	304	353	0.87 (Metal foam design), 0.58 (PFF)	Numerical	Current density was increased by the addition of baffle plates and metal foam.	[36]
PFF with blockages	5.1	0.8	0.8	0.8	15	101.3	333	0.800 (with 2 staggered block), 0.725 (without block) (approx.)	Numerical	The maximum power density increased by 4.2% and 11.1% for the in-line and staggered designs respectively over the baseline design.	[40]
PFF with subchannels	196 (14×14)	1	1	1	NA	101.3	333	0.490 (conventional design), 0.460 (SIP 30%, SFR 70%) (approx.)	Numerical	Influence of sub channels along the channel was analysed	[44]
PFF with micro distributor	26.01 (5.1×5.1)	1	1	1	25	101.3	333	0.700 (PFF with micro distributor), 0.569 (PFF) (approx.)	Numerical	Decrease in size of micro distributor increased the performance	[45]
PFF with sub channels and porous parts	4.18 & 5.06 (2.2×1.9 & 2.3×2.2)	19, 22	19, 22	Inlet 0.85, outlet 0.35	13	150	363	NA	Numerical	The porous ribs at bottom of the flow field improved the performance.	[47]
PFF – 4×3 structure	3.4 (approx.)	2	NA	2.5	4	0.101, 0.325	338	NA	Numerical	3D FF increased the EMTC and cell performance	[49]
PFF with zigzag wavy cooling channel	225 (15×15)	2	2	1	37	NA	333	NA	Numerical	Cooling effect of zigzag flow channel was better	[52]

Table 2. continued

Type of Flow channel/Flow field design	Active area cm²	Channel width (CW) W_c mm	Landing or Rib width (RW) W_r mm	Channel height or depth D_c mm	Number of channels N_{ch}	Pressure P kPa	Temperature T K	Power density W/cm²	Type of study	Remarks	Ref.
Sinusoidal FF	9.5 (approx.)	NA	NA	NA	9	100	353	0.650 (Sinusoidal), 0.300 (Parallel)	Numerical	Performance was better due to uniform reactant distribution.	[53]
SFF	0.2	1.5	0.5	1.5	1	304	353	NA	Numerical	Serpentine channel showed better results	[56]
SFF – single and multi passes	10	0.8	0.8	1	1,2,5,5	101	343	NA	Numerical	Performance of 2-SFF was higher at higher humidity.	[57]
FF:3 (MPSFF)	3, 4.5 & 6	0.8	0.7	0.8	2,3,4	101.3	NA	0.464 (4 pass), 0.463 (2 pass)	Numerical	At 0.35 V, Performance of 3 pass SFF was better than 2 and 4 passes.	[58]
FF:3 (MPSFF)	200	0.8	0.7	0.8	3,6,9	150	323	0.449 (3 pass), 0.476 (6 pass)	Numerical	6 pass SFF yielded more power output than 3 and 9 passes.	[59]
4-SFF & 1-SFF	24.8 (4.96×5)	1	1	1	4,1	291	333, 323	NA	Numerical	Parallel flow increased the performance of 4-SFF and 1-SFF	[60]
3-SFF	9.5	1	1	1	3	200	343	0.4754	Numerical	Maximum power density was obtained at maximum humidification and at GDL porosity of 0.6	[61]
PIS	25	0.75	1.5	0.75	3	150	373 to 453	0.26 (100 °C), 0.31 (120 °C), 0.35 (140 °C), 0.39 (160 °C), 0.42 (180 °C)	Numerical	Performance of cell was improved with the increase of temperature	[62]
PIS	5	0.8	0.8	0.8	3,5	101 (anode), 325 (cathode)	333	NA	Numerical	Performance of 3PIS & 5PIS were higher than FF:3	[63]
FF:3 (MPSFF)	26.21, 24.80, 25.20, 25.40, 25.60, 24.60, 24.01, 23.52	0.5, 0.6, 0.6, 0.8, 1, 1, 1, 1	0.8, 0.6, 1, 0.8, 0.6, 0.8, 1, 1.5	0.6, 0.6, 0.4, 0.4, 0.4, 0.4, 0.4, 0.4	4,5,6,8	101.3	333	NA	Numerical	Most excellent possible SFF for the running condition with geometrical specifications was found.	[64]
FF:3 (MPSFF)	200	0.9	0.9	0.55	3,6, 13,26	101.3	343	NA	Numerical	The 13-channel was better than 26-channel, because of the differences in membrane hydration.	[66]

Table 2. continued

Type of Flow channel/Flow field design	Active area (cm²)	Channel width (CW) W_c mm	Landing or Rib width (RW) W_r mm	Channel height or depth D_c mm	Number of channels N_{ch}	Pressure P kPa	Temperature T K	Power density W/cm²	Type of study	Remarks	Ref.
FF:4 (SBFF)	2.3×2.3	1	1	1	3	NA	323	0.7195 (SBFF1), 0.7464 (SBFF2), 0.7649 (SBFF3), 0.6519 (SFF)	Numerical	Baffles induced the higher-pressure differences between adjacent channels.	[68]
FF:7 (CESFF)	10.24 (3.2×3.2)	0.8	0.8	1	variable	101	343	0.82 (CESFF 4-3), 0.67 (SFF)	Numerical	The under-rib convection removed the water from the active area	[72]
FF:8 (MSFF)	18.6 & 25.8 (3.1×6 & 4.3×6)	1	1	1	3,5,7	101.3	353	0.461 (MSFF-3-7), 0.419 (PFF)	Numerical	Serpentine path turns and the reactant transportation under the landing have improved the performance of FF:8	[75]
FF:9 (ECSSFF)	55.5	1	1	1	3	200	323, 333, 343, 353	0.83 (ECSSFF), 0.75 (TSFF)	Numerical	At 0.5 V, 353 K and RH 100%, FF:9 gave 7.51% of higher power density.	[78]
FF:9 (ECSSFF), FF:11 (TSFF)	50, 100, 150, 200	2	1	1	3	200	343	1.35 (100 cm² FF:9), 1.15 (200 cm² TSFF) (approx.)	Numerical	Power was increased 4.5 to 13.5% in FF:9 compared to FF:11.	[79]
SFF, FF:12 (SVSFF), 2-1 SFF	50	1, 0.8	1	1	1,2	10 (back pressure)	343	0.370 (FF:12), 0.300 (SFF), 0.275 (2-1 SFF) (approx.)	Numerical	2-1 SFF showed better performance above −5°C.	[80]
Compound FF	25	1	1	1	5	101	343	0.92 (Compound FF & SFF), 0.68 (PFF)	Numerical	Prevention of water flooding by compound FF was better than SFF.	[81]
4 pass serpentine channel	5.29 (2.3×2.3)	1	1	1	1	NA	323	NA	Numerical	With proper length and height reduction ratios, cell performance was increased.	[85]
SFF with modified channel width	6.168 (2.57×2.4)	1, 1.8 to 0.2, 1.9 to 0.1, 1.6 to 0.4, 1.5 to 0.5	1.3	1	1	101.3	323	0.630 (TS), 0.600 (OS)	Numerical	Convergent serpentine flow slab TS36 gave 1.35 times higher current density.	[86]

Table 2. continued

Type of Flow channel/Flow field design	Active area cm²	Channel width (CW) W_c mm	Landing or Rib width (RW) W_r mm	Channel height or depth D_c mm	Number of channels N_{ch}	Pressure P kPa	Temperature T K	Power density W/cm²	Type of study	Remarks	Ref.
5 pass 4 turn SFF	25	NA	NA	NA	5,10	101.3	348	0.40 (SFF with subchannel), 0.380 (SFF). (approx.)	Numerical	The power output of the SFF having sub-channels was higher.	[87]
Serpentine channels with Horizontal and vertical orientations	26.52	1.5	1	1	1	NA	298.15	NA	Numerical	Horizontal channel with upright manifold showed better performance.	[88]
IFF with rectangular parallelepiped (H1 = Bipolar plate thick, H = Channel & two Landing widths, H2 = Channel width or Rectangular pipe width, H3 = Rectangular pipe height	25	H/ H1 = 1.5, H2/ H1 = 0.5, H3/ H1 = 0.6	NA	NA	1	101.3	313, 333, 353	0.8 (Novel design), 0.65 (original design)	Numerical	The optimum combination of operating parameters and location of pipes were found.	[102]
Straight & IFF	NA	0.762	0.1905	0.762	1	150	353	NA	Numerical	Forced convection led to better water transport in interdigitated channel.	[106]
2 pass IFF	49	1,2	1,2	1	2	101	313,323, 333,343	0.292 (C:L of 2:1), 0.272 (C:L of 1:2)	Numerical	2:1 (C:L) yielded the maximum power density.	[107]
FF:14 (HSI)	48.067	0.8	0.8	0.8	1,2	101.3	333	0.7652 (2-IO FF:14), 0.7323 (1S or SFF), 0.5121 (1I-2O FF:14)	Numerical	2-IO FF:14 showed better cell performance due to uniform gas distributions.	[109]
Multiple concentric spirals	16.6	0.8	1.5	1.0	1,2,3,4,6,8	202	343	Power of 0.52 W (4 channel), 0.44 W (8 channel). (approx.)	Numerical	The flow field with 3 and 4 channels gave better performance. Power of 8 channels was 15% lower than 4 channels.	[110]
Tubular cylindrical with serpentine, interdigitated & straight designs	5.49	0.8	0.8	0.8	15,2,1	202	343	Power of 1.63 W (PFF), 1.57 W (IFF), 1.44 W (SFF)	Numerical	Tubular SFF gave better performance due to less pressure drop and better water removal. The conventional FF on cylindrical configurations were better than rectangular configurations.	[112]
BI	24.6	2	1	1	1	101.3	323	1.1 (BI), 0.80 (PFF), 0.45	Numerical	Higher power densities of 26% and 56% were ob-	[115]

Table 2. continued

Type of Flow channel/Flow field design	Active area	Channel width (CW)	Landing or Rib width (RW)	Channel height or depth	Number of channels	Pressure	Temperature	Power density	Type of study	Remarks	Ref.
	– cm^2	W_c mm	W_r mm	D_c mm	N_{ch} –	P kPa	T K	– W/cm^2			
								– (SFF) (approx.)	–	tained for BI over PFF and SFF respectively.	
Bionic	4	1	variable	1	More	101.3	353	0.760	Numerical	Due to secondary channels, more gas consumption ratio, even reactant distribution and low ohmic losses, the bionic flow field had high performance.	[116]
Biomimetic	7.2	0.5 to 3 mm	0.5 to 3 mm	0.2 and 2.5 mm.	More	101.3	353	0.85 (Bio), 0.82 (SFF), 0.700 (PFF) (approx.)	Numerical	Biomimetic FF yielded higher power, uniform distribution of gases and easy removal of water.	[117]
Serpentine and Tubular cells with double parallel, double bisector & triple parallel (Square tubular-simple, DPIE, DBIE, TPIE)	NA	NA	NA	0.05 0.025 0.025 0.025 0.025	2,4,6	304	353	0.9 (DPIE), 0.85 (DBIE), 0.80 (simple) (approx.)	Numerical	Double bisector channels showed better performance	[125]
Honeycomb	12.6 (2×6.3)	1.5	1.3	1.5	NA	110	353	0.34	Numerical	The hexagonal pins increased the diffusion rate of oxygen through GDL by 10 times.	[128]
Land-pillar	257 (25.2×10.2)	2, 3	2	2	Variable	NA	NA	NA	Numerical	3 mm CW, single inlet and 76% flow area showed higher performance	[129]
Cascade	100	2	NA	1	Variable	NA	NA	NA	Numerical	More H_2 inlets at entry of flow field were the best.	[130]
SFF	34	2,3,4	1	3	1	101.3	299	NA	Numerical	The best open ratio of air breathing cathode channel was found.	[132]
Constructal	25	NA	NA	NA	16,64, 256	101	300	0.45 (Constructal), 0.36 (Parallel) (approx.)	Numerical	Constructal 256 design with fractal structure had a good hydrodynamic performance	[135]
Multipass SFF	25 & 200	0.9 1.0 0.7	0.9 0.7 1.0	0.55	3	101, 274	343 353	NA	Numerical	The best rib to channel ratio for automotive and stationary applications were found.	[136]
SFF,PFF, HSI (FF:14)	26.01	0.4, 0.6, 0.8, 1.0, 1.2	1.6, 1.4, 1.2, 1.0, 0.8	1	1	101.3	323	0.966 (SFF), 0.902 (IFF), 0.692 (PFF)	Numerical	While increasing rib width and decreasing channel width, the performance of cell was improved.	[137]

Table 2. continued

Type of Flow channel/Flow field design	Active area cm²	Channel width (CW) W_c mm	Landing or Rib width (RW) W_r mm	Channel height or depth D_c mm	Number of channels N_{ch}	Pressure P kPa	Temperature T K	Power density W/cm²	Type of study	Remarks	Ref.
SFF	2.56	0.27 to 4	NA	0.27 to 4	1	101.3	343	0.480 (10/06), 0.440 (06/10)	Numerical	Channel with a high cross-section aspect ratio gave better performance.	[138]
Single channel	0.3, 0.6, 0.9, 1.2	0.5, 1, 1.5, 2	0.5, 1, 1.5, 2	0.5, 1, 1.5, 2	1	150	323	0.4473 (0.5×0.5), 0.4347 (1×1), 0.4146 (1.5×1.5), 0.3751 (2×2)	Numerical	Various landing to channel width ratios were analyzed.	[139]
PFF with open cathode	100	1.26, 1.58, 2, 2.5, 2.53, 3.16	1.26, 0.94, 2, 1.5, 2.53, 1.9	1.58, 1.26, 2.5, 2, 3.16, 2.53	40, 25, 20	101.3	348	0.16 (approx.)	Numerical	Performance of the cell was not much affected by aspect ratio and cross-sectional area.	[143]
SFF	25	1, 1.25, 1.5, 1.75	1, 0.75, 0.5, 0.25	0.34, 0.5, 0.67, 0.83	5	101	348	0.420 (approx.)	Numerical	Increasing the CW caused the membrane dehydration.	[144]
Rectangular, trapezoidal & parallelogram flow channels	0.5076	0.8, 0.9, 0.8	0.4, 0.35, 0.4	1, 1, 1	1	101.3	343	NA	Numerical	Rectangular channel showed better performance	[145]
SFF with Rectangle and Triangle cross-section	50	1.37	1.45	0.37 & 0.76	5	200	353	NA	Numerical	PTFE coating on water clogging and effect of channel cross-section were found.	[146]
Rectangular, trapezoidal, stepped flow channels	2	0.8, 1.05, 1.05	0.65	0.8, 0.8, 0.8	1	101.3	353	NA	Numerical	Rectangular channel exhibited good electrical performance	[147]
PFF with Rectangle, Triangle, Trapezoid and Circular cross-sections	196 (14×14)	1	1	0.5, 1	12	101.3	NA	0.67 (Trianle), 0.60 (Retangle) (approx.)	Numerical	Different channel cross-sections were compared. At low cell voltage, the triangle channel showed maximum performance.	[148]
SFF with triangle, hemisphere and rectangular shapes	16 (4×4)	0.5, 1, 1.5, 2, 3, 4	0.5, 1, 1.5, 2, 3, 4	1.5	1	202	350	NA	Numerical	Best channel shape was found to increase H_2 consumption and performance.	[149]

Table 2. continued

Type of Flow channel/Flow field design	Active area cm²	Channel width (CW) W_c mm	Landing or Rib width (RW) W_r mm	Channel height or depth D_c mm	Number of channels N_{ch}	Pressure P kPa	Temperature T K	Power density W/cm²	Type of study	Remarks	Ref.
Straight channels	2.4	0.8	variable	0.8	1	101.3	343	0.315 (Trp-I-Trp)	Numerical	Trapezoidal-Inverted Trapezoidal shape gained higher power density upto 4.65%	[152]
Taper Channel (taper in height and width)	198.87	1	1	0.1 0.5 1.8	9	101.3	323	NA	Numerical	Increasing the width of the taper channel gave better performance	[154]
Single taper channel	1.5 approx.	1	NA	variable	1	101	353	0.25 (approx.)	Numerical	Power density was increased 8% by 0.75° inclination	[155]
Converging-Diverging flow channels	13.4 (6.7×2.0)	0.5	1	0.5	14	101.3	333	NA	Numerical	The channel angle of 0.3° gave better performance due to over rib velocity	[156]
Convergent & Divergent SFF	2	1	0.5	0.25 0.5 1.0	1	101.3	353	NA	Numerical	Convergent FF gave better performance	[159]
IFF	NA	1	1	NA	NA	101.3	298	NA	Numerical	Better oxygen transport and performance were found in the narrower channels	[161]
SFF with slope turn	NA	1	1	1	1	NA	NA	NA	Numerical	Slope turns increased the performance.	[162]
SFF	100	1	1	1	1,2,3,4,5,6 channels	101.3	323	NA	Numerical	Channel curvature and number of channels for better performance were found.	[163]
SFF	60	2	2	0.72	1	NA	NA	NA	Numerical	Effects of the curvature ratios and Reynolds number on the pressure losses of flow pattern were analysed.	[164]
SFF	0.20	1	1	1	1	304	353	NA	Numerical	The 1.2 mm bend size had less pressure drop and uniform temperature distribution	[165]

NA – Not Available

wavy SFF, Sinusoidal SFF, MSI, MSS of plate type FF and the tubular cylindrical FF are some of the designs developed from SFF. The important points obtained from SFF are as follows;

- There is a considerable balance among the flow distribution and pressure drop with robust operation of PEMFC in FF : 3 than single pass SFF
- The under rib convection in FF : 4 and FF : 7 and the enhanced cross flow in FF : 9 have increased the cell performance. Further, the pressure drop of the reactants can be greatly reduced by using FF:9
- FF : 5 design has the advantages of both Parallel Serpentine Flow Field Plate (FF : 6) and IFF Plate
- The bends and wavy shapes on SFF have improved performance over the conventional SFF. The sub-channels and DEA in SFF have increased the cell performance
- To enhance the performance of SFF with better water management, a specially made PCI and PSI can be inserted along the cathode ribs at different positions and sizes. Due to globalized water absorption, the staggered arrangement of PCI and PSI showed better performance in MSS than MSI

4. The IFF design changes the diffusion transfer mechanism of the gases to/from CL into the forced convection mechanism. Even though the performance of IFF is higher than SFF, the pressure drop of reactants is much more, due to the dead end of channels. Further, the use of oxygen instead of air in the cathode side provides better results. The important points obtained from IFF are as follows;
   - The FF:14 (HSI) design has the advantages of both SFF and IFF The FF : 14 can be used for commercial applications due to the simple design and manufacturability
   - The proper position of baffles in inlet and outlet channels on the IFF has improved the cell performance
   - The novel flow field which can be exchanged between PFF and IFF was designed

5. The spiral, concentric spiral, radial, cylindrical, and tubular flow fields showed higher performance than planar flow fields, but their design and fabrication are complex.
   - The cylindrical SFF has better performance than cylindrical PFF and cylindrical IFF
   - The cylindrical PEMFC are having high gravimetric and volumetric power density compared to the planar PEMFC
   - The innovative radial flow field with control rings showed a superior flow distribution and water

removal, utilization of active area and lower pressure drop than parallel and serpentine types

6. The Natural inspired or Bio inspired flow fields namely BI, Bionic, Biomimetic, Lung, Bio-inspired IFF, Ginkgo and Net leaf flow fields, etc. were developed from the nature designs.
   - The Bio-inspired (BI) flow field developed from the leaf flow patterns, showed the higher power densities than SFF and PFF
   - The Bio-inspired IFF designed based on Murray's law has improved the fuel cell performance than IFF and 5 channeled parallel-in-series designs
   - The interdigitated designs with a Pitchfork pattern has uniform current density distributions
   - The peak power density of Ginkgo flow field is higher than PFF
   - A semi cylindrical shaped obstacle along the daughter channels of natural inspired flow field is higher

7. The intersectant FF with optimum porosity gave superior performance than the SFF. The perforated FF which consists of 169 holes generated more power densities on comparison with SFF. The honeycomb FF having the hexagonal pins increased the diffusion rate of oxygen through GDL by 10 times. Compared to the uniform type, the zigzag pin type FF showed a higher performance due to even distribution of reactant. The fractal designs of flow fields have lower performance than serpentine. For portable applications, the tubular cylindrical configurations are deemed as a possible choice than conventional designs.

8. The length and number of channels, width and height of landing and channel and number of inlets have an influence on the cell performance. The bending curvature, slope and width have an influence on fuel cell performance. In automotive applications, a wide channel with narrow width and the co-current flow gives higher performance, whereas, for stationary applications, a narrow channel with wide width and the co-current flow gives higher performance.

9. The rectangular cross-section of the channel with sharp curve resulted in better performance when compared to other cross-sections like triangular, trapezoid, stepped channel etc. The Trapezoidal-Inverted Trapezoidal shape gained greater power density upto 4.65 %.

10. For commercial applications of fuel cell, the flow field with active area of 100, 200 and 300 cm^2 and above are more suitable. For increasing the output voltage and current, the cells can be connected in series and parallel respectively to form a stack.

11. The Converging-Diverging flow channels, the convergent serpentine channels and the taper in width and height of channels have improved the reactant

flow and cell performance. The performance of the taper channels is better than the conventional ones.

12. With proper channel design, operating parameters and orientations of channels, the performance of fuel cell can be improved. Finally, almost care must be given while choosing the correct flow field design for higher performance of PEMFC.

Nomenclature

Symbols

CO_2	Carbon dioxide
D_c	Depth of channel
f	Branching factor
H_2	Hydrogen
H_2O	Water
N_{ch}	Number of channels
NOx	Nitrogen oxide
O_2	Oxygen
P	Pressure
Pt	Platinum
SOx	Sulphur oxide
T	Temperature
W_c	Width of channel
W_r	Width of rib
W_{GP}	Gross power
W_{NP}	Net power
W_{PP}	Pumping power
1-S, 2-S, 3-S	Single, double and triple serpentine respectively
η	Channel to rib width ratio

Abbreviations

ABFC	Air Breathing Fuel Cell
AB-PEMFC	Air Breathing – Proton Exchange Membrane Fuel Cell
BI	Bio Inspired
CL	Catalyst Layer
C:L	Channel to Landing width ratio
CW	Channel Width
DBIE	Double Bisectors Intermediate Electrode
DEA	Dead End Anode
DE-PEMFC	Direct Ethanol- Proton Exchange Membrane Fuel Cell
DMFC	Direct Methanol Fuel cell
DPIE	Double Parallel Intermediate Electrode
EMTC	Effective Mass Transfer Coefficient
EASA	Electrochemical active surface area
FCEV	Fuel Cell Electric Vehicle
FF	Flow Field

FF:1	Parallel Trapezoid Baffle Plate Flow Field (PTBPFF)
FF:2	Staggered Trapezoid Baffle Plate Flow Field (STBPFF)
FF:3	Multi-Path Serpentine Flow Field (MPSFF)
FF:4	Serpentine Baffle Flow Field (SBFF)
FF:5	Parallel Serpentine-Baffle Flow Field Plate (PSBFFP)
FF:6	Parallel Serpentine Flow Field Plate (PSFFP)
FF:7	Convection Enhanced Serpentine Flow Field (CESFF)
FF:8	Modified Serpentine Flow Field (MSFF)
FF:9	Enhanced Cross Flow Split Serpentine Flow Field (ECSSFF)
FF:10	Single Serpentine Flow Field (SSFF)
FF:11	Triple Serpentine Flow Field (TSFF)
FF:12	Single Variable Section Serpentine Flow Field (SVSFF)
FF:13	Waved Serpentine Flow Field (WSFF)
FF:14	Hybrid Serpentine Interdigitated (HSI)
GC	Gas Channel
GDE	Gas Diffusion Electrode
GDL	Gas Diffusion Layer
HTPEMFC	High Temperature PEMFC
LIF	Laser Induced Fluorescence
MF	Maldistribution Factor
MSI	Modified Serpentine flow field with Inline arrangement of porous inserts
MSS	Modified Serpentine flow field with Staggered arrangement of porous inserts
NIDO	Nature inspired design with obstacle
PCB	Printed Circuit Board
PCI	Porous Carbon Inserts
PEMFC	Proton Exchange Membrane Fuel Cell
PIS	Parallel In Series
PSI	Porous Sponge Inserts
PTFE	Polytetrafluoroethylene
RW	Rib Width
S	conventional Serpentine
SC	Convergent Serpentine
SD	Divergent Serpentine
SFF	Serpentine Flow Field
SFR	Sub-channel Flow Rate
SIP	Sub-channel Inlet Position
SP	Square Peripheral
TPA	Through-Plane Array
TPIE	Triple Parallel Intermediate Electrode
1S	One channel serpentine
3DFF	Three Dimensional Flow Field

Acknowledgement

References

[1] W. Bernhart, S. Riederle, M. Yoon, W. G. Aulbur, *Auto Tech Rev.* **2014**, *3*, 18–23.

[2] R. Q. Nafil, **Fuel Cells as a Source of Green Energy** in (Ed.: M. S. M. E.-P. Vizureanu), IntechOpen, Rijeka, **2020**, p. Ch. 11.

[3] M. C. Williams, **Chapter 2 - Fuel Cells**,in (Eds.: D. Shekhawat, J. J. Spivey, D. A. B. T.-F. C. T. for F. P. Berry), Elsevier, Amsterdam, **2011**, pp. 11–27.

[4] A. R. Vijay Babu, P. Manoj Kumar, G. Srinivasa Rao, *Alexandria Eng. J.* **2018**, *57*, 3953–3958.

[5] M. Muthukumar, *Ph.D Thesis* **2016**.

[6] M. Muthukumar, N. Rengarajan, B. Velliyangiri, M. A. Omprakas, C. B. Rohit, U. Kartheek Raja, *Mater. Today Proc.* **2020**, DOI https://doi.org/10.1016/j.matpr.2020.03.679.

[7] A. Ajanovic, R. Haas, *Fuel Cells* **2019**, *19*, 515–529.

[8] O. Saritas, D. Meissner, A. Sokolov, *J. Knowl. Econ.* **2019**, *10*, 1183–1203.

[9] I. Alvarez-Meaza, E. Zarrabeitia-Bilbao, R. M. Rio-Belver, G. Garechana-Anacabe, *Sustain.* **2020**, *12*, DOI 10.3390/su12062334.

[10] Frost, Sullivan, *Fuel Cell Electr. Veh. Genes. a New Era or a Myth. New Energy Veh. Technol. open access Gov. Organ. Sept.* **2018**.

[11] V. Thiagarajan, P. Karthikeyan, R. Manoharan, S. Sampath, A. Hernández-Ramírez, M. E. Sánchez-Castro, I. L. Alonso-Lemus, F. J. Rodríguez-Varela, *Electrocatalysis* **2018**, *9*, 582–592.

[12] V. Thiagarajan, R. Manoharan, P. Karthikeyan, E. Nikhila, A. Hernández-Ramírez, F. J. Rodriguez-Varela, *Int. J. Hydrogen Energy* **2017**, *42*, 9795–9805.

[13] V. Thiagarajan, P. Karthikeyan, K. Thanarajan, S. Neelakrishnan, R. Manoharan, R. Chen, A. Fly, R. Anand, T. R. Karuppa Raj, N. Sendhil Kumar, *Int. J. Hydrogen Energy* **2019**, *44*, 13415–13423.

[14] M. Muthukumar, P. Karthikeyan, M. Eldho, P. Nagarathinam, E. P. Panneer Selvam, R. Prasanna, *J. Adv. Chemistry.* **2017**, *13*, 6462–6467.

[15] M. Kumar, P. Karthikeyan, A. P. Kumar, *Asian J. Res. Soc. Sci. Humanit.* **2016**, *6*, 1387.

[16] S. Praveenkumar, M. Kumar, S. Muruganantham, *Int. J. Appl. Chem* **2015**, *11*, 505–513.

[17] P. Karthikeyan, M. Muthukumar, S. Vignesh Shanmugam, P. Pravin Kumar, S. Murali, A. P. Senthil Kumar, *Procedia Eng.* **2013**, *64*, 409–418.

[18] S. S. Kocha, *Polymer Electrolyte Membrane (PEM) Fuel Cells: Automotive Applications BT- Fuel Cells and Hydrogen Production: A Volume in the Encyclopedia of Sustainability Science and Technology*, in (Eds.: T. E. Lipman, A. Z. Weber), Springer New York, New York, NY, **2019**, pp. 135–171.

[19] F. Ramin, H. Sadeghifar, A. Torkavannejad, *Int. J. Heat Mass Transfer* **2019**, *129*, 1151–1160.

[20] P. Manoj Kumar, A. K. Kolar, *Int. J. Hydrogen Energy* **2010**, *35*, 671–681.

[21] J.-K. Kuo, T.-H. Yen, C.-K. Chen, *J. Power Sources* **2008**, *177*, 96–103.

[22] G. Cai, Y. Liang, Z. Liu, W. Liu, *Energy* **2020**, *192*, 116670.

[23] Z. Wan, W. Quan, C. Yang, H. Yan, X. Chen, T. Huang, X. Wang, S. Chan, *Energy Convers. Manage.* **2020**, *205*, 112386.

[24] H.-W. Wu, H.-W. Ku, *Appl. Energy* **2011**, *88*, 4879–4890.

[25] S. O. Obayopo, T. Bello-Ochende, J. P. Meyer, *Int. J. Hydrogen Energy* **2012**, *37*, 10286–10298.

[26] M. Bilgili, M. Bosomoiu, G. Tsotridis, *Int. J. Hydrogen Energy* **2015**, *40*, 2303–2311.

[27] S. Barati, B. Khoshandam, M. M. Ghazi, *Int. J. Hydrogen Energy* **2018**, *43*, 21928–21939.

[28] S. Maharudrayya, S. Jayanti, A. P. Deshpande, *J. Power Sources* **2005**, *144*, 94–106.

[29] S. Maharudrayya, S. Jayanti, A. P. Deshpande, *J. Power Sources* **2006**, *157*, 358–367.

[30] M. Sajid Hossain, B. Shabani, C. P. Cheung, *Int. J. Hydrogen Energy* **2017**, *42*, 5272–5283.

[31] B. H. Lim, E. H. Majlan, W. R. W. Daud, M. I. Rosli, T. Husaini, *Int. J. Hydrogen Energy* **2017**, *42*, 9210–9218.

[32] B. H. Lim, E. H. Majlan, W. R. W. Daud, M. I. Rosli, T. Husaini, *Chem. Eng. Sci.* **2020**, *217*, 115499.

[33] A. R. Vijay Babu, P. Manoj Kumar, G. Srinivasa Rao, *Arabian J. Sci. Eng.* **2016**, *41*, 3415–3423.

[34] A. Ghanbarian, M. J. Kermani, *Energy Convers. Manage.* **2016**, *110*, 356–366.

[35] E. Afshari, M. Mosharaf-Dehkordi, H. Rajabian, *Energy* **2017**, *118*, 705–715.

[36] A. Azarafza, M. S. Ismail, M. Rezakazemi, M. Pourkashanian, *Renewable Sustainable Energy Rev.* **2019**, *116*, 109420.

[37] X. Wang, Y. Qin, S. Wu, X. Shangguan, J. Zhang, Y. Yin, *J. Power Sources* **2020**, *457*, 228034.

[38] J. Chen, *J. Power Sources* **2010**, *195*, 1122–1129.

[39] H. Heidary, M. J. Kermani, S. G. Advani, A. K. Prasad, *Int. J. Hydrogen Energy* **2016**, *41*, 6885–6893.

[40] H. Heidary, M. J. Kermani, A. K. Prasad, S. G. Advani, B. Dabir, *Int. J. Hydrogen Energy* **2017**, *42*, 2265–2277.

[41] D. Quan, Z. Hong-Liang, W. Zhong-Min, Y. Yan-Ru, Y. Chen, W. Xiao-Dong, *J. Energy Eng.* **2020**, *146*, 4020054.

[42] M. Rahimi, B. Aghel, A. A. Alsairafi, *Chem. Eng. Process.* **2010**, *49*, 689–696.

[43] S. Dabiri, M. Hashemi, M. Rahimi, M. Bahiraei, E. Khodabandeh, *Energy* **2018**, *152*, DOI 10.1016/j.energy.2018.04.005.

[44] Y. Wang, S. Wang, G. Wang, L. Yue, *Int. J. Hydrogen Energy* **2018**, *43*, 2359–2368.

[45] H. Liu, W. Yang, J. Tan, Y. An, L. Cheng, *Energy Convers. Manage.* **2018**, *176*, 99–109.

[46] R. Koresawa, Y. Utaka, *Int. J. Hydrogen Energy* **2015**, *40*, 8172–8181.

[47] Y. Utaka, A. Okabe, Y. Omori, *J. Power Sources* **2015**, *279*, 533–539.

[48] Y. Cai, Z. Fang, B. Chen, T. Yang, Z. Tu, *Energy* **2018**, *161*, 28–37.

[49] J. Shen, Z. Tu, S. H. Chan, *Appl. Therm. Eng.* **2020**, *164*, 114464.

[50] S. Arun Saco, R. Thundil Karuppa Raj, P. Karthikeyan, *Energy* **2016**, *113*, 558–573.

[51] M. K. Vijayakrishnan, K. Palaniswamy, J. Ramasamy, T. Kumaresan, K. Manoharan, T. K. Raj Rajagopal, T. Maiyalagan, V. R. Jothi, S.-C. Yi, *Int. J. Hydrogen Energy* **2020**, *45*, 7848–7862 DOI https://doi.org/10.1016/j.ijhydene.2019.05.205.

[52] E. Afshari, M. Ziaei-Rad, M. M. Dehkordi, *J. Energy Inst.* **2017**, *90*, 752–763.

[53] S. A. Atyabi, E. Afshari, *J. Therm. Anal. Calorim.* **2019**, *135*, 1823–1833.

[54] M. Whiteley, L. Rasha, T. Neville, J. Millichamp, R. Luca, P. Shearing, D. J. L. Brett, *J. Power Sources* **2019**, *442*, 227218.

[55] Y. Xu, Z. Penga, Q. Xu, H. Su, W. Shi, F. Barbir, *AIChE J.* **2020**, DOI 10.1002/aic.16957.

[56] F. Hashemi, S. Rowshanzamir, M. Rezakazemi, *Math. Comput. Model.* **2012**, *55*, 1540–1557.

[57] D. H. Jeon, S. Greenway, S. Shimpalee, J. W. Van Zee, *Int. J. Hydrogen Energy* **2008**, *33*, 1052–1066.

[58] M. Muthukumar, P. Karthikeyan, V. Lakshminarayanan, A. P. Senthil Kumar, M. Vairavel, R. Girimurugan, *Appl. Mech. Mater.* **2014**, *592–594*, 1728–1732.

[59] M. Muthukumar, S. Saravanaperumal, V. Lakshminrayanan, A. P. Senthil Kumar, *Int. J. Appl. Eng. Res.* **2015**, *10*, 22429–22435.

[60] I. khazaee, H. Sabadbafan, *Energy* **2016**, *101*, 252–265.

[61] E. E. Kahveci, I. Taymaz, *EJSDR* **2017**, *2*, 155–163.

[62] D. G. Caglayan, B. Sezgin, Y. Devrim, I. Eroglu, *Int. J. Hydrogen Energy* **2016**, *41*, 10060–10070.

[63] N. Limjeerajarus, P. Charoen-amornkitt, *Int. J. Hydrogen Energy* **2015**, *40*, 7144–7158.

[64] A. Ghanbarian, M. J. Kermani, J. Scholta, M. Abdollahzadeh, *Energy Convers. Manage.* **2018**, *166*, 281–296.

[65] F. Mojica, M. A. Rahman, J. M. Mora, J. D. Ocon, P.-Y. A. Chuang, *Fuel Cells* **2020**, *20*, 547–557. DOI 10.1002/fuce.202000002.

[66] S. Shimpalee, S. Greenway, J. Van Zee, *J. Power Sources* **2006**, *160*, 398–406.

[67] V. Velisala, G. N. Srinivasulu, *Arabian J. Sci. Eng.* **2018**, *43*, 1225–1234.

[68] X.-D. Wang, Y.-Y. Duan, W.-M. Yan, *J. Power Sources* **2007**, *173*, 210–221.

[69] P. Martins Belchor, M. M. Camargo Forte, D. E. Ortiz Suman Carpenter, *Int. J. Hydrogen Energy* **2012**, *37*, 11904–11911.

[70] G. Benetti, P. Barbieri, E. Mathias, J. Bottin, M. Klein, M. M. Forte, P. Belchor, *Renew. Energy Power Qual. J.* **2015**, 62–65.

[71] C. Xu, T. S. Zhao, *Electrochem. Commun.* **2007**, *9*, 497–503.

[72] F. B. Baz, S. Ookawara, M. Ahmed, *Int. J. Hydrogen Energy* **2019**, *44*, 30644–30662.

[73] E. Alizadeh, M. Rahimi-Esbo, S. M. Rahgoshay, S. H. M. Saadat, M. Khorshidian, *Int. J. Hydrogen Energy* **2017**, *42*, 14708–14724.

[74] D. Singdeo, T. Dey, S. Gaikwad, S. J. Andreasen, P. C. Ghosh, *Appl. Energy* **2017**, *195*, 13–22.

[75] C. Min, J. He, K. Wang, L. Xie, X. Yang, *Energy Convers. Manage.* **2019**, *180*, 1217–1224.

[76] P. V. Suresh, S. Jayanti, A. P. Deshpande, P. Haridoss, *Int. J. Hydrogen Energy* **2011**, *36*, 6067–6072.

[77] S. Abdulla, M. M. Seepana, V. S. Patnaikuni, *Arabian J. Sci. Eng.* **2020**, DOI 10.1007/s13369-020-04803-0.

[78] A. Sheikh, V. S. Patnaikuni, *Int. J. Energy Res.* **2019**, DOI 10.1002/er.4368.

[79] S. Abdulla, V. S. Patnaikuni, *Int. J. Hydrogen Energy* **2020**, DOI https://doi.org/10.1016/j.ijhydene.2020.01.199.

[80] Y. Zhu, R. Lin, Z. Jiang, D. Zhong, B. Wang, W. Shangguan, L. Han, *Int. J. Hydrogen Energy* **2019**, *44*, 7505–7517.

[81] Y. Vazifeshenas, K. Sedighi, M. Shakeri, *Int. J. Hydrogen Energy* **2015**, *40*, 15032–15039.

[82] H. A. Dhahad, W. H. Alawee, A. K. Hassan, *Renew. Energy Focus* **2019**, *30*, 71–77.

[83] M. Seyhan, Y. Akansu, M. Murat, Y. Korkmaz, S. Akansu, *Int. J. Hydrogen Energy* **2017**, *42*, 25619–25629.

[84] W. Li, Q. Zhang, C. Wang, X. Yan, S. Shen, G. Xia, F. Zhu, J. Zhang, *Appl. Energy* **2017**, *195*, 278–288.

[85] W.-M. Yan, H.-Y. Li, P.-C. Chiu, X.-D. Wang, *J. Power Sources* **2008**, *178*, 174–180.

[86] C.-T. Wang, Y.-T. Ou, B.-X. Wu, S. Thangavel, S.-W. Hong, W.-T. Chung, W.-M. Yan, *Energy Procedia* **2017**, *142*, 667–673.

[87] S.-H. Jang, G. Shin, H. Hwang, K.-S. Choi, H.-M. Kim, *World Renewable Energy Congress* **2011**, *10*, 1205–1210.

[88] M. Ashrafi, M. Shams, *Appl. Energy* **2017**, *208*, 1083–1096.

[89] A. Iranzo, J. Biesdorf, M. Cochet, A. Salva, P. Boillat, F. Rosa, *Fuel Cells* **2016**, *16*, 777–783,.

[90] P. Karthikeyan, R. J. Vasanth, M. Muthukumar, *Int. J. Hydrogen Energy* **2015**, *40*, 4641–4648.

[91] P. Karthikeyan, M. Marappan, V. Jothi, *Int. J. Hydrogen Energy* **2016**, *41*, 2867–2874.

[92] M. Karthikeyan, P. Karthikeyan, C. Mathan, M. Muthukumar, *J. Ceram. Process. Res.* **2019**, *20*, 490–498.

[93] a) M. Karthikeyan, P. Karthikeyan, M. Muthukumar, V. Magesh Kannan, K. Thanarajan, T. Maiyalagan, C.-W. Hong, V. R. Jothi, S.-C. Yi, *Int. J. Hydrogen Energy* **2019**, *45*, 7863–7872; b) M. Marappan, R. Narayanan, K. Manoharan, M. K. Vijayakrishnan, K. Palaniswamy, S. Karazhanov, S. Sundaram, *Molecules* **2021**, *26*, 286.

[94] R. Liu, W. Zhou, S. Li, F. Li, W. Ling, *Int. J. Hydrogen Energy* **2020**, *45*, 17833–17843.

[95] J. Siegel, D. Mckay, A. Stefanopoulou, D. Hussey, D. Jacobson, *J. Electrochem. Soc.* **2008**, *155*, DOI 10.1149/1.2976356.

[96] J. W. Choi, Y.-S. Hwang, S. W. Cha, M. S. Kim, *Int. J. Hydrogen Energy* **2010**, *35*, 12469–12479.

[97] Y. Yang, X. Zhang, L. Guo, H. Liu, *Int. J. Hydrogen Energy* **2017**, *43*, DOI 10.1016/j.ijhydene.2017.10.137.

[98] T. V. Nguyen, *J. Electrochem. Soc.* **1996**, *143*, L103–L105.

[99] T. V. Nguyen, W. He, *Handb. Fuel Cells* **2010**, DOI doi:10.1002/9780470974001.f303031.

[100] W.-M. Yan, S.-C. Mei, C.-Y. Soong, Z.-S. Liu, D. Song, *J. Power Sources* **2006**, *160*, 116–122.

[101] V. Thitakamol, A. Therdthianwong, S. Therdthianwong, *Int. J. Hydrogen Energy* **2011**, *36*, 3614–3622.

[102] H.-W. Ku, H.-W. Wu, *J. Power Sources* **2013**, *232*, 199–208.

[103] P. Karthikeyan, P. Velmurugan, A. J. George, R. Ram Kumar, R. J. Vasanth, *Int. J. Hydrogen Energy* **2014**, *39*, 11186–11195.

[104] P. Hu, L. Peng, W. Zhang, X. Lai, *J. Power Sources* **2009**, *187*, 407–414.

[105] A. D. Santamaria, N. J. Cooper, M. K. Becton, J. W. Park, *Int. J. Hydrogen Energy* **2013**, *38*, 16253–16263.

[106] S. Um, C. Y. Wang, *J. Power Sources* **2004**, *125*, 40–51.

[107] V. Lakshminarayanan, K. Niveda, S. Akash, P. Anand, *Int. J. Ambient Energy* **2019**, 1–5.

[108] A. D. Santamaria, J. Bachman, J. W. Park, *Int. J. Hydrogen Energy* **2013**, *38*, 5807–5812.

[109] N. Limjeerajarus, T. Santiprasertkul, *Int. J. Hydrogen Energy* **2019**, DOI https://doi.org/10.1016/j.ijhydene.2018.12.160.

[110] D. Juarez-Robles, A. Hernandez-Guerrero, B. Ramos-Alvarado, F. Elizalde-Blancas, C. E. Damian-Ascencio, *J. Power Sources* **2011**, *196*, 8019–8030.

[111] J.-Y. Jang, C.-H. Cheng, W.-T. Liao, Y.-X. Huang, Y.-C. Tsai, *Appl. Energy* **2012**, *99*, 67–79.

[112] J. M. Sierra, S. J. Figueroa-Ramírez, S. E. Díaz, J. Vargas, P. J. Sebastian, *Int. J. Hydrogen Energy* **2014**, *39*, 16694–16705.

[113] S. R. Suseendiran, S. Pearn-Rowe, R. Rengaswamy, *Int. J. Hydrogen Energy* **2020**, *45*, 10549–10558.

[114] B. R. Friess, M. Hoorfar, *Int. J. Hydrogen Energy* **2012**, *37*, 7719–7729.

[115] R. Roshandel, F. Arbabi, G. K. Moghaddam, *Renewable Energy* **2012**, *41*, 86–95.

[116] T. Chen, Y. Xiao, T. Chen, *Energy Procedia* **2012**, *28*, 134–139.

[117] H. Ruan, C. Wu, S. Liu, T. Chen, *Heat Mass Transfer* **2016**, *52*, 2167–2176.

[118] A. Ozden, M. Ercelik, D. Ouellette, C. O. Colpan, H. Ganjehsarabi, F. Hamdullahpur, *Int. J. Hydrogen Energy* **2017**, *42*, 21546–21558.

[119] S. R. Badduri, G. N. Srinivasulu, S. S. Rao, *Int. J. Green Energy* **2019**, *16*, 1591–1601.

[120] N. Guo, M. C. Leu, U. O. Koylu, *Int. J. Hydrogen Energy* **2014**, *39*, 21185–21195.

[121] A. Arvay, J. French, J.-C. Wang, X. Peng, A. Kannan, *Open Electrochem. J.* **2015**, *6*, 1–9.

[122] H. C. Kang, K. M. Jum, Y. J. Sohn, *Int. J. Hydrogen Energy* **2019**, *44*, 24036–24042.

[123] H. Kahraman, A. Coban, *Arabian J. Sci. Eng.* **2020**, DOI 10.1007/s13369-020-04368-y.

[124] B. Osanloo, A. Mohammadi-Ahmar, A. Solati, *Int. J. Hydrogen Energy* **2016**, *41*, 10844–10853.

[125] A. Mohammadi-Ahmar, A. Solati, B. Osanloo, M. Hatami, *Energy* **2017**, *137*, 302–313.

[126] D. Wen, L. Yin, Z. Piao, C. Lu, G. Li, Q. Leng, *Int. J. Heat Mass Transfer* **2018**, *121*, 775–787.

[127] S. Subramaniam, G. Rajaram, K. Palaniswamy, V. R. Jothi, *J. Energy Inst.* **2017**, *90*, 363–371.

[128] S. A. Atyabi, E. Afshari, *J. Cleaner Prod.* **2019**, *214*, 738–748.

[129] K. H. Gopi, A. Nambi, N. Rajalakshmi, *Fuel Cells* **2020**, *20*, 33–39.

[130] L. Valiño, R. Mustata, M. I. Gil, J. Martín, *Int. J. Hydrogen Energy* **2010**, *35*, 11425–11436.

[131] S. H. Han, N. H. Choi, Y. D. Choi, *Int. J. Hydrogen Energy* **2015**, *40*, 4819–4829.

[132] W. Ying, T.-H. Yang, W.-Y. Lee, J. Ke, C.-S. Kim, *J. Power Sources* **2005**, *145*, 572–581.

[133] L. He, M. Hou, Y. Gao, D. Fang, P. Wang, B. Lv, Z. Shao, *Energy Convers. Manage.* **2020**, *205*, 112335.

[134] K. Tüber, A. Oedegaard, M. Hermann, C. Hebling, *J. Power Sources* **2004**, *131*, 175–181.

[135] B. Ramos-Alvarado, A. Hernandez-Guerrero, F. Elizalde-Blancas, M. W. Ellis, *Int. J. Hydrogen Energy* **2011**, *36*, 12965–12976.

[136] S. Shimpalee, J. W. Van Zee, *Int. J. Hydrogen Energy* **2007**, *32*, 842–856.

[137] Y. Kerkoub, A. Benzaoui, F. Haddad, Y. K. Ziari, *Energy Convers. Manage.* **2018**, *174*, 260–275.

[138] A. P. Manso, F. F. Marzo, M. G. Mujika, J. Barranco, A. Lorenzo, *Int. J. Hydrogen Energy* **2011**, *36*, 6795–6808.

[139] M. Muthukumar, P. Karthikeyan, M. Vairavel, C. Loganathan, S. Praveenkumar, A. P. S. Kumar, *Procedia Eng.* **2014**, *97*, 1534–1542.

[140] W. J. Yang, H. Y. Wang, Y. B. Kim, *Int. J. Hydrogen Energy* **2014**, *39*, 9430–9439.

[141] V. Lakshminarayanan, P. Karthikeyan, *Prog. Comput. Fluid Dyn. An Int. J.* **2019**, *19*, 328.

[142] S. Kiattamrong, A. Sripakagorn, *Energy Procedia* **2015**, *79*, 612–619.

[143] S. Kreesaeng, B. Chalermsinsuwan, P. Piumsomboon, *Energy Procedia* **2015**, *79*, 733–745.

[144] K.-S. Choi, H.-M. Kim, S.-M. Moon, *Int. J. Hydrogen Energy* **2011**, *36*, 1613–1627.

[145] D. H. Ahmed, H. J. Sung, *J. Power Sources* **2006**, *162*, 327–339.

[146] J. P. Owejan, T. A. Trabold, D. L. Jacobson, M. Arif, S. G. Kandlikar, *Int. J. Hydrogen Energy* **2007**, *32*, 4489–4502.

[147] A. L. R. Paulino, E. F. Cunha, E. Robalinho, M. Linardi, I. Korkischko, E. I. Santiago, *Fuel Cells* **2017**, *17*, 27–36.

[148] X.-D. Wang, G. Lu, Y.-Y. Duan, D.-J. Lee, *Int. J. Hydrogen Energy* **2012**, *37*, 15778–15786.

[149] A. Kumar, R. G. Reddy, *J. Power Sources* **2003**, *113*, 11–18.

[150] L. Varadharajan, P. Karthikeyan, M. Kumar, A. P. Senthil Kumar, B. Kavin, A. Kavyaraj, *Appl. Mech. Mater.* **2014**, *592–594*, 1672–1676.

[151] M. Muthukumara, P. Karthikeyanb, *Int J AdvEngg Tech/Vol. VII/Issue II/April-June* **2016**, *302*, 305.

[152] A. Mohammedi, Y. Sahli, H. Ben Moussa, *Fuel* **2020**, *263*, 116713.

[153] P. Wawdee, S. Limtrakul, T. Vatanatham, M. W. Fowler, *Int. J. Hydrogen Energy* **2015**, *40*, 3739–3748.

[154] W.-M. Yan, H.-C. Liu, C.-Y. Soong, F. Chen, C. H. Cheng, *J. Power Sources* **2006**, *161*, 907–919.

[155] É. Fontana, E. Mancusi, A. da Silva, V. C. Mariani, A. A. Ulson de Souza, S. M. A. G. Ulson de Souza, *Int. J. Heat Mass Transfer* **2011**, *54*, 4462–4472.

[156] N. Zehtabiyan-Rezaie, A. Arefian, M. Kermani, A. Karimi, M. Abdollahzadeh, *Energy Convers. Manage.* **2017**, *152*, 31–44.

[157] J. Lee, M. Gundu, N. Lee, K. Lim, S. Jang, J. Kim, H. Ju, *Int. J. Hydrogen Energy* **2019**, DOI 10.1016/j.ijhydene.2019.07.128.

[158] M. Z. Chowdhury, Y. E. Akansu, *Int. J. Hydrogen Energy* **2017**, *42*, 25686–25694.

[159] M. Z. Chowdhury, B. Timurkutluk, *Energy* **2018**, *161*, 104–117.

[160] R. R. Kumar, S. Suresh, T. Suthakar, V. K. Singh, *Int. J. Hydrogen Energy* **2020**, *45*, 15642–15649.

[161] S. Chen, Z. Xia, X. Zhang, Y. Wu, *Energy Procedia* **2019**, *158*, 1678–1684.

[162] H. Liu, J. Tan, L. Cheng, W. Yang, *Energy Convers. Manage.* **2018**, *176*, 227–235.

[163] N. Jaruwasupant, Y. Khunatorn, *Energy Procedia* **2011**, *9*, 326–337.

[164] S. Maharudrayya, S. Jayanti, A. P. Deshpande, *J. Power Sources* **2004**, *138*, 1–13.

[165] L. Rostami, P. Nejad, A. Vatani, *Energy* **2016**, *97*, 400–410.

[166] X. Li, I. Sabir, J. Park, *J. Power Sources* **2007**, *163*, 933–942.

[167] W. R. Chang, J. J. Hwang, F. B. Weng, S. H. Chan, *J. Power Sources* **2015**, *166*, 149–154.

[168] T. J. Mason, J. Millichamp, T. P. Neville, A. El-kharouf, B. G. Pollet, D. J. L. Brett, *J. Power Sources* **2012**, *219*, 52–59.

[169] A. Jung, J. Oh, K. Han, M. S. Kim, *Appl. Energy* **2016**, *175*, 212–217. https://doi.org/10.1016/j.apenergy.2016.05.016.

[170] I. V. Zenyuk, D. Y. Parkinson, L. G. Connolly, A. Z. Weber, *J. Power Sources* **2016**, *328*, 364–376.

[171] C–C. Chen, D. Shaw, K.-L. Hsueh, *Int. J. Hydrogen Energy* **2017**, *42(5)*, 3185–3196.

[172] X. Wang, Y. Song, Bi Zhang, *J. Power Sources* **2008**, *179*, 305–309.

[173] N. Kulkarnia, M. D. R. Koka, R. Jervisa, F. Iacoviello, Q. Meyera, P. R. Shearinga, D. J. L. Bretta, *J. Power Sources* **2019**, *426*, 97–110.

[174] X. Q. Xing, K. W. Lum, H. J. Poh, Y. L. Wu, *J. Power Sources* **2010**, *195*, 62–68.

[175] R. Chen, Y. Qin, Q. Du, J. Peng, *SAE [Tech. Pap.]* **2018**, 2018-01-1718, doi:10.4271/2018-01-1718.

[176] H. Li, Y. Tang, Z. Wang, Z. Shi, S. Wu, D. Song, J. Zhang, K. Fatih, J. Zhang, H. Wang, Z. Liu, R. Abouatallah, A. Mazza, *J. Power Sources* **2008**, *178*, 103–117.